

**STUDIES ON SOME SUPPORTED TRANSITION
METAL COMPLEXES**



**THESIS SUBMITTED TO THE
COCHIN UNIVERSITY OF SCIENCE AND TECHNOLOGY
IN PARTIAL FULFILMENT OF THE
REQUIREMENTS FOR THE DEGREE OF**

DOCTOR OF PHILOSOPHY

IN

CHEMISTRY

IN THE FACULTY OF SCIENCE

BY

RANI ABRAHAM

**DEPARTMENT OF APPLIED CHEMISTRY
COCHIN UNIVERSITY OF SCIENCE AND TECHNOLOGY
KOCHI-682 022, KERALA**

NOVEMBER 1999



COCHIN UNIVERSITY OF SCIENCE AND TECHNOLOGY
DEPARTMENT OF APPLIED CHEMISTRY
KOCHI - 682 022, INDIA

Phone: 0484-555804 Telex: 885-5019 CUIN Grams: CUSAT
Fax: 91-484-532495; email: chemist@vsnl.com

Dr. K.K. Mohammed Yusuff
Professor and Head

1st November, 1999

CERTIFICATE

This is to certify that the thesis entitled "*Studies on some supported transition metal complexes*" submitted for the award of the Degree of Doctor of Philosophy of Cochin University of Science and Technology, is a record of bonafide research work carried out by Ms. Rani Abraham under my supervision in the Department of Applied Chemistry.

(K.K. MOHAMMED YUSUFF)

PREFACE

Studies in the area of supported transition metal complexes are receiving wide attention due to their various advantages. The difficulties encountered during the practical application of the homogeneous metal complexes are minimised by 'supporting' or 'heterogenising' them. Moreover, a combination of the benefits of both homogeneous and heterogeneous catalysts is achieved by the process of heterogenization.

In this thesis an attempt has been made to heterogenise some transition metal complexes with two types of supports. One is zeolite Y which is inorganic in nature and the other is polystyrene which is an organic polymer. A consideration of the influence exerted by the ligands on the structure and properties of the metal complexes led to the choice of two biologically important ligands, embelin and 2-aminobenzimidazole. Studies involving the metal complexes of biologically important ligands are often attempted, as they might function as models of biologically important molecules like enzymes and might give an insight into the functioning of these type molecules. A sincere effort has been made to characterise the synthesized complexes with the available techniques. The ability of these supported systems in catalysing the deoxo reaction was investigated. A study of the decomposition of hydrogen peroxide involving the supported complexes were also undertaken. The catalase like activity of one of the complexes was ascertained by a detailed study of the reaction mechanism.

The general conclusions drawn from the study are summarised at the end of the thesis. The zeolite turned out to be a better support in terms of mechanical as well as thermal stability. The abilities of the ligands in tuning the potential of the metal ion were apparent from the study.

CONTENTS

CHAPTER I	INTRODUCTION	1	
	1.1	General types of immobilization.	3
	1.2	Supports for anchoring metal complexes	4
	1.2.1	Inorganic materials as supports	4
	1.2.2	Organic polymers as supports	5
	1.3	Zeolite encapsulated transition metal complexes	5
	1.3.1	Structure of zeolites	7
	1.3.2	Methods of encapsulation of transition metal complexes inside the zeolite structure.	7
	1.3.3	Zeolite encapsulated complexes-evidence for intrazeolite location.	8
	1.3.4	Zeolite encapsulated metal complexes – Applications	9
	1.4	Polymer supported transition metal complexes	11
	1.4.1	Procedure for anchoring a complex on a polymer support	13
	1.4.2	Polymer anchored complexes-characterization	13
	1.4.3	Polymer anchored complexes-limitations	13
	1.4.4	Polymer anchored complexes-applications	14
	1.5	Role of ligands in metal complexes	15
	1.6	Scope of the present investigation	16
		References	18
CHAPTER II	EXPERIMENTAL TECHNIQUES	23	
	2.1	Reagents	23
	2.2	Modification of supports	24
	2.2.1	Zeolites	24
	2.2.2	Polystyrene	24
	2.3	Preparation of the ligands	25
	2.3.1	Extraction of embelin	25
	2.3.2	Preparation of Schiff base with polymer bound aldehyde and 2-aminobenzimidazole	26
	2.3.3	Preparation of Schiff base with polymer bound amine and embelin	26
	2.4	Analytical methods	26
	2.4.1	Analysis of the zeolite samples for Si, Al, Na and transition metal ions by the complete dissolution method.	26
	2.4.2	Analysis of the polymer samples for metal	27
	2.4.3	CHN analyses	27
	2.4.4	Estimation of chlorine	27

	2.5	Physico chemical methods	28
	2.5.1	Magnetic susceptibility measurements	28
	2.5.2	Surface area analyses	28
	2.5.3	Infra red spectra	28
	2.5.4	Optical spectra	29
	2.5.5	EPR	29
	2.5.6	XRD	30
	2.5.7	SEM	30
	2.5.8	TG	30
	2.5.9	GC	31
		References	32
CHAPTER III		STUDIES ON TRANSITION METAL COMPLEXES OF EMBELIN AND 2-AMINOBENZIMIDAZOLE IN ZEOLITE Y	33
		Introduction	33
	3.1	Studies on the transition metal complexes of embelin encapsulated in zeolite Y	34
	3.1.1	Experimental	34
	3.1.1.1	Materials	34
	3.1.1.2	Preparation of the complexes in NaY	34
	3.1.1.3	Preparation of a reaction blank	35
	3.1.2	Physicochemical characterization	35
	3.1.2.1	Elemental Analysis	35
	3.1.2.2	Surface Area Analysis	37
	3.1.2.3	Magnetic susceptibility measurements	37
	3.1.2.4	Infrared Spectra	42
	3.1.2.5	Electronic Spectra	43
	3.1.2.6	EPR studies	47
	3.1.2.7	X-Ray Diffraction	52
	3.1.2.8	Thermal behaviour	53
	3.2	Studies on the transition metal complexes of 2-aminobenzimidazole in zeolite Y	56
	3.2.1	Experimental	56
	3.2.1.1	Materials	56
	3.2.1.2	Preparation of the complexes in Na Y	56
	3.2.1.3	Preparation of a reaction blank	56
	3.2.2	Physicochemical characterization	57
	3.2.2.1	Elemental Analysis	57
	3.2.2.2	Surface area analysis	57
	3.2.2.3	Magnetic susceptibility measurements	57
	3.2.2.4	Infrared Spectra	57
	3.2.2.5	Electronic Spectra	59
	3.2.2.6	EPR Spectra	61
	3.2.2.7	XRD	63

	3.2.2.8 Thermal behaviour	63
	References	65
CHAPTER IV	TRANSITION METAL COMPLEXES OF POLYMER BOUND SCHIFF BASES	67
	Introduction	67
4.1	Transition metal complexes of the schiff base derived from polymer bound amine and embelin	68
4.1.1	Experimental	68
4.1.1.1	Materials	68
4.1.1.2	Preparation of the complexes	68
4.1.1.3	Analytical methods	68
4.1.2	Results and discussion	69
4.1.2.1	Magnetic susceptibility measurements	71
4.1.2.2	Surface area Analyses	72
4.1.2.3	Infrared Spectra	75
4.1.2.4	Electronic Spectra	75
4.1.2.5	EPR Spectra	76
4.1.2.6	Thermal behaviour	78
4.1.2.7	SEM	78
4.2	Transition metal complexes of the schiff base derived from polymer bound aldehyde and 2-aminobenzimidazole	80
4.2.1	Experimental	80
4.2.1.1	Materials	80
4.2.1.2	Synthesis of the complexes	80
4.2.2	Results and discussion	80
4.2.2.1	Magnetic measurements	82
4.2.2.2	Surface area analyses	82
4.2.2.3	Infrared Spectra	82
4.2.2.4	Electronic Spectra	86
4.2.2.5	EPR Spectra	86
4.2.2.6	Thermal behaviour	88
4.2.2.7	SEM	88
	Reference	89
CHAPTER V	ACTIVITY OF THE SUPPORTED TRANSITION METAL COMPLEXES IN CATALYSING THE HYDROGEN-OXYGEN REACTION	91
	Introduction	91
5.1	Experimental	93
5.1.1	Materials	93
5.1.2	Preparation of the catalysts	93

5.1.3	Analysis of the complexes	93
5.1.4	Reaction setup	93
5.2	Results and discussion	94
5.2.1	Influence of oxygen concentration	97
5.2.2	Influence of catalyst weight	97
5.2.3	Influence of temperature	97
5.2.4	Life cycle of the catalyst	100
	Reference	101
CHAPTER VI	CATALYTIC DECOMPOSITION OF HYDROGEN PEROXIDE- A KINETIC AND MECHANISTIC STUDY	102
6.1	Introduction	102
6.2	Experimental	104
6.2.1	Materials	104
6.2.2	Experimental setup	104
6.3	Screening studies	106
6.3.1	Catalysis by zeolite encapsulated complexes	06
6.3.2	Catalysis by polymer supported complexes	108
6.4	Kinetic study of the decomposition of hydrogen peroxide in the presence of the zeolite encapsulated copper embelin complex	109
6.4.1	Kinetic procedure	109
6.4.2	Results	110
6.4.3	Discussion	113
	References	118
	SUMMARY AND CONCLUSIONS	119

CHAPTER I

INTRODUCTION

The importance of coordination compounds or transition metal complexes is evident from their numerous applications in almost every field of life. They play an active role in nature as exemplified by the function of macromolecules such as haemoglobin, chlorophyll, etc. that regulate various enzymatic processes in biological systems. Many enzymes contain coordinated metal ions as their active centres. Metal containing compounds are also important in the process of energy transfer. Therefore, studies on metal complexes, have always been a subject of interest, intrigue and challenge to the chemist particularly to the inorganic chemist. A survey of current literature in this field reveals that synthetic coordination chemistry has advanced so much as to be able to produce complexes that mimic and therefore challenge biological systems in terms of energy capture.

Many metal complexes are labile and coordinatively unsaturated. These properties have led to their use in the field of homogeneous catalysis. A large number of coordination compounds are used as catalysts (1) for hydrocarbon transformations. Examples include the well known Wilkinson's hydrogenation catalyst, chlorotris(triphenylphosphine)rhodium(I); the catalyst used in the oxo process, dicobaltoctacarbonyl; the Rh complex catalyst $[\text{RhCO}_2\text{I}_2]$ - used by the Monsanto company for the production of acetic acid; Zeigler Natta catalyst and the Wacker catalysts. Chiral metal complexes are now being increasingly used in enantioselective synthesis in the pharmaceutical industry (2). As a result, there is a continuing interest in the development of catalytically efficient metal complexes, and also in the modification of the existing catalysts.

Homogeneous catalysis is attractive, because it is often highly selective towards the formation of a desired product. Also these reactions can be performed under mild conditions. However, the application of these systems to large scale processes often lead to significant problems such as:

- (i) difficulties in the separation of the catalyst from the reaction medium as well as with respect to catalyst recovery. This is a severe disadvantage especially when complexes of precious metals like Pd, Pt, Rh etc. are used.
- (ii) instability (thermal as well as mechanical) of homogeneous catalytic systems.
- (iii) possible corrosive effect of catalyst solutions.

In several cases, these disadvantages restrict the use of metal complex catalysts, despite their highly selective nature. On the other hand, application of heterogeneous catalysts is more practical from a technological point of view. They often possess high stability, and are therefore easily recoverable from the reaction medium. However, heterogeneous catalysts prove to be insufficiently selective and active for many processes for which effective homogeneous systems exist. Most of these processes are energy consuming as they require high temperature and often high pressure. These factors have been the impetus for the development of 'hybrid' or heterogenized homogeneous systems.

The term 'heterogenization' refers to the process whereby a transition metal complex is immobilized on or anchored to an inert polymer or inorganic support. The heterogenized systems combine the merits of both the homogeneous and heterogeneous systems, while minimizing the demerits of both. In the beginning, heterogenization of known catalysts were attempted (3,4). Later on, the trend in research moved in the direction of finding novel heterogenized systems and in evaluating their catalytic potentials. Different techniques and materials were evaluated for effective heterogenization, and this itself has turned out to be a very interesting subject. The increasing interest in the area of heterogenized

homogeneous catalytic systems is evident from the large number of papers published on various classes of anchored catalysts (5-7).

Classification of catalysts containing immobilized complexes is not completely outlined. Most often, the classification is based on the type of matrix used, the nature of anchoring sites on the matrix surface, the nuclearity of attached catalytic centres and the manner in which the metal complex is immobilized.

I.1 GENERAL TYPES OF IMMOBILIZATION:

Complexes in the volume of the matrix:

Complexes can be immobilized in the volume of the matrix which is a separate phase with respect to the medium. The encapsulation of complexes in the cages of zeolites (7), immobilization of complex catalysts in the volume of polymer gels, mica type silicates and graphites, etc., (8) comes under this category.

Complexes supported on a matrix surface:

Complexes can be anchored to a matrix with a large surface area and pore size. This type of matrices allows the diffusion of reagents to the anchored catalysts. The following techniques are usually employed for the surface immobilization of complexes:

(a) *Binding complexes by chemical bonds with surface anchoring sites* (8) - this technique of immobilization involves the synthesis of surface compounds of general composition:



where || is the support surface; $\sim \text{L}$ is the anchoring site (surface ligand), which is bonded to the support surface by a chemical bond; M is the metal atom, X are the ligands not bonded to the support ("external ligands"); and l, m, x are the

stoichiometric numbers. This approach may provide a great variety of catalysts due to the possibility of varying the type of transition metal and its ligand environment.

(b) immobilization of complexes in a film of non volatile solvent - In this technique, the pores of the support are filled with the solution of catalytically active complexes in a non volatile solvent (4).

(c) formation of dispersed phase of supported metal complex on matrix surface - this technique involves impregnation of the support with a solution of the complex compound and subsequent removal of the solvent (5).

1.2 SUPPORTS FOR ANCHORING METAL COMPLEXES:

Sheldon in his review (10) of the recent advances that have been made in the transformation of homogenous to solid catalysts, describes the use of metal complexes immobilized on organic and inorganic supports. Information on solid acids and bases, redox molecular sieves as solid catalysts for liquid phase oxidations, zeolite encapsulated complexes and supported liquid phase catalysts is also given in this review. The various approaches towards the rational design of novel catalysts based on the concept of confinement of redox active centers in molecular sieves is again discussed by Sheldon et al. in another review (11).

1.2.1 Inorganic materials as supports:

A variety of inorganic materials are used as catalyst supports. Zeolites, Oxides, Silica, Alumina, and Clay are the common supports used. (7, 9). They have the following characteristic features:

- (i) rigidity of the matrix surface
- (ii) thermal stability - this property permits the use of catalysts supported in materials at moderate and high temperatures.
- (iii) availability of the methods of large scale production of supports with the required surface area and pore volume.

1.2.2 Organic polymers as supports:

Many different polymer materials, natural and synthetic, prepared both by addition polymerization or condensation, are reported as matrices to anchor complexes. The cross linked copolymers with styrene and divinylbenzene are used extensively. A detailed description of polymer supported complexes is presented in forthcoming section (1.4).

It is interesting to note that the functions of the anchored metal complexes are largely influenced by the supports used and in view of this, different supports including both organic and inorganic have been experimented with.

1.3 ZEOLITE ENCAPSULATED TRANSITION METAL COMPLEXES:

Zeolites with their intracrystalline cage and channel structure have long fascinated the scientists. Encapsulation of transition metal complexes in these materials might combine some characteristics of the support (like pore diameter, cavity size and electrostatic potential) with the electronic and stereochemical properties of the complex; and therefore could lead to the highly selective formation of certain products with a precise structure. According to Herron (12) and Mitchell (13), zeolite encapsulated complexes can be considered as inorganic analogues of enzymes. These materials have an internal structure of linked channels which open into wider cages rather as underground streams open into a cave. Chemically they are constructed of SiO_4 and AlO_4 tetrahedra linked through oxygen bridges (Fig.1.1). Channels and cages of different shapes and sizes are created by the linking of the tetrahedra to each other. This structure of the zeolite is somewhat similar to the tertiary protein structure of an enzyme. In an enzyme the active site is embedded in the protein chain. This protein chain protects the active site from bad reactions, such as self destructions via bimolecular path ways. It also acts as a sieve towards the substrate molecules, and permits only those capable of passing through the protein

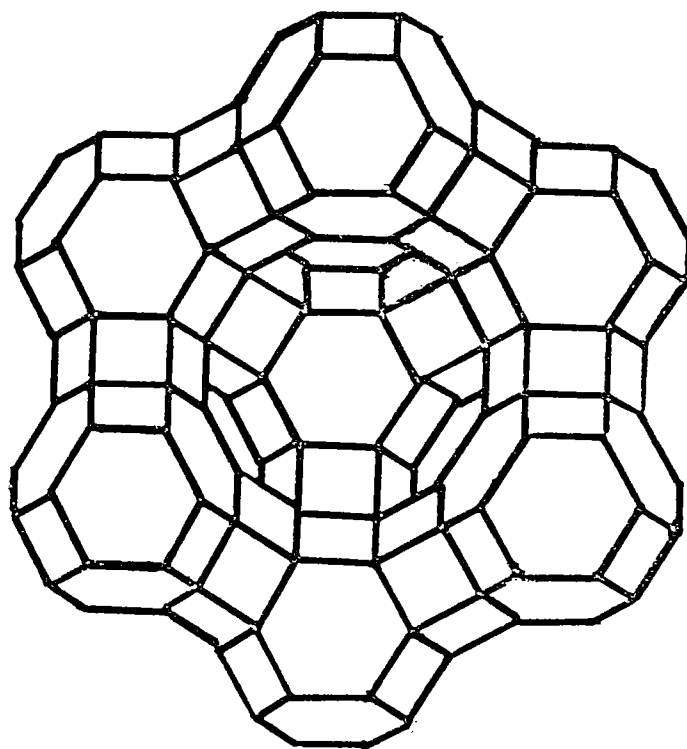


Fig I.1: Zeolite Y.

channels to access the embedded active metal site. As a result of this sieving action the enzyme exhibits high substrate selectivity. An interesting similarity of the enzymes and zeolites in this context is the use of zeolites as molecular sieves in the separation of gas mixtures and also as shape and size-selective catalysts. The protein chain of the enzyme also provides a stereochemically demanding void near the active site, where the substrate must reside during the reaction, leading to transformation at specific bonds within the substrate molecule. A similar role can be expected for zeolites in the case of zeolite encapsulated complexes.

The intracrystalline cage and channel structure of the zeolite can be exploited by encapsulating a metal complex within the cage. The species thus obtained can then be compared to an enzyme with the metal complex as the active site and the zeolite framework concealing it like the protein chain. The properties of the molecules in the cage are modified by the electric field created within the cage by the framework atoms. These framework atoms which are themselves catalytically active, also improve the steric constraints on the complex causing it to distort and thereby changing its stability and reactivity. The dimerisation of complexes which lead to its deactivation are also strongly retarded by encapsulation.

For encapsulating a metal complex within the cage of a zeolite, the zeolite must possess an optimum cage size. Due to this reason only some of the zeolites like zeolite Y, X, etc., can function as metal complex supports. A discussion on the structure of these type of zeolites is presented in the following sections. The different methods for encapsulating the metal complexes in the zeolites and the available physicochemical techniques for their characterisation are also discussed. The importance of the zeolite encapsulated complexes in catalysis as evidenced by the large number of publications in literature is also discussed.

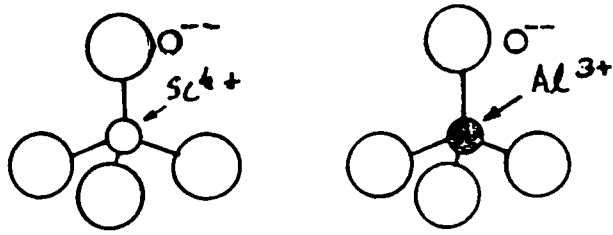
1.3.1 Structure of Zeolites (14):

The silica and alumina tetrahedra which constitutes the basic building units of zeolites can be arranged in different manners to form different porous crystal structures. For example, 24 tetrahedra form a sodalite unit (fig.I.2), which is a cubo-octahedron consisting of six four membered faces (the cube faces) and eight six membered rings (the octahedral faces). These sodalite units are the basic building blocks for A, X and Y type molecular sieves. When the sodalite units are linked to one another at their hexagonal faces through hexagonal prisms of six oxygen atoms, the X and Y zeolite structures are formed. This structure has two types of pores or cavities in it. The sodalite cages enclose a supercage or α cage with diameter 13\AA and a cage mouth opening of 8\AA (fig.I.2). Because of these large spatially accessible pores, the X and Y type zeolites are suitable candidates for encapsulating transition metal complexes.

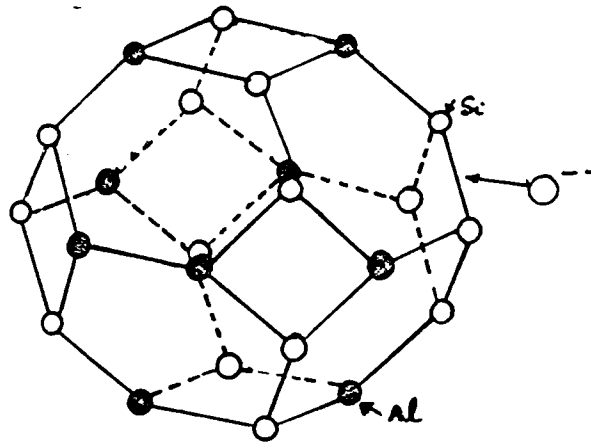
1.3.2 Methods of encapsulation of transition metal complexes inside the zeolite structure:

Metal complexes can be encapsulated in the cages of a zeolite by different routes. The various strategies for the preparation of the zeolite encapsulated complexes with sufficient examples have been presented in the paper of Balkus and Gabrielov (15). Evidence for the intrazeolite location of the metal complexes as well as the prevailing interpretation of these results are organized in terms of various methods of characterization. A brief summary of the known reactivity studies of zeolite encapsulated metal complexes including catalytic oxidation and hydrogenation is also presented in this paper.

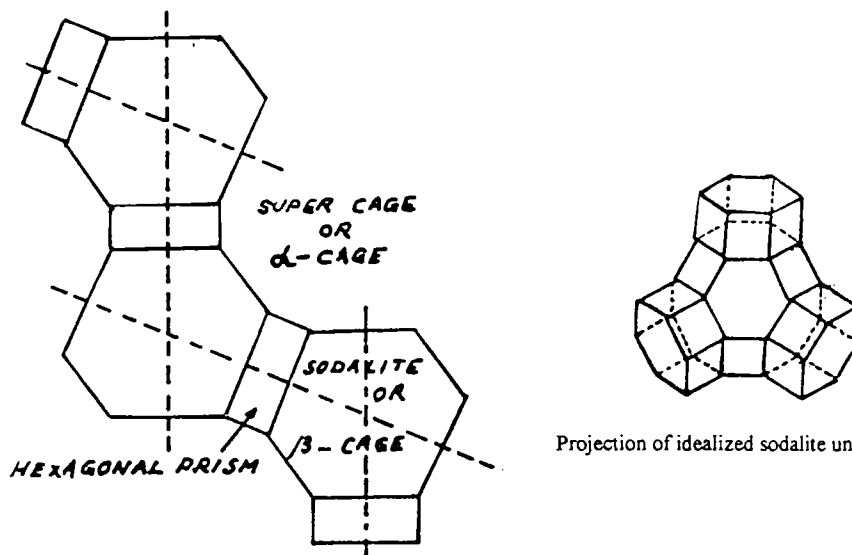
One of the methods for introducing a metal complex into the cavities is the flexible ligand method, wherein the ligand, which is flexible enough to diffuse freely through the pores, is allowed to react with the metal-ion exchanged zeolite. The



SiO₄ and AlO₄ tetrahedra.



Sodalite Unit



Projection of idealized sodalite unit and hexagonal prism.

Cross sectional view of the type of cages in molecular sieves X and Y.

Fig. 1.2: Structural units of Zeolite Y.

ligand upon complexation becomes too large and rigid to escape the cages (16-19). Examples of complexes encapsulated by this method include the cobalt complexes of salen, bipyridyl, etc., (20). Another approach to the synthesis of encapsulated complex is the template method (21) which is exemplified by the preparation of intrazeolite metallophthalocyanine. Dicyanobenzene molecules diffuse into the zeolite pores, where four molecules can cyclize around a resident metal ion, to form a tetradentate macrocycle which is too large to exit from the cavities. A recent approach is the zeolite synthesis (22, 23) method in which the metal complex added possibly play the role of the template during the crystallisation of the zeolite host.

1.3.3 Zeolite encapsulated complexes - evidence for intrazeolite location:

A battery of techniques are used to reveal the presence of the complexes in the cavities of the zeolite. The analytical data indicates the presence of intrazeolite matter. Various techniques are used to check whether the synthesized complexes are in the cages or are simply deposited on the external surface (24). The scanning electron microscope can be used to detect externally deposited complexes. X-ray photoelectron spectroscopy (XPS) will probe the depth of an internal atom relative to a surface atom. In this technique, electrons are ejected from core levels when a substance is irradiated with X-rays. Only electrons from atoms near the surface (within 50 Å⁰) can escape and contribute to XPS. Hence by comparing XPS intensities we can determine whether atoms of a particular element are within a particle or at the surface (13). A useful chemical procedure is to treat a zeolite complex with a substance, which is too big to enter the channels but can react with the surface complexes. If there is no reaction, it can be concluded that the complex is in the internal cage(25, 26).

The presence of the complexes is further confirmed by the infrared spectrum of the sample. The spectrum is either compared to that of its unencapsulated analogue or to that of the ligands forming the complex (24). Several workers have

elucidated the structure of the complexes in the cages by a combination of diffuse reflectance and magnetic studies(27-29). Zeolite samples do not show specific d-d absorptions when analyzed in the absorbance mode. This is because the zeolite surface scatters the radiations falling on it. Hence measurements are usually done in the diffuse reflectance mode. The electron paramagnetic studies (EPR) are very useful in understanding the environment about the paramagnetic cation. EPR studies of zeolite encapsulated complexes have been performed by several workers (27,28,30). Electrochemical techniques such as cyclic voltammetry provide information on the oxidation state and redox chemistry of the active metal centre and the ligand. Even subtle structural features may be elucidated through differences in potential shifts between two different complex structures (31-33). X-ray diffraction studies (XRD), surface area analyses, and thermal analyses (24) are also used to characterize the zeolite encapsulated complexes.

1.3.4 Zeolite encapsulated metal complexes – Applications:

The metal complexes physically entrapped in the cavities of the zeolites on the basis of their size, are also referred to as 'ship-in-a-bottle' complexes. These complexes have excited the imagination of chemists because of their ability to bind reversibly, small molecules such as oxygen. Their size and shape selectivities, and the possibilities of metalloenzyme mimicry are also of interest. In a number of instances the effect of complexation is to make a metal exchanged zeolite more selective. The ligands modify or fine tune the electronic and structural environment of a metal ion. Thus encapsulated metal complexes have catalytic properties which differ from those of cation exchanged zeolites.

Biomimetic chemistry based on zeolites is a theme which has been pursued by a number of research groups. Herron (12) has demonstrated the ability of zeolite complexes to reproduce the control typical of enzyme protein with the help of Co(salen) in zeolite Y. Lunsford and Howe have used the transition metal complexes

of ethylene diamine in zeolite Y as catalysts for the oxidation of pyrocatechol with the aim of investigating the possibility of using these systems for activating molecular oxygen within zeolite for attack on appropriate substrates in a manner similar to that of enzymes. Zeolite encapsulated oxomolybdenum sulfur complexes have been employed as models of molybdenum oxidase / reductase enzymes (13).

The ability of the zeolite encapsulated complexes to bind oxygen reversibly have prompted the scientists to explore the possibility of using them as efficient oxygen carriers. Interestingly, the majority of reactions catalysed by zeolite encapsulated complexes are oxidation reactions.

Selective oxidations (16) of various olefins on the basis of their size was achieved by the use of Mn(salen) complexes in zeolite Y. Iron phthalocyanine in zeolite Y was found to be a good catalyst for the selective oxidation of saturated hydrocarbons (34). The unencapsulated complex when used for the oxidation of alkanes suffers from low turn over numbers which is due in part to irreversible dimerisation or oxidative degradation of the macrocycles. The inclusion of the complex in Y-zeolite (35) results in a catalyst which is 1000 times more active than the homogeneous catalysts. This particular complex was also applied for catalysing the mild oxidation of hydroquinone to benzoquinone(36). Selective aerobic oxidation of styrene as well as methanol have been performed over zeolite encapsulated complexes with good results (37,38). Highly active oxidation catalysts have been prepared by treating dehydrated NaY with a tetranuclear Cu(II) complex (39). Catalytic activity of zeolite encapsulated cobalt phthalocyanine have been reported for thiol oxidation (40). The activity of different zeolites were compared with carbon supports for the above reaction and it was found that the zeolite was more reactive than the usual carbon supports.

Zeolite encapsulated Cu(II) salen complex was found to be active in the oxidation of cyclohexanol (41). The encapsulated complexes also function as good

epoxidation catalysts. Well characterised vanadyl bis(bipyridyl) complexes encapsulated in NaY zeolite have been found to show good epoxide selectivity during oxidation of cyclohexane and cyclohexene with different peroxides (42). Bridged bis(2-pyridinecarboxamide) derived manganese complexes in NaY zeolites were used as catalysts for the epoxidation of olefins with H_2O_2 and t-BuOH (43). Iron and cobalt phthalocyanines encapsulated in zeolite Y effects the oxidation of cis-pinane to 2-pinane hydroperoxide (44). Adipic acid could be produced in high yield by the oxidation of cyclohexene with hydrogen peroxide in presence of manganese diimine catalysts in faujasite zeolites (45). A zeolite encapsulated complex of pyrazole was found to function as an effective catalyst for the oxidation of ascorbic acid (90).

Several encapsulated complexes have been found to function as efficient catalysts (18,46-49) for several other reactions like water gas shift reaction, carbonylation of methanol and aromatic compounds, hydroformylation and hydrogenation of alkenes. A manganese(salen)Cl₂ complex in NaY catalyzed the homologation of methanol in presence of CO and an iodate promoter at 30 atm CO and 150^oC to give dimethylether and acetic acid as the main products (50).

The examples given above are by no means complete nor exhaustive. Only the recent reports have been included to reflect the continuing interest in this field. Design of new zeolite metal complex supramolecules have been illustrated in the review by De Vos et al (51).

1.4 POLYMER SUPPORTED TRANSITION METAL COMPLEXES:

Immobilization of transition metal complexes on organic polymers has many real advantages and considerable potential for catalysis. The most obvious advantage is of course the experimental advantage of heterogeneity. A polymer bound catalyst can be used in a continuous processes in which the polymer bound catalyst is used as part of a fixed bed into which reactants enter and products exit. The flexibility of a

crosslinked polymer and, in turn, the extent of interaction between reactive sites on such a polymer can be controlled either by varying the extent of crosslinking in the polymer backbone or by changing the loading of catalyst species on the polymer.

In polymer bound metal complexes, the polymer bound ligand differ considerably from the simple ligands in their complexation behaviour due to a macroenvironment created at the center which causes steric, electrostatic, hydrophobic and conformational effects (52-54). In many catalytic reactions, the activity of the complex depends on the polymer backbone as well as on the metal complex (55). Further, the polymer bound metal complex has various degrees of accessibility to the substrate, and the catalytic process becomes comparable to that of a metalloenzyme like haemoglobin: In haemoglobin the protein bound haem is the active site and the protein part plays an important role by providing a hydrophobic environment and thus improving the catalytic activity (56).

Although various types of organic polymers have been chemically modified for use as catalyst precursors, divinylbenzene (DVB) crosslinked polystyrene has been the most widely used polymer (57). This particular polymer is easily derivatised either before or after polymerisation by unexceptional electrophilic aromatic substitution reactions. Furthermore, the physical restraints imposed by the polymer backbone on chemical reactivity of the attached complexes are also readily controllable by varying the percentage of DVB crosslinking reagent and the polymerization method. For example, rigid macroporous DVB crosslinked polystyrene possessing relatively large pores, whose size is not very solvent dependent or gel type microporous DVB crosslinked polystyrene for which access to interior catalyst sites is very solvent dependent are both readily available or can be readily prepared.

1.4.1 Procedure for anchoring a complex on a polymer support:

The immobilization procedures (57) involve functionalising the organic polymer so that it can bind the transition metal. In fact, virtually every imaginable type of ligand can be or have been incorporated into polymers. The diversity of types of ligands attached to organic polymeric surfaces has led to a corresponding diversity in terms of the type of polymer bound complexes.

1.4.2 Polymer anchored complexes -characterization:

Analytical data of the complexes gives an idea of its composition. Infrared spectroscopy is the most frequently used analytical procedure to characterize these complexes. It is particularly useful when the complex has a functional group like carbonyl. Techniques employed to elucidate the structure of simple metal complexes has been put to use in the case of polymer supported complexes also. These techniques include UV-Vis-near IR and EPR spectroscopic studies (58). Scanning electron microscopy can be used to detect the presence of the complex on the surface of the polymer (59).

1.4.3 Polymer anchored complexes - limitations:

In spite of all the modern techniques available, it would be difficult to determine the actual chemical structure of the metal complex species attached to the polymer. The determination of the distribution of the reactive species on the solid surface is also difficult. Further, there can be disadvantages associated with the polymer structures and the immobilization process. The possible reactivity of the polymer backbone to a particularly reactive catalyst, the physical diffusional restraints which complicate catalyst immobilization, or the hydrophobicity of the interior of organic polymers like polystyrene could impose chemical restraints on the type of species which could exist within the interior of a polystyrene matrix.

Potential experimental problems include the mechanical fragility of organic polymer systems and low thermal stability relative to inorganic supports like zeolites (57).

1.4.4 Polymer anchored complexes - applications:

The first example of catalysis by polymer metal complexes was presented by Lautsch et al. (60). Since then, a large number of reactions have been reported to be catalysed by polymer supported catalysts which include oxidation, hydrogenation, hydroformylation, decomposition of hydrogen peroxide, initiation of radical polymerization, asymmetric synthesis, optical resolution, etc.(61)

The progress made in the preparation and use of polymer supported complexes have been reviewed by several authors (9,61,62). Shuttleworth et al. has reviewed the progress made in the field of polymer supported complexes till 1997 (63). Benedetto and Karel (64) have presented a detailed review of the polymer supported catalysts and the reactions where they have replaced the conventional catalysts. A review (65) by Li Hong et al describes the effect of polymer supports on the activity and selectivity of metal complex catalyst for ring opening metathesis, polymerization of cycloolefins and metathesis, hydroformylation and selective hydrogenation of olefins.

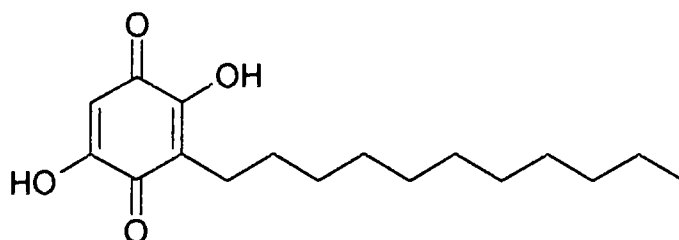
A polystyrene bound manganese(III) porphyrin has been found to act as an efficient catalyst for alkene oxidation by sodium periodate (66). Polymer supported $\text{PdCl}_2\text{-Co(OAc)}_2$ exhibits very high catalytic activity for the hydrodechlorination of organic chlorides under mild conditions (67). Polymer bound Pd catalysed cross coupling reactions of halides and triflates with organoboron compounds to form carbon-carbon bonds was achieved under mild conditions (68). Chemically and structurally designed chiral and macroporous matrices can be obtained upon aminolysis with enantiomerically pure amino acids of an activated ester functionality pendant from the backbone of precursor crosslinked copolymers (69). Polymer

bound triphenyl complexes of nickel, rhodium, ruthenium complexes (70,71) in hydrogenation reactions yielded excellent results. Polymer bound complexes are also reported to exhibit catalase like activity.

1.5 ROLE OF LIGANDS IN METAL COMPLEXES:

The metal centre of a complex is bound to coordinating ligands which may number as two or as many as six. These ligands exert a profound influence on the activity of the metal centre. Studies on metal complexes of biologically active ligands are important since they can sometimes be considered as models of the more complex biological systems (72-76). With this view, large number of metal complexes of biologically important ligands have been synthesized and studied.

Quinones and their substituted derivatives have long been known to possess a number of chemically and biologically significant properties with many important applications in several areas (77-79). Embelin (2,5-dihydroxy-3-undecyl-2,5-cyclohexadiene-1,4-dione) is a naturally occurring derivative of benzoquinone and is an orange pigment isolated from the berries of the Indian shrub *Embelia ribes*.

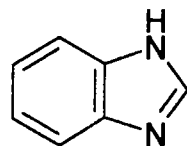


EMBELIN

This compound is of great medicinal importance. It possess antihelmintic(80), antifertility (81), analgesic (82), free radical scavenging (83) (antioxidant status) properties. Transition metal complexes of this ligand are

reported (84) to have a polymeric structure. However, very little is known about the activity of the metal complex.

Benzimidazoles are another group of molecules which play a significant role in determining the function of a number of biologically important metal complexes (85). A very large number of research papers have been published on transition metal complexes of benzimidazole derivatives. Reports are available on the applied aspects of these complexes such as their role in the protection of metal from corrosion, their use as antifungal, antibacterial, antiviral, and antifouling agents. A large number of papers also deal with the synthesis and structural studies of these complexes. Benzimidazoles and imidazoles as axial bases facilitate oxygen binding by haem iron (86-88).



BENZIMIDAZOLE

Such complexes can be considered as models for myoglobin. The oxygen binding constant is at least 3800 times greater for the imidazole compound than that for the pyridine analogue. The π donor ability of the imidazole ring is suggested as an explanation for its increased binding capacity (89).

1.6 SCOPE OF THE PRESENT INVESTIGATION:

Supported metal complexes have attracted wide attention due to their possible applications in catalysis. The properties of such complexes are very much dependent on the type of support and the type of ligands used. Ease of catalyst separation from the reaction products, higher selectivity of reaction and milder/ non-corrosive conditions have undoubtedly accelerated research in this area. The

synthesis and application of new, supported, metal complexes will enhance the interaction between homogeneous and heterogeneous catalysis. Moreover, the use of biologically important ligands in preparing supported metal complexes and the application of such complexes as catalysts might shed some light on the mechanism by which enzymes catalyze biological reactions. The present investigation has therefore been undertaken with the following objectives:

- (i) To synthesize and characterize a few supported transition metal complexes of biologically important ligands
- (ii) To determine the effect of the support on the structure and geometry of the complexes.
- (iii) To study the catalytic activity and thermal degradation characteristics of the supported complexes and thereby ascertain the influence of heterogenization on the above properties.

With these objectives, the zeolite encapsulated and polymer supported complexes of embelin and 2-aminobenzimidazole were synthesized and their catalytic activity was studied.

REFERENCES

- [1] J.E. Huheey; E.A. Keiter and R.C. Keiter, *Principles of Structure and Reactivity, Inorganic Chemistry*; IV Ed.; Harper and Collins, 1993.
- [2] R. Noyori, *Science*, **1990**, 248, 1194; **1992**, 258, 584.
- [3] G.J.K. Acres; G.C. Bond; B.J. Cooper and J.A. Dawson, *J. Catal.*, **1966**, 6, 139.
- [4] K.K. Robinson; F.E. Paulik; A. Hershman and J.E. Roth, *J. Catal.*, **1969** 15, 245.
- [5] W.A. Hermann and B. Cornils, *Appl. Homogeneous Catal. Organomet. Compd.*, **1996**, 2, 1167.
- [6] P. Peter and W. Stefan, *Appl. Homogeneous Catal. Organomet. Compd.*, **1996**, 2, 605-623 (CA: 127, 14, 190297p)
- [7] C. Guiezi; S. Giobilos and G. Palji; *J. Mol. Catal. A: Chem.*, **1996**, 107, 1-3.
- [8] Y.I. Yermakov; B.N. Kuznetsov and V.A. Zakharov, *In catalysis by metal complexes, Stud. Surf. Sci. Catal.* 1981, 8, 1.
- [9] D.C. Bailey and S.H. Langer; *Chem. Rev.*; **1981**, 81, 109.
- [10] R.A. Sheldon, *Curr. Opin. Solid State Mater. Sci.*; **1996**, 1 (1), 101.
- [11] R.A. Sheldon; I.W.C.E. Arends and H.E.B. Lempers, *Catal. Today*, **1998**, 41(1), 387.
- [12] N. Herron, *Chemtech.*, **1989**, 542.
- [13] Philip. C.H. Mitchell, *Chem. Ind.*, **1991**, 308.
- [14] P.G. Menon *In Lectures on Catalysis*, 41st Ann. Meeting, Ind. Acad. Sci., Ramasheshan Ed., 1975.
- [15] K.J. Balkus Jr and A.G. Gabrielov, *J. Inclusion Phenom. Mol. Recognit. Chem.*, **1995**, 21(1-4) 159.
- [16] C. Bowers and P.K. Dutta, *J. Catal.*, **1990**, 122.
- [17] N. Herron, *Inorg. Chem.*, **1986**, 25, 4714.

- [18] S. Kowalak; R.C. Weiss and K.J. Balkus Jr., *J. Chem. Soc. Chem. Commun.*, 1991, 57.
- [19] K.J. Balkus Jr; A.A. Welch and B.E. Gnade, *Zeolites*, 1990, 10, 122
- [20] K. Mizuno and J.H. Lunsford, *Inorg. Chem.*, 1983 22, 3484.
- [21] G. Meyer; D. Whorle; M. Mohl and G. Schulz Ekloff, *Zeolites*, 1984, 4, 30
- [22] K.J. Balkus Jr; C.D. Hargis and S. Kowalak, *Am. Chem. Soc. Symp. Ser.*, 1992, 499, 347.
- [23] K.J. Balkus Jr; S. Kowalak; K.T. Ly and C.D. Hargis, *Stud. Surf. Sci. Catal.*, 1991, 69, 93.
- [24] P.M. Edgardo; G. Nyole; L. Fabio; D.D. Acosta; P. Pasquale; G.L. Aldo; R. Patricio and D. Bernard, *J. Phys. Chem.* 1993, 97, 12819.
- [25] K. Mizuno; S. Imamura and J.H. Lunsford, *Inorg. Chem.*, 1984, 23, 3510.
- [26] P.K. Dutta and R.E. Zaykoski, *J. Phys. Chem.*, 1989, 93, 2603.
- [27] R.A. Schoonheydt and J. Pelgrims, *J.C.S. Dalton*, 1981, 914.
- [28] R.A. Schoonheydt; D.R. Wouwe; M.V. Hove; E.F. Vansant and J.H. Lunsford, *J. Chem. Soc. Chem. Commun.*, 1980, 33.
- [29] S.K. Tiwary and S. Vasudevan, *Inorg. Chem.*, 1998, 37, 5239.
- [30] R.F. Howe and J.H. Lunsford, *J. Phys. Chem.*, 1975 79, 17.
- [31] F. Bedioui; L. Roue; J. Devynck and K.J. Balkus Jr., *In Zeolite and Related microporous materials; Stud. Surf. Sci. Catal.*, 1994, 84, 917.
- [32] K.J. Balkus Jr; A.G. Gabrielov; S. L. Bell; F. Bedioui; L. Roue; and J. Devynck, *Inorg. Chem.*, 1994, 33, 67.
- [33] F. Bedioui; E.D. Boysson; J. Devynck and K.J. Balkus Jr, *J. Chem. Soc. Faraday. Trans.* 1991, 24, 87, 3831.
- [34] N. Herron; G.D. Stucky and C.A. Tolman, *J. Chem. Soc. Chem. Commun.*; 1986, 1521.
- [35] R.F. Parton; D.R.C. Huybrechts and P.A. Jacobs, *Stud. Surf. Sci. Catal.* 1991, 65, 110.
- [36] K. Lazar; A.N. Szeleezky; F. Notheisz and A. Zsigmond, *Stud. Surf. Sci. Catal.*, 1995, 94, 720.

- [37] S.P. Varkey and C.R. Jacob, *Ind. J. Chem.*, **1998**, 37A, 407.
- [38] S.P. Varkey and C.R. Jacob, *Ind. J. Chem.*, **1999**, 38A, 320.
- [39] T.A Fattah; D. Geoffrey; B.V. Romanovsky; L. S. Olga; A.N Larin; S.A. Jansen and M.J. Palmieri, *Catal. Today*, **1997**, 33,1-3, 313.
- [40] F. Thibault Starzyk; V. Mark; R.F. Parton and P.A. Jacobs, *J. Mol. Catal. A: Chem.*, **1996**, 109, 1, 75-99
- [41] R. Chandra; A. Murugkar; S. Padhye and S.A. Pardhy, *Ind. J. Chem.*, **1996**, 35A, 1-3
- [42] P.P. Knops Gerrits; C.A. Treijillo; B.Z. Zhan and P.A. Jacobs, *Top. Catal.*, **1996**, 3, 3-4, 437
- [43] P.P. Knops Gerrits; M. L'abbe and P.A. Jacobs, *Stud. Surf. Sci. Catal.*, **1997**, 108, 445.
- [44] A.A. Valente and J. Vital, *Stud. Surf. Sci. Catal.*, **1997**, 108, 461.
- [45] P.P. Knops Gerrits; F. Thibault Starzyk and P.A. Jacobs, *Stud. Surf. Sci. Catal.*, **1994**, 84, 1411.
- [46] P.A. Jacobs; R. Chantillon; P. Dhaet; J. Verdonek and M. Tilem, *ACS.Symp. Ser.*, **1983**, 218, 439.
- [47] A. Auroux; V. Bolis; P. Wierzchowski; P. Gravelle and J. Vedrine *J. Chem. Soc. Faraday Trans.*, **1979**, 2, 75, 2544.
- [48] M. Iwamoto; H. Kusano and S. Kagawa, *Inorg. Chem.*, **1983**, 22, 3366
- [49] E. Mantovani; N. Palladino and A. Zarrobi, *J. Mol. Catal.*, **1977**, 3, 285.
- [50] S.B. Halligudi; S. Samant; D. Chatterjee; D.B. Shukla and R.S. Somani, *Stud. Surf. Sci. Catal.*, **1998**, 113, 841.
- [51] D.E. De Vos; F. Thibault Starzyk; P.P. Knops Gerrits; R.F. Parton and P.A. Jacobs, *Macromol. Symp.*, **1994**, 157.
- [52] M.N. Hughes, *The Inorganic Chemistry of Biological Processes*, 2nd ed. 1981, Wiley, Chichester.
- [53] R.W. Hay, *Bioinorganic Chemistry*, 1984, Horwood; England.
- [54] G.L. Eicchorn Ed., *Inorganic Biochemistry*; Elsevier; Amsterdam.

- [55] E.W. Neuse; *Encyclopedia of Polymer science and Technology*, 8, 1968, Interscience; NewYork.
- [56] M.M. Taqui Khan *In Lectures on Catalysis*, 41st Ann. Meeting Ind. Acad. Sci., S. Ramasheshan Ed., 1975.
- [57] D.E. Bergbreiter *In Chemically Modified Surfaces in Catalysis and Electrocatalysis*; ACS Symp. Ser. 192., J.S.Miller Ed.; 1982.
- [58] A. Syamal and M.M. Singh, *Ind. J. Chem.*, **1998**, 37A, 350.
- [59] J.N. Shah; D.T Gokak and R.N. Ram, *J. Mol. Catal.*, **1990**, 60, 141.
- [60] W. Lautsch; W.Rothkegel; W.Brosler; W.Baidermann; V.Doering and H. Zoschke, *J. Polym. Sci.* **1952**, 8, 191; 17 (1955) 479.
- [61] E. Tsuchida and H.Nishide, *Advances in Polymer Science*, **1977**, 24.
- [62] (a) A. Akelah and D.C.Sherrington, *Chem. Rev.*, **1981**, 557 (b) A. Akelah and D.C Sherrington, *Polymer*, **1983**, 24, 1369.
- [63] S.J. Shuttleworth; S.M.Allin and P.K.Sarma, *Synthesis*, **1977**, 1217.
- [64] C. Benedetto and J. Karel, *Chem. Ind.*, **1996**, 78, 563.
- [65] Li Hong and Hi Bingleue, *Chin. J. Polym. Sci.*, **1998**, 16(4), 362.
- [66] S. Tangestaninjad and V. Mirkhani, *J. Chem. Res. Synop.*, **1998**, 12, 788.
- [67] Li Haiqing; Liao Shyij Xu and Yun Yu Daorang, *Synth. Commun.*, **1997**, 27(5), 825.
- [68] Jang Su Bum, *Tetrahedron Lett.*, **1997**, 38(10),1793.
- [69] M. Boaro; B. Corain and K. Jerabek, *J. Mol. Catal. A. Chem.*, **1996**, 109(2).
- [70] C.U. Pittman Jr; L.R. Smith and R.M. Hames, *J. Am. Chem. Soc.*, **1975**, 97, 7
- [71] W.O. Haag and D.I. Whitehurst, *In Proc. V. Int. Congr. Catal.*, Miami Ed., J.W. Hightower Abstrc. 29 1972.
- [72] N. Farrell; D. Dolphin and B.K. James, *J. Am.Chem. Soc.*, **1978**, 100, 324.
- [73] W.S. Brinagar; C.K. Chang; J. Geibel and T.G. Traylor, *J. Am. Chem. Soc.*, **1974**, 102, 5597.
- [74] F. Basolo; B.M. Hoffman and J.A. Ibers, *Acc. Chem. Res.*, **1975**, 8, 384.
- [75] J.C. Stevens; P.J. Jackson; W.P. Schammel; G.C. Christoph and D.H. Busch, *J.Am. Chem. Soc.*, **1980**, 102, 3283.

- [76] J.P. Collman and K.S. Sushik, *Pure Appl. Chem.*, **1978**, 50, 951.
- [77] R.A. Morton Ed., *Biochemistry of Quinones*, Academic Press, New York, 1965.
- [78] R.H. Thomson, *Naturally occurring Quinones*, Academic Press, New York, 1971.
- [79] S. Patai, *The Chemistry of Quininoid Compounds, Part II*, Wiley, London, 1974.
- [80] L.F. Fieser and E.M. Chamberlin, *J. Am. Chem. Soc.*, **1948**, 70, 71.
- [81] V.P. Dixit and P. Khanna, *Indian Patent 144370*, **1978** {CA (2: 82417c)}.
- [82] C.K. Atal; M.A. Siddiqui; Z. Usha; V. Amla; R.K. Johri; R.G. Rao and S.J. Kour, *Ethnopharmacol.*, **1984** 309. {CA 101: 183865}.
- [83] M. Chitra; C.S. Devi Syamala and E. Sukumar, *Filoterapia*, **1994**, 65(4), 317.
- [84] K.K.A. Rashid; J. Chacko and P.N.K. Nambisan, *Polyhedron*, **1983**, 2, 293.
- [85] P. N. Preston, *Chem. Rev.* **1974**, 74
- [86] J.F. Drake and R.J.P. Williams, *Nature*, **1958**, 182, 1084.
- [87] A.H. Corwin and Z. Reyes, *J. Am. Chem. Soc.*, **1956**, 78, 2437.
- [88] A.H. Corwin and S.D. Bruck, *J. Chem. Soc.*, **1958**, 80, 4736.
- [89] C.R. Chang and T.G. Traylor, *J. Am. Chem. Soc.*, **1973**, 95, 8475.
- [90] K.K.M. Yusuff and J. Mathew, *Ind. J. Chem.*, **1998**, 36A, 303.
- [91] R. Sreekala and K.K.M. Yusuff, *Ind. J. Chem.*, **1995**, 34A, 994.
- [92] R. Krishnan and S. Vancheesan, *Stud. Surf. Sci. Catal.*, **1998**, 113, 845.

CHAPTER II

EXPERIMENTAL TECHNIQUES

This chapter gives a brief account of the general reagents used and the various analytical and physicochemical techniques employed for the characterisation of the ligands and the supported complexes. Procedural details regarding the synthesis of the complexes and their activity studies are given in the appropriate chapters.

2.1. REAGENTS

The following metal salts were used: $\text{MnCl}_2 \cdot 4\text{H}_2\text{O}$ (E. Merck, GR), $\text{CoCl}_2 \cdot 6\text{H}_2\text{O}$ (E. Merck, GR); FeCl_3 anhydrous (Qualigens); $\text{NiCl}_2 \cdot 6\text{H}_2\text{O}$ (BDH, GR); $\text{CuCl}_2 \cdot 2\text{H}_2\text{O}$ (E. Merck, GR).

2-Aminobenzimidazole (E. Merck, GR) was used as one of the ligands. The berries of embelia ribes used for the extraction of embelin was purchased from the local market.

Synthetic Y-type zeolites were obtained from United Catalysts India Ltd., Baroda. Chloromethylated polystyrene beads of 200-400 mesh size, crosslinked with 2% divinylbenzene and containing 12.9% chlorine (Fluka) were used in the present study.

Hydrogen peroxide (30% aqueous solution) used for the kinetic studies was the product of E. Merck and was used as such.

2.2. MODIFICATION OF SUPPORTS

2.2.1 Zeolites:

The synthetic Y type zeolites was stirred in 0.1M solution of sodium chloride for 24 hours to convert any other ions, if present, to Na⁺ ion. After stirring, the zeolite was filtered and washed several times with deionised water until the filtrate was free of chloride ions. It was then dried in an air oven for one hour and stored for further use.

The incorporation of metal ions into the zeolite matrix is a prerequisite for encapsulation of metal complexes in the zeolite cages by the flexible ligand method. Zeolites have a remarkable ability for ion exchange. The sodium ions can be replaced with monovalent, bivalent or trivalent ions. For the introduction of Mn²⁺, Co²⁺, Ni²⁺ and Cu²⁺ ions, zeolite Y (2.5g) was stirred in a 0.01M solution of the respective metal chloride at 70⁰C for 4 hours. It was then filtered and dehydrated at 400⁰C for 2 hrs. The pH of the metal salt solution was adjusted to be between 4.0 and 4.5, as aluminium ions are removed from the lattice at pH below 4 and the structural framework will collapse (1). The Fe³⁺ ion was introduced into the lattice with a very dilute solution of ferric chloride (0.0025M), as dealumination takes place at high concentrations.

2.2.2. Polystyrene

The polymer support should contain proper functional groups for anchoring the ligand or metal complex. Hence, chloromethylated polystyrene was functionalised with amino and aldehydic groups respectively, the procedures of which are given below.

Preparation of Aminomethylpolystyrene (2):

Chloromethylpolystyrene (11.0g) was suspended in 200ml of DMF and hexamethylenetetramine (11.2g) and potassium iodide (13.28g) were added to this suspension. This solution was heated with stirring under reflux at 100⁰C in an oil bath for 10 hours. The resin was filtered and washed with 6N hydrochloric acid and water. It was then stirred with a solution of NaOH (10%, 150ml) for 2 hrs, filtered, washed several times with water and methanol (50ml×3min×4 times) and dried in vacuum to constant weight. A test portion of the resin on heating with ninhydrin reagent (12ml) gave a deep blue colour.

Preparation of Aldehyde Resin

The polymer bound benzaldehyde was prepared according to the following procedure (3). A mixture of chloromethylpolystyrene (20.0g), dimethylsulphoxide (300ml) and sodium bicarbonate (19.0g) was stirred at 138-140⁰C for 12 hours. The resultant resin was filtered, washed with hot ethanol, methylene chloride and benzene and dried in vacuo over anhydrous calcium chloride.

2.3. PREPARATION OF THE LIGANDS

2.3.1. Extraction of embelin

Pure natural embelin was prepared by the method of Fieser and Chamberlin (4). The sun dried berries of embelia ribes were partially crushed to remove the outer crust and extracted with solvent ether in a soxhlet extractor. The crude embelin thus isolated was purified by defatting twice with petroleum ether (60-80⁰C) and recrystallising twice from absolute alcohol. Pure natural embelin was obtained in 2% yield.

2.3.2. Preparation of Schiff base with the polymer bound aldehyde and 2-aminobenzimidazole:

The following procedure (5) was adopted for the condensation. Polymer bound benzaldehyde (10.0g) was swollen in dioxan (50ml) for 24 hours. Afterwards dioxan was decanted off and 2-aminobenzimidazole (4.0g) in absolute ethanol was added. This mixture was refluxed on a water bath for ten hours. The polymer bound Schiff base was filtered, washed several times with dioxan and ethanol and dried in vacuo over anhydrous calcium chloride.

2.3.3. Preparation of Schiff base with polymer bound amine and embelin

The polymer bound amine was swollen with dioxan as described above. After decanting the solvent, embelin (6.0g) dissolved in ethanol was added and the mixture was refluxed for 10-12 hours on a water bath. It was then filtered, washed and dried as described in the above case.

2.4. ANALYTICAL METHODS

2.4.1. Analysis of the zeolite samples for Si, Al, Na and transition metal ions by the complete dissolution method:

The dried zeolite sample was accurately weighed ('x' g) and transferred to a beaker. Conc. sulphuric acid (about 40ml) was added and heated until SO₃ fumes were evolved. It was diluted with water (200ml) and filtered through an ashless filter paper (filtrate A). The residue was dried at 1000⁰C in a platinum crucible, cooled and weighed ('a' g). Hydrofluoric acid (10ml) was then added and evaporated carefully and finally ignited to 1000⁰C ('b' g). The percentage of silica (SiO₂) was calculated using the equation

$$\%SiO_2 = \frac{(a-b)}{x} \times 100$$

Potassium persulphate was added to this residue and heated until a clear melt was obtained. The melt was dissolved in water and this solution was combined with filtrate A. The sodium, aluminium and transition metal ions in this solution were determined by atomic absorption spectroscopy (AAS). The unit cell formula of the zeolite was calculated from the Si/Al ratio (δ).

2.4.2. Analysis of the polymer samples for metal:

The organic part of the polymer samples was completely eliminated before estimation of the metal. This was done by treating the complex with aqua regia for 24 hrs. at 100°C. The resulting solution was filtered and the metal ion concentration in the solution was determined by atomic absorption spectrophotometry.

2.4.3 C H N analyses:

Microanalyses for carbon, hydrogen and nitrogen in the polymer as well as in the zeolite samples were done at Regional Sophisticated Instrumentation Centre, IIT Chennai, Central Drug Research Institute, Lucknow or Central Salt and Marine Chemicals Research Institute, Bhavanagar.

2.4.4. Estimation of Chlorine:

Chlorine in the samples was analyzed by the Volhard's method (7). The polymer supported samples were digested with pyridine for two hours at 100°C. The mixture was then quantitatively transferred to a conical flask containing 50% acetic acid (30ml) and concentrated nitric acid (5ml). To this solution standard silver nitrate solution was added with stirring, and this mixture was allowed to stand for 5 minutes. Afterwards, about 50ml of water was added to this followed by 5 ml of toluene. The solution was mixed thoroughly using a stirrer. The unreacted silver nitrate was determined by titration with standard thiocyanate solution.

2.5. PHYSICO-CHEMICAL METHODS

2.5.1. *Magnetic Susceptibility Measurements.*

Magnetic susceptibility measurements were done at room temperature on a simple Guoy balance. Due to the lack of facilities, variations of magnetic susceptibility with temperature could not be studied. The Guoy tube was standardised using $[\text{HgCo}(\text{CNS})_4]$ as recommended by Figgis and Nyholm (8). The effective magnetic moment was calculated using the equation,

$$\mu_{\text{eff}} = 2.84 (\chi_{\text{M}}^{\text{corr}} T)^{1/2} \text{ BM}$$

where T is the absolute temperature and $\chi_{\text{M}}^{\text{corr}}$ is the molar susceptibility corrected for diamagnetism of the atoms in the complex using Pascals constants.

2.5.2. *Surface Area Analyses*

Surface area of the samples were measured by multipoint BET method using a Micromeritics Gemini 2360 surface area analyzer. Nitrogen gas was used as the adsorbate at liquid nitrogen temperature.

2.5.3. *Infrared spectra:*

Infrared spectra of the ligands and supported complexes in the region 4600-400 cm^{-1} were taken by the KBr pellet technique using Shimadzu 8000 Fourier Transform Infrared Spectrophotometer (FT). Through FT analysis the background spectrum of the support could be subtracted and thus, the species present in low concentrations could be identified.

2.5.4. Optical Spectra:

The optical spectra of the zeolite samples were recorded on a Cary Win spectrophotometer in the diffuse reflectance mode at Regional Sophisticated Instrumentation Centre, Indian Institute of Technology, Chennai. The spectrum was plotted as percentage reflectance versus wavelength. A Kubelka-Munk (9,10) analysis was performed on the reflectance data. The Kubelka-Munk factor, $F(R)$ is given by

$$F(R) = (1-R)^2 / 2R = k/s$$

where R is the diffuse reflectance of the sample as compared to the standard, k is the molar absorption coefficient and s is the scattering coefficient of the sample. The standard used in this case was MgO .

Electronic spectra were also recorded in the absorption mode for the polymer supported complexes using a Shimadzu 200 UV-Vis spectrophotometer by the mull technique following a procedure recommended by Venanzi (11). The procedure is briefly described below.

Small filter paper strips were impregnated with a paste of the sample in nujol. This paper strip was placed over the entrance to the photocell housing in the sample cell holder. A nujol treated paper strip of similar size and shape was used as the blank.

2.5.5. EPR:

The EPR spectra of the powdered samples were recorded at liquid nitrogen temperature using a Varian E-109 X/Q band spectrophotometer. The g values were determined relative to tetracyanoethylene (TCNE, $g = 2.0027$). μ_{eff} values were also determined from the EPR parameters by substituting g_{\perp} and g_{\parallel} in the following equation (12)

$$\mu_{\text{eff}}^2 = g_{\parallel}^2/4 + g_{\perp}^2/4 + 3kT/\lambda_0 (g-2)$$

where λ_0 is the spin orbit coupling constant for the free metal ion.

The density of unpaired electrons at the central atom can be computed (13) from the equation

$$\alpha_{\text{Cu}}^2 = (A_{\parallel}/P) + (g_{\parallel} - 2) + 3/7(g_{\perp} - 2) + 0.04$$

where $1-\alpha^2$ measures the covalency associated with the bonding of metal ion to the ligand and $P = .036\text{cm}^{-1}$.

2.5.6 XRD:

In the present study the parent zeolite and the zeolite encapsulated complexes were analyzed by powder X-ray diffraction for comparing their crystallinities. The X-ray diffractometer used in the present investigation is Rigaka D-Max C. Measurements were done with a stationary X-ray source, Ni filtered Cu $K\alpha$ radiation ($\lambda=1.5404$) and a movable detector which scans the intensity of the diffracted radiation as a function of the angle 2θ between the incident and diffracted beams.

2.5.7 SEM:

The morphology of the samples were examined by scanning electron microscopy at Sree Chitra Thirunal Institute of Medical Science and Technology, Thiruvananthapuram.

2.5.8 TG:

The thermogravimetric analyses were done on a Shimadzu TGA-50 or on a TGA.V5.1A DuPont 2000 at a heating rate of $20^{\circ}\text{C min}^{-1}$ in an inert atmosphere using a Pt crucible. The mass of the samples used were in the range 2-8mg.

2.5.9 GC:

The catalytic activity studies were performed with a Chemito 8510 Gas Chromatograph (Spherocarb column) equipped with a thermal conductivity detector. The gas chromatograph was connected to a microcatalytic reactor.

REFERENCES

- [1] P.G. Menon *In Lectures on Catalysis*, 41st Ann. Meeting, Ind. Acad. Sci., S. Ramasheshan Ed.; 1975.
- [2] K.S. Devaki and V.N.R. Pillai, *Eur. Polym. J.*, **1988**, 24, 209.
- [3] J.M.J. Frechet and K.E. Haque, *Macromolecules*, **1975**, 8, 130.
- [4] L.F. Fieser and E.M. Chamberlin, *J. Am. Chem. Soc.*, **1948**, 70, 71.
- [5] K.K.M. Yusuff and R. Sreekala, *J. Polym. Sci. Chem. Ed.*, **1992**, 30, 2595.
- [6] C. Tollman and N. Herron, *Symposium in Hydroc. Oxidation*, 194th National Meeting of the Am. Chem. Soc. , New Orleans, LA, Aug. 30-Sept. 4, 1987.
- [7] A.I. Vogel, *A Text Book of Quantitative Inorganic Analysis*; Longmans-Green, London, 1978.
- [8] B.N. Figgis and R.S. Nyholm, *J. Chem. Soc.*, **1958**, 4190.
- [9] H.G. Hecht In *Modern Aspect of Reflectance Spectroscopy*; W.W. Wendlandt Ed.; Plenum Press, New York, 1968.
- [10] S.K. Tiwary and S. Vasudevan, *Inorg. Chem.*, **1998**, 37, 5239.
- [11] G. Dyer, J.G. Hartley and L.M. Venanzi, *J. Chem. Soc.*, **1965**, 1293.
- [12] B.V. Agarwala, *Inorg. Chim. Acta*, **1979**, 36, 209.
- [13] D. Kivelson and R. Neiman, *J. Chem. Phys.*, **1961**, 35, 149.

CHAPTER III

STUDIES ON TRANSITION METAL COMPLEXES OF EMBELIN AND 2-AMINOBENZIMIDAZOLE IN ZEOLITE Y

INTRODUCTION

There is a growing interest in synthesizing novel zeolite encapsulated complexes and in utilizing them in the fields of catalysis, gas purification etc., The isolation of metal complexes in the cages and the influence of the zeolite architecture on the structure of the complexes hold a lot of promise in the above fields. These factors prompted us to synthesize a few encapsulated complexes of the transition metal ions Mn(II), Co(II), Fe(III), Ni(II) and Cu(II) with two biologically important ligands viz., embelin (2,5-dihydroxy-3-undecyl-2,5-cyclohexadiene-1,4-dione) and 2-aminobenzimidazole. These molecules coordinate to the metal ions in the zeolite resulting in the formation of encapsulated complexes. The ligands are reported to augment the oxygen binding capacity of the metal ions (*1*) and hence the complexes may be presumed to behave as ideal catalysts for oxidation reactions.

Studies on the preparation and characterization of the zeolite encapsulated complexes of embelin and 2-aminobenzimidazole are presented in this chapter. Elemental analysis, FTIR, electronic (absorption and diffuse reflectance) and epr spectral studies; magnetic susceptibility measurements; TG; surface area analyses and X-ray diffraction studies were used in understanding the presence, composition and structure of the complexes. This chapter is divided into two sections. The first section includes the studies on the complexes of embelin, while the second section comprises the preparation and characterization of the complexes of 2-aminobenzimidazole.

3.1. STUDIES ON THE TRANSITION METAL COMPLEXES OF EMBELIN ENCAPSULATED IN ZEOLITE NaY.

Zeolite encapsulated complexes of embelin with the metal ions Mn(II), Fe(III) Co(II), Ni(II), and Cu(II) were prepared and characterised by the different physicochemical techniques. A detailed discussion of these aspects is presented in this section.

3.1.1 EXPERIMENTAL

3.1.1.1 Materials:

The metal salts used for the preparation of the complexes are listed in chapter II. The preparation of the ligand embelin is also described therein.

3.1.1.2 Preparation of the complexes in NaY:

The transition metal complexes of embelin were entrapped in the cavities of the zeolite by the flexible ligand method (2). The ligand was entrapped either by simply refluxing a mixture of embelin and the metal ion-exchanged zeolite in methanol for several hours or by sealed heating. The metal exchanged zeolite (about 1g) was introduced into a round bottomed flask containing embelin (~0.1g) dissolved in methanol and was refluxed for 4-6 hrs. In the sealed heating procedure the metal ion exchanged zeolite (1g) is mixed with embelin (~0.1 g). This mixture was taken in a glass tube, sealed and heated to 130⁰C for 2 hrs. The encapsulated complexes thus obtained were further purified by soxhlet extraction with methanol and then with acetone for 48-72 hrs. This exhaustive extraction process is meant to remove the complexes formed on the surface. Uncomplexed metal ions remaining in the zeolite were removed by back exchange of the zeolite with NaCl (0.01M) solution for 12 hrs. It was then washed with hot water to remove chloride ions and then dried in vacuum

dried in vacuum over anhydrous calcium chloride. Scanning electron microscopy of a representative complex (Fig. III.1) before and after the soxhlet extraction indicates that the material formed on the external surfaces can be removed by soxhlet extraction. Once formed the internally confined species are too large to be extracted

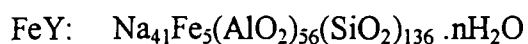
3.1.1.3 Preparation of a Reaction Blank.

A reaction blank was prepared by reacting zeolite NaY (1.0g) with embelin (1.0 gm) following the same preparation and purification procedures described above. Most of the ligand did escape on filtration and on further washing and purification, the solid turned colourless indicating the complete removal of the ligand (which was confirmed by infrared spectroscopic studies).

3.1.2 PHYSICOCHEMICAL CHARACTERIZATION:

3.1.2.1 Elemental Analysis:

Details regarding the elemental analyses of the samples are given in chapter II. The results of the elemental chemical analysis are presented in Table III.1. Elemental analyses reveal a Si/Al ratio of 2.4 for NaY that corresponds to a unit cell formula, $\text{Na}_{56}(\text{AlO}_2)_{56}(\text{SiO}_2)_{136} \cdot n\text{H}_2\text{O}$ for NaY(3). The following unit cell formulae have been calculated for the metal exchanged zeolites using the elemental analyses data.



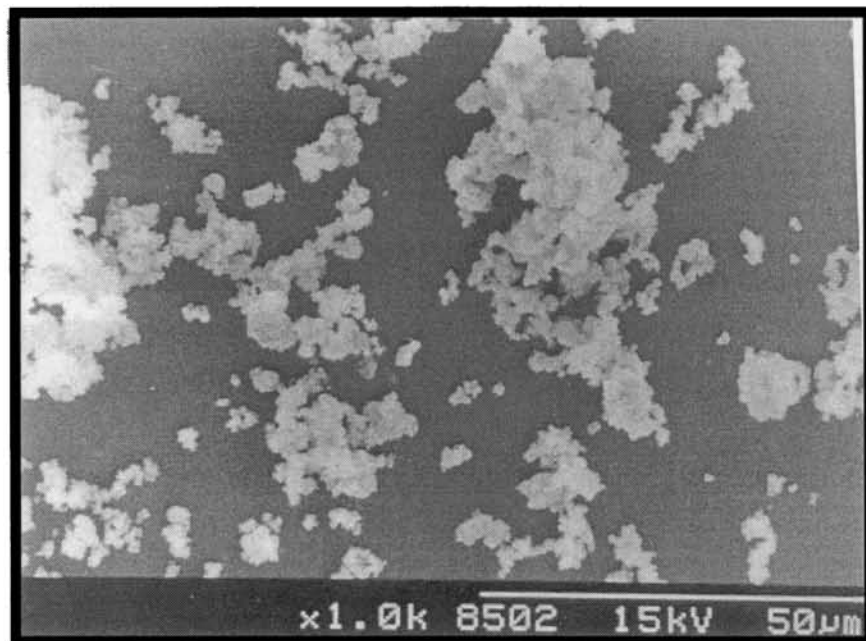
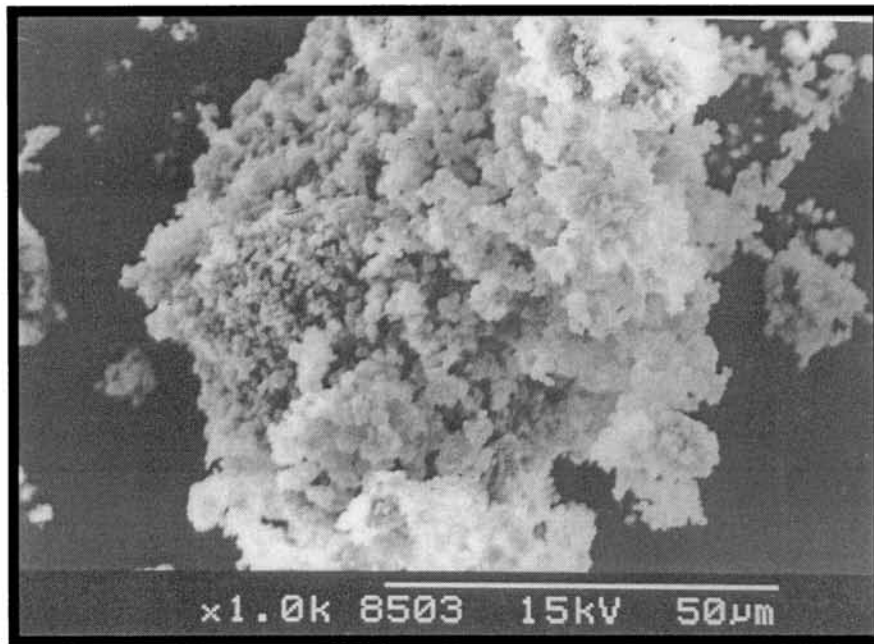


*Fig. III. 1 Scanning Electron Micrograph of YCuEm
(a) before soxhlet extraction (b) after soxhlet extraction.*

TABLE III.1*Analytical data of the Zeolite encapsulated complexes of Embelin*

Sample	Elements (%)				
	Si	Al	Na	Metal	C
NaY	22	8.7	7.4		
MnY	20.7	8.2	3.74	3.8	
YMnEm	20.5	8.1	5.2	2.06	7.65
FeY	20.6	8.2	5.7	1.5	
YFeEm	22	8.7	6.6	0.9	3.52
CoY	20.7	8.2	5.5	1.92	
YCoEm	22	8.75	6.0	1.8	6.5
NiY	20.4	8.1	3.6	4.23	
YNiEm	19.2	7.6	3.7	3.54	8.2
CuY	20.85	8.24	3.26	5.2	
YCuEm	22	8.7	3.96	4.7	1.95

3.1.2.2 Surface Area Analysis:

Surface area analyses of the zeolite samples determined by the BET method are presented in Table III.2. The parent zeolite, zeolite NaY has a surface area of 509 m²/g. The results indicate that there is only a small decrease in surface area of the zeolite as a result of metal exchange. However, the surface area of the zeolites after the encapsulation of the complexes are significantly low. This large reduction in surface area could be interpreted as due to the formation of compounds in the cavities of the zeolite. Such extent of reductions in surface area of zeolites due to inclusion of metal complexes in the pores has been reported by Balkus and Gabrielove (2). There are reports on the reductions in surface area of NaY zeolite from 699 m²/g to 378 m²/g as a result of the encapsulation of the cobalt phthalocyanine (4). The surface area reported for MnCl₄ salen-X and MnBr₄ salen-X was 133 m²/g and 71 m²/g respectively, which is very much lower (5) when compared to that of the zeolite (690 m²/g)

3.1.2.3 Magnetic susceptibility measurements:

The magnetic susceptibility of the metal ion exchanged zeolites and the zeolite encapsulated complexes were measured at room temperature by Guoy method. Magnetic measurements of the zeolite samples are usually done by the Faraday method (6). Due to the lack of facilities we could not measure the magnetic susceptibility by this method; and hence, an attempt has been made to get a qualitative idea of the magnetic behavior of the prepared samples by the Gouy method. The unit cell formula computed earlier was used for the calculation of magnetic moment values. Diamagnetic and paramagnetic (due to iron impurities) contributions of the zeolite frame work were subtracted from the values obtained. For this purpose, the susceptibility of the parent zeolite, NaY, was measured directly. In the case of the encapsulated complexes the diamagnetic contribution of the ligand part was also taken into account. In almost all the cases conclusions arrived from the μ_{eff} values (Tables III.4 & III.5) nearly agree with those from the other experimental results.

TABLE III.2

Surface area of the ion exchanged zeolites and zeolite encapsulated complexes of embelin

Sample	BET Surface area (m ² /g)
NaY	507
MnY	480
YMnEm	267
FeY	470
YFeEm	266
CoY	482
YCoEm	340
NiY	478
YNiEm	315
CuY	492
YCuEm	370

Manganese(II) complex:

A room temperature magnetic moment of 6.0 B.M is observed for the manganese(II) complex of embelin in NaY (YMnEm). This value is very close to the spin only value of 5.92 B.M. Complexes of divalent manganese are known both in high spin ($S = 5/2$) and low spin ($S = 1/2$) configurations. The high spin complexes are expected to exhibit magnetic moments very close to the spin only value (for a d^5 ion) independent of temperature and irrespective of whether the ligand arrangement is of octahedral, tetrahedral or lower symmetry. Room temperature magnetic moments in the range of 5.7 - 6.0 B.M have been reported for a large number Mn(II) complexes in the octahedral geometry (7). Hence the observed moment of 6.0 B.M indicates an octahedral geometry for the metal ion. An octahedral geometry around Mn(II) ion is indicated for the manganese(II) exchanged zeolite (MnY), as it exhibits a μ_{eff} value of 5.8 B.M.

Iron(III) complex:

The iron(III) complex exhibits a value of 5.9 B.M. The free ion ground state is S^6 for iron(III) which becomes 6A_1 in a weak ligand field. Ions with a 6A_1 ground state will not have any orbital contribution to the magnetic moment. Magnetic moment values in the range 5.7 to 6 B.M are frequently observed for Fe(III) complexes irrespective of whether the ligand arrangement is in an octahedral or tetrahedral fashion (8,9). Hence, it is not possible to distinguish between tetrahedral and octahedral symmetry on the basis of magnetic moments alone.

A magnetic moment of 5.8 B.M is observed for the Fe(III) exchanged zeolite which also falls in the range of values expected for an Fe(III) octahedral high spin complex.

Cobalt(II) complex:

The magnetic moment obtained for the cobalt(II) complex in NaY (YCoEm) is about 5.5 B.M. This is much higher than the spin only value of 3.89 B.M for 3 unpaired electrons. In the case of high spin octahedral cobalt(II) complexes (d^7 ion) a large orbital contribution to the magnetic moment is expected because of the three fold orbital degeneracy of the ${}^4T_{1g}$ ground state. Mixing of a singlet excited state lowers the moment but generally values ranging from 4.7 to 5.2 B.M are expected. Magnetic moments in the range 4.7 to 5.2 B.M have been reported for a large number of octahedral complexes (8,9). Thus it seems that the cobalt complex (YCoEm), might probably be in an octahedral configuration.

A magnetic moment value of 4.3 B.M is obtained for the Co(II) exchanged zeolite (CoY). Values in the range 4 - 4.6 B.M have been reported for dehydrated CoY. Based on the magnetic measurements Egerton and coworkers (10) concluded that on dehydration Co^{2+} species which exist as octahedral aquo complexes in the large cavities migrates to the sodalite units and attains a tetrahedral geometry.

Nickel(II) complexes:

The nickel(II) complex of embelin in NaY Zeolite (YNiEm) exhibits a μ_{eff} value of 3.4 B.M. This value is higher than the spin only value of 2.83 B.M for 2 unpaired electrons. The d^8 ion in an octahedral environment has a ground state electron configuration of $t_{2g}^6 e_g^2$. In this configuration, the orbital angular momentum will be quenched and the μ_{eff} value should be close to the spin only value of 2.83 B.M. However, the first excited triplet state ${}^3T_{2g}$ having the configuration $t_{2g}^5 e_g^3$ offers 3 possible ways of arranging the five t_{2g} electrons while retaining the rotational properties of d_{yz} and the d_{xz} orbitals with respect to the z axes. This level has therefore an orbital angular momentum and the spin orbital coupling of nickel(II) is large enough to allow mixing of this level with the lowest level to produce the true

ground state. Therefore the orbital angular momentum is not completely quenched by the ligand field, and magnetic moments normally found for the octahedral complexes of nickel(II) are in the range 2.9 to 3.3 B.M (11).

In tetrahedral fields, large orbital contributions to the magnetic moment are expected because of the three fold degeneracy of the 3T_1 ground state. Magnetic moments in the range 3.7 to 4.1 B.M are frequently observed for the tetrahedral complexes of nickel(II) (9,11). Square planar complexes of nickel(II) are usually diamagnetic. The above factors when taken into account indicate that YNiEm has an octahedral structure.

A μ_{eff} value of 3.1 B.M is observed for the nickel(II) exchanged zeolite Y (NiY) which indicates an octahedral geometry around nickel(II) ion.

Copper (II) complex:

A value of 1.9 B.M has been calculated from the observed susceptibility for the embelin complex (YCuEm). Copper(II) complexes in general have μ_{eff} values ranging between 1.75 to 2.2 B.M. Magnetic moments, strictly, cannot be used to identify the stereochemistry of the copper(II) complexes. However, lower magnetic moments are frequently attributed to square planar configurations, whereas higher values indicate increasing distortion from planar configuration. The value observed for the embelin complex could be due to a tetrahedral distortion from planar geometry (9).

The copper (II) exchanged ZeoliteY (CuY) also exhibits a moment around 1.9 B.M This can also be interpreted as due to a slight distortion from the planar configuration.

3.1.2.4 Infrared spectra:

The IR spectra is the most often used technique that gives an indication as to whether the complex formation has taken place. In the case of zeolite encapsulated complexes several workers have confirmed the formation of metal complexes inside the zeolite matrix by a comparison of the infrared spectra of the simple complexes with that of the encapsulated ones (4). A comparison of the spectra of the simple and the encapsulated complex (Fig's III.3-III.7) reveals a similarity between these complexes.

The IR spectral data is given in table III.3. The ligand embelin has a strong infrared absorption at 1610 cm^{-1} (Fig. III.2) which is due to the C=O stretching of the carbonyl group of embelin (12). In this type of ligands coordination of the carbonyl oxygen to the metal is indicated by a shift of C=O stretching frequencies to lower values. In the case of the zeolite encapsulated complexes this band is shifted to 1526 cm^{-1} for the Mn(II) complex, to 1537 cm^{-1} for the Fe(III) complex, to 1520 cm^{-1} for the Co(II) complex, to 1512 cm^{-1} for the Ni(II) complex and to 1460 cm^{-1} for the Cu(II) complex. A similar shift in frequency has been observed for the corresponding free metal complexes of embelin (13). The Cu(II) complex of 2,5 dihydroxy-1 - 1,4 benzoquinone also exhibits a similar shift for the carbonyl stretching frequency (14).

The extent of shifting of the carbonyl frequency is generally regarded as an indication of the metal-oxygen bond strength. The lowering of the -C=O stretching frequency upon coordination has been compared for the chelate polymers of various dihydroxyquininoid ligands (15). The Cu(II) complex of 2,5- dihydroxy-1,4-benzoquinone exhibited the lowest carbonyl frequency among this group. The carbonyl frequency is decreased by about 150 cm^{-1} in the copper(II) complex; whereas for the other metal complexes it is lowered only by 90 cm^{-1} . Hence, the copper(II) complex can be regarded as having the maximum strength for its metal-oxygen bond.

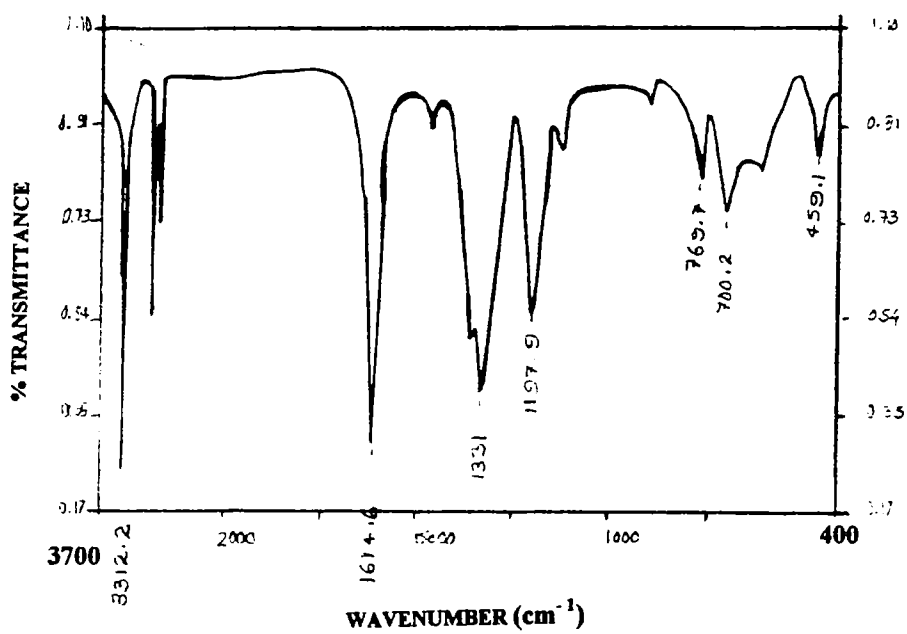


Fig III.2: FTIR Spectrum of Embelin

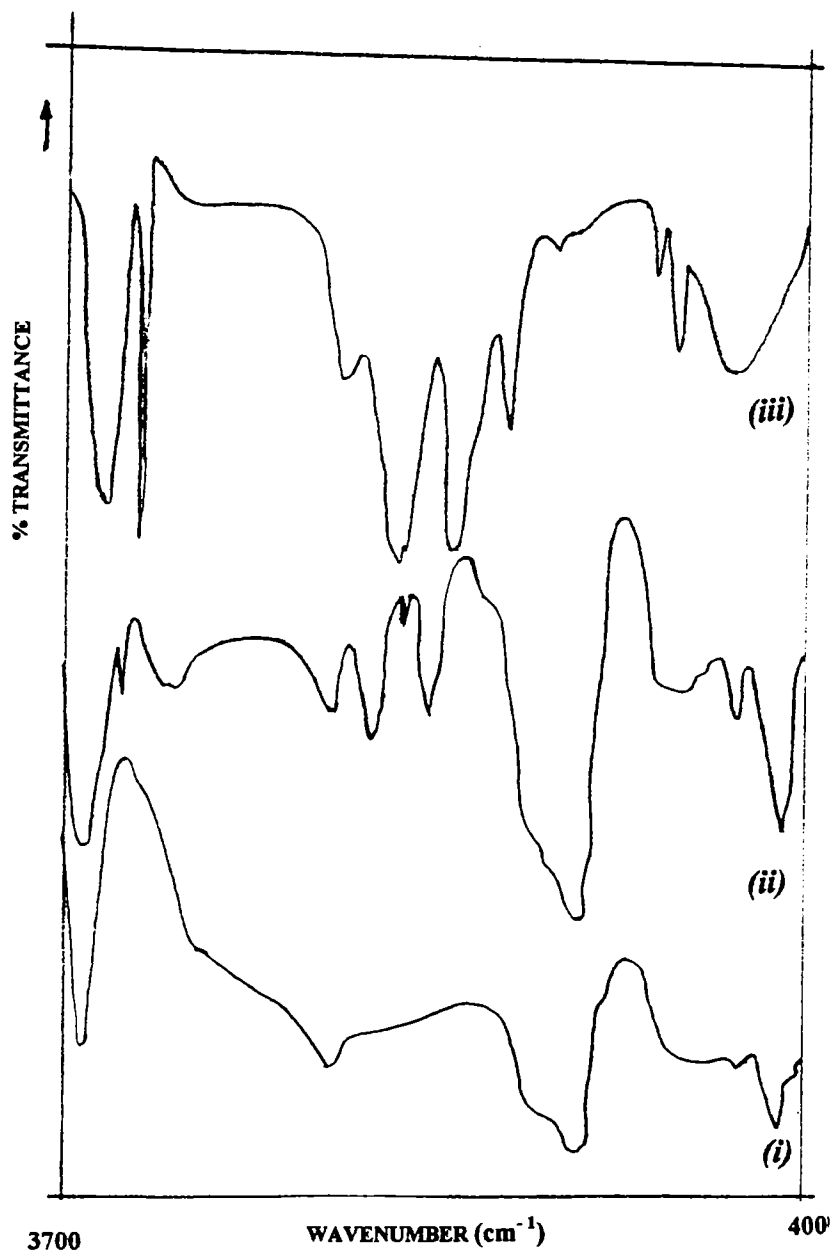


Fig III.3: FTIR Spectrum of (i) MnY (ii) YMnEm (iii) MnEm

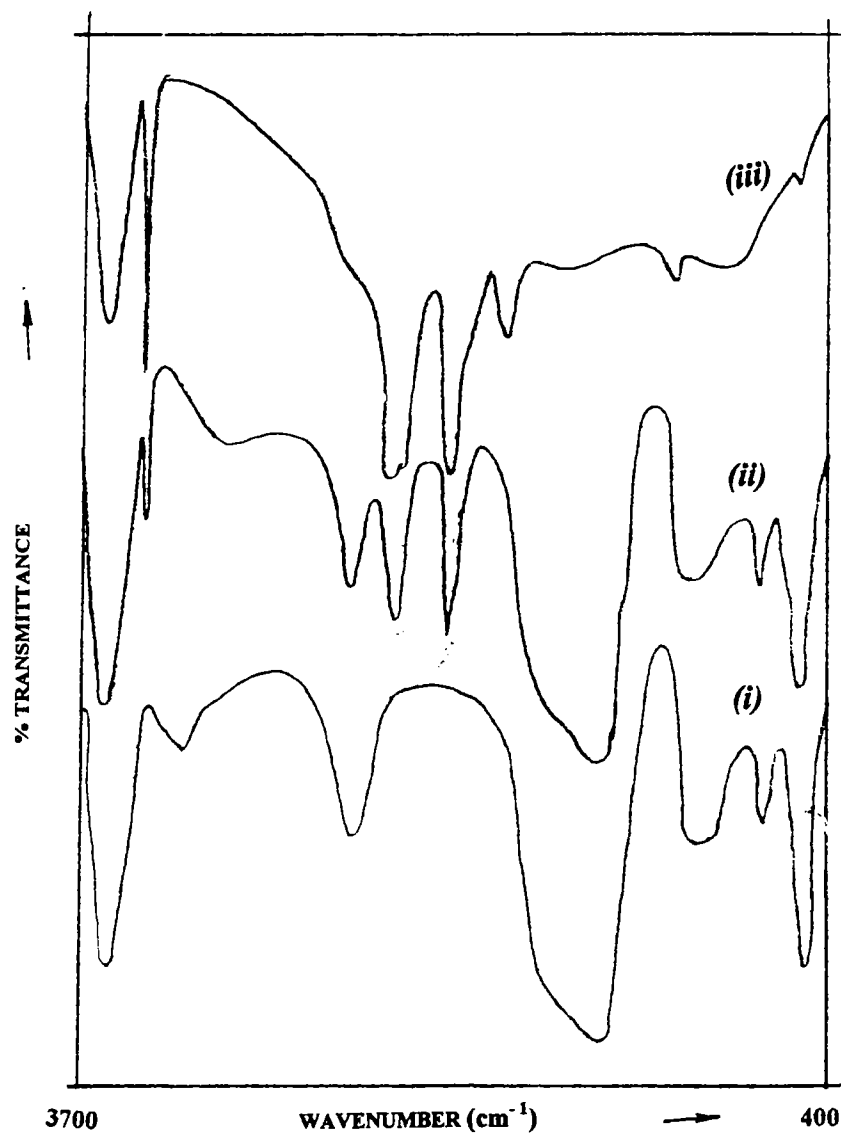


Fig III.4: FTIR Spectrum of (i) FeY (ii) YFeEm (iii) FeEm

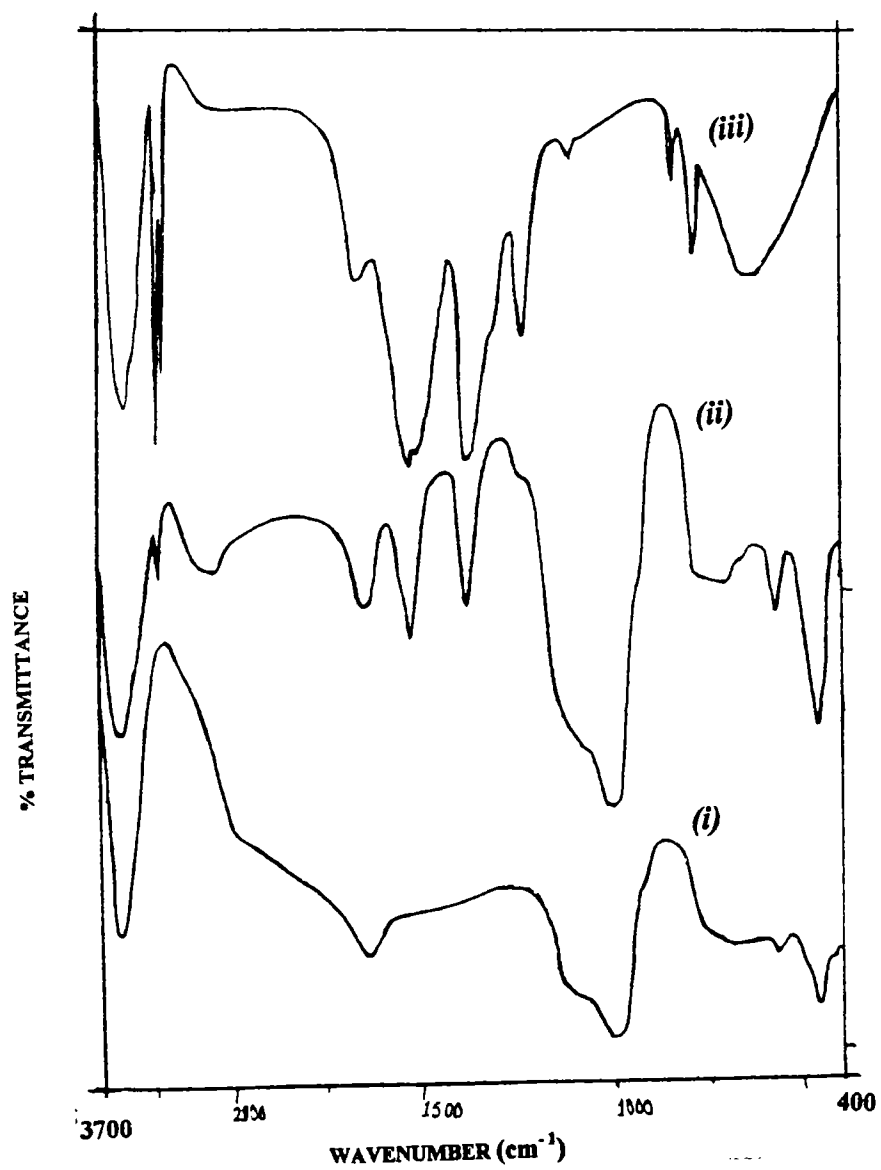


Fig III.5: FTIR Spectrum of (i) CoY (ii) YCoEm (iii) CoEm

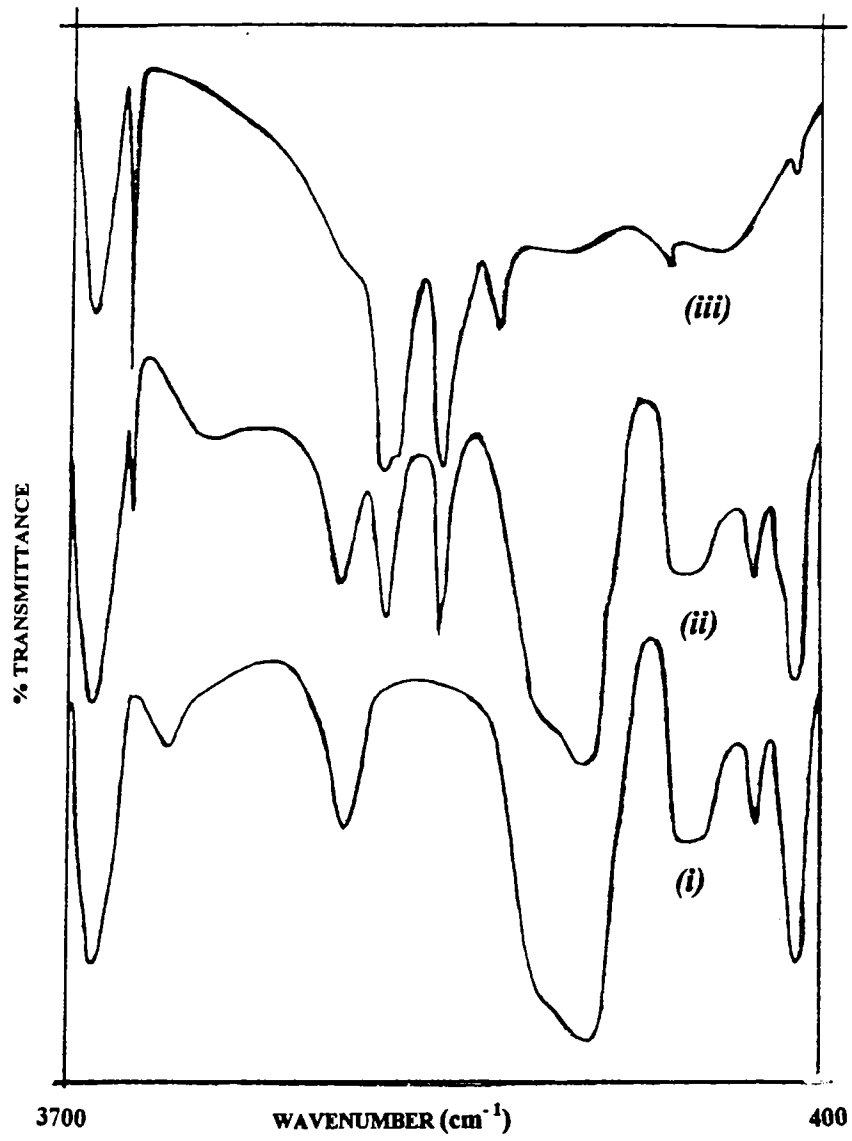


Fig III.6: FTIR Spectrum of (i) NiY (ii) YNiEm (iii) NiEm

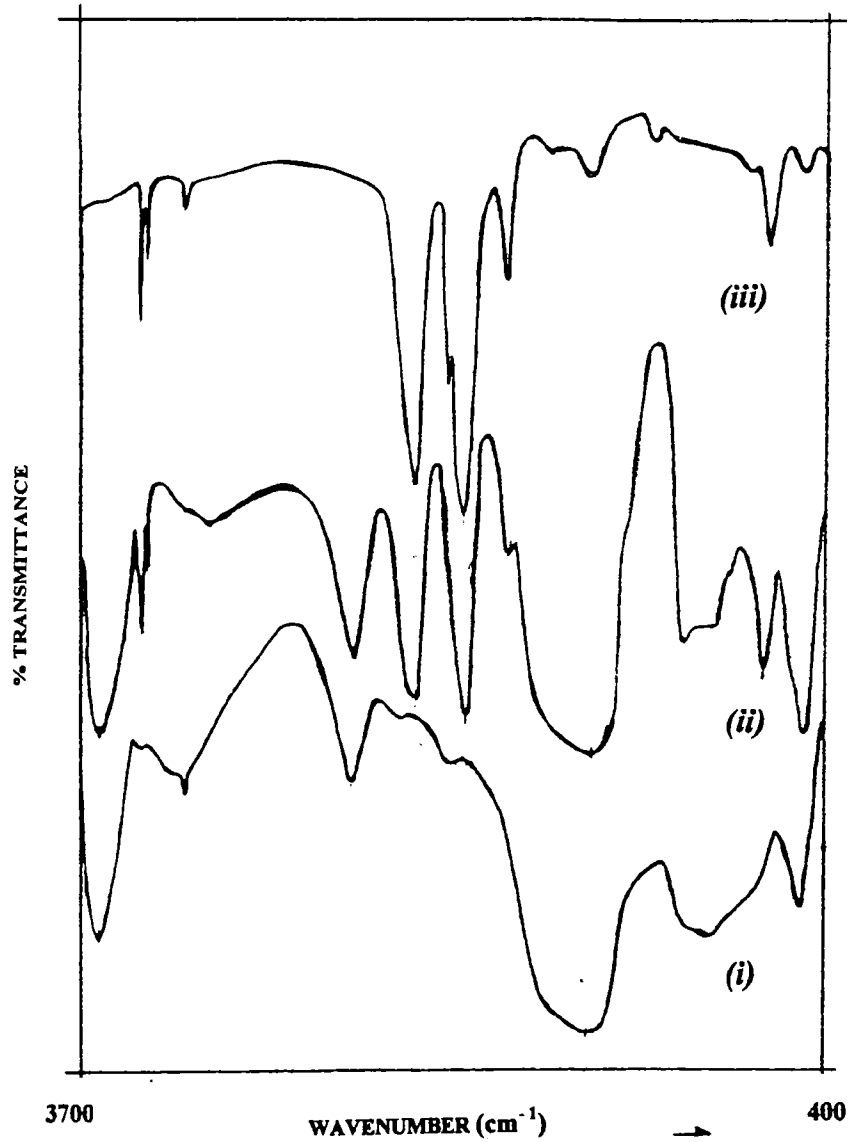


Fig III.7: FTIR Spectrum of (i) CuY (ii) YCuEm (iii) CuEm

A strong band observed at 3300 cm^{-1} in the spectrum of embelin is due to the O-H stretching. In the case of the free metal chelates, this band is absent and the disappearance of this band is due to the complexation and consequent loss of phenolic hydrogen as a result of chelation (13). However, in the case of the zeolite encapsulated complexes, the presence of this band cannot be inferred as due to non-coordination of the phenolic OH group; and might be due to the presence of the O-H stretching frequency of the large number of water molecules in the zeolite lattice.

3.1.2.5 *Electronic spectra*:-

The surface of the zeolite scatters the radiations falling on it and no relevant information is obtained from spectral measurements in the absorption mode. Hence measurements were made in the diffuse reflectance mode. The spectrum obtained is a plot of percentage reflectance vs wavelength. The wavelength corresponding to minimum reflectance was found out. A Kubelka-Munk analysis (6) was also performed on the spectral data and was replotted as $F(R)$ vs wavelength or wavenumber. The absorption maxima for the samples are given in Tables III.4 and III.5. The bands at 5128 cm^{-1} (1950 nm) and 6896 cm^{-1} (1450 nm) are observed for all the zeolite samples regardless of the nature of the metal ion or of other species present. These two bands are attributed (16) to the overtones $2\nu_1$ and $2\nu_3$ and to the combinations $\nu_1+\nu_2$ and $\nu_3+\nu_2$ of the stretching and bending vibrations of water molecules [which appear in the IR spectrum as broad bands at $3100 - 3500\text{ cm}^{-1}$ (ν_3 and ν_1) and in the range $1638-1645\text{ cm}^{-1}$ (ν_2)]. Due to the low concentration of the metal ions species in the zeolite, the absorption bands are of very low intensity. Furthermore, ligand absorptions and charge transfer transitions complicate the assignment of bands in the UV and high energy visible region. The representative spectra are given in Fig III.8.

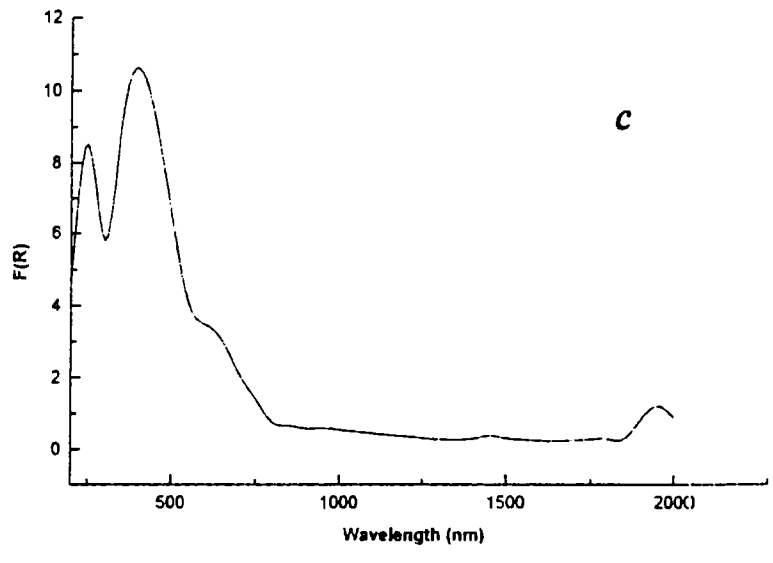
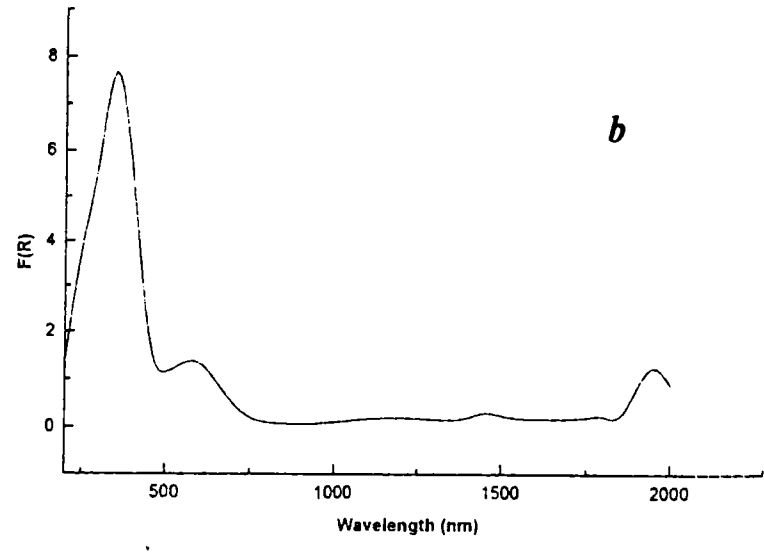
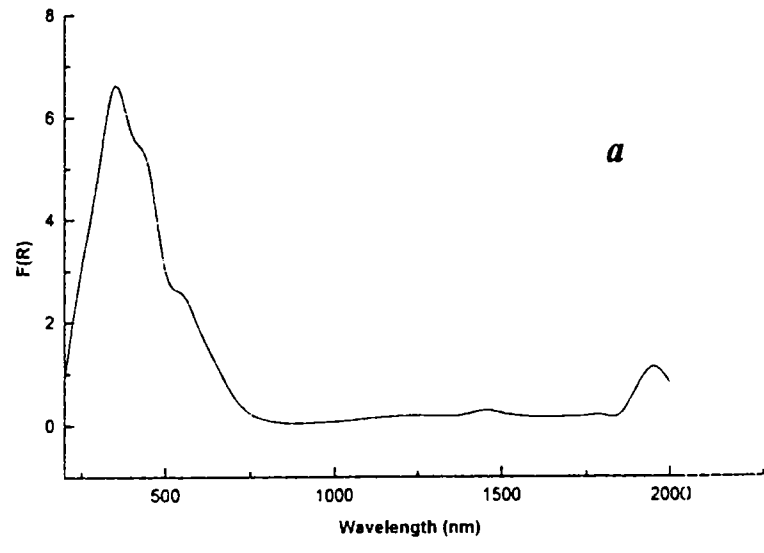


Fig III.8: Diffuse Reflectance Spectrum of (a) YCoEm (b) YNiEm (c) YCuEm

Manganese(II) complex:

In a weak ligand field the ground state term 6S become 6A_1 . All the excited states of this d^5 ion have different spin multiplicities. The absence of any sextet term implies that all the transitions from 6A_1 ground state are spin forbidden as well as Laporte forbidden. Hence the bands in the spectrum of Mn(II) ions (apart from those in the UV region due to charge transfer or ligand absorption) are of very low intensity. The bands observed for the YMnEm complex are very weak. The band at 21750 cm^{-1} may be assigned to the ${}^4A_{1g}(G) \leftarrow {}^6A_{1g}$, ${}^4E_g(G) \leftarrow {}^6A_{1g}$ doublet and that at 19000 cm^{-1} to the ${}^4T_{2g}(G) \leftarrow {}^6A_{1g}$ transition. The band at 17850 cm^{-1} is probably the ${}^4T_{1g}(G) \leftarrow {}^6A_{1g}$ transition. The observed spectral bands along with the magnetic moment value of 6.0 B.M suggest an octahedral structure for the complexes (17).

The bands observed in the spectrum of MnY could not be assigned properly. The weak d-d transitions, if any, might be obscured by the strong charge transfer transitions.

Iron(III) complex

The 6S free ion term for the Fe(III) changes to 6A_1 in a weak crystal field. All the excited states of the d^5 ion are of different multiplicity and the absence of any other sextuplet state accounts for all the transitions to be spin forbidden and hence of low intensity. In the case of tetrahedral coordination of the Fe(III) ion the absorptions are somewhat more intense as the tetrahedral structure lacks a center of symmetry. The band observed at 16300 cm^{-1} could probably be attributed to a forbidden d-d transition probably in a near octahedral geometry (17).

The Fe(III) exchanged zeolite Y (FeY) exhibits a bands around 22200 cm^{-1} which can be attributed (17) to the ${}^4T_1 \leftarrow {}^6A_1$ transition of Fe(III) in tetrahedral geometry.

Cobalt(II) complex:

Cobalt(II) is a d^7 ion with 4F ground state. In a cubic field, three spin allowed transitions are anticipated because of the splitting of the free ion ground term 4F and the accompanying 4P term. In an octahedral complex, the spectrum usually consists of a band in the near IR which may be assigned as ν_1 ; $^4T_{2g}(F) \leftarrow ^4T_{1g}(F)$ and another in the visible region, ν_3 ; $^4T_{1g}(P) \leftarrow ^4T_{1g}(F)$ often with a shoulder on the low energy side. The transition ν_2 ; $^4A_{2g}(F) \leftarrow ^4T_{1g}(F)$, being an essentially two electron transition, is expected to be weak, and hence appears as the shoulder. The ν_2 band which is usually absent may appear in the spectra and the reason may be spin-orbit coupling or distortions from the regular octahedral geometry (9). The band at 23530 cm^{-1} in the spectrum of YCoEm can be assigned to the $^4T_{1g}(P) \leftarrow ^4T_{1g}(F)$ transition. The band at 18850 cm^{-1} could be due to the $^4A_{2g}(F) \leftarrow ^4T_{1g}(F)$ transition. The appearance of this band in the spectrum could be due to a distortion of the structure of the complex from the regular octahedral geometry. The weak band at 8150 cm^{-1} can be attributed to the $^4T_{2g}(F) \leftarrow ^4T_{1g}(F)$ transition (9,17). The above mentioned spectral bands along with the magnetic moment value of 6.0 B.M thus suggest an octahedral geometry for the complex, YCoEm.

For CoY spectral bands are observed at 18500 cm^{-1} , 16150 cm^{-1} and at 5600 cm^{-1} . The spectral changes of CoY on dehydration have been reported by Hutta and Lunsford (18). Their studies indicate a tetrahedral coordination of the Co^{2+} ion after dehydration at 300°C when they are situated inside the sodalite cages. On dehydration at a temperature above 400°C the cobalt(II) ion tend to migrate into the hexagonal prisms where they experience a distorted octahedral environment

Nickel(II) complexes:

In a cubic field three spin allowed transitions are expected for the d^8 nickel(II) ion. The bands observed at, 17450 cm^{-1} and 8500 cm^{-1} can be assigned to the $^3T_{1g}(F) \leftarrow ^3A_{2g}(F)$ and $^3T_{2g}(F) \leftarrow ^3A_{2g}(F)$ transitions respectively. The band

expected in the range 19000 cm^{-1} - 26000 cm^{-1} for the ${}^3T_{1g}(P) \leftarrow {}^3A_{2g}(F)$ transition is probably obscured by the intense charge transfer transitions. These transitions along with the magnetic moment value of 3.4 B.M indicate an octahedral structure for the nickel complex inside the zeolite (17).

The bands observed at 24450 cm^{-1} , 14300 cm^{-1} and 8210 cm^{-1} for NiY can be assigned to the ${}^3T_{1g}(P) \leftarrow {}^3A_{2g}(F)$, ${}^3T_{1g}(F) \leftarrow {}^3A_{2g}(F)$ and ${}^3T_{2g}(F) \leftarrow {}^3A_{2g}(F)$ transitions respectively. The positions of these bands are consistent with a Ni(II) ion in a distorted octahedral geometry (19).

Copper(II) complexes:

The copper complexes of embelin in zeolite Y (YCuEm) exhibits bands at 17250 cm^{-1} , and 12800 cm^{-1} . The band at 17250 cm^{-1} is observed as a shoulder to the transition at 12800 cm^{-1} . The great majority of Cu(II) compounds have a broad absorption band in the region 11000 to 16000 cm^{-1} (9). However, distortions result in a number of transitions and the band becomes unsymmetrical. The presence of the band at 12800 cm^{-1} with a shoulder suggests a penta coordination for the complex and the appearance of the shoulder as a greater intensity absorption to the higher energy side hints at a square pyramidal configuration (17). Hence the Cu(II) might be in a five coordinate state with the fifth position being loosely bound by an H_2O molecule.

For CuY zeolite a broad band is seen around $\sim 13500\text{ cm}^{-1}$ indicative of a square planar geometry (17).

3.1.2.6 EPR Studies:

Several workers have aimed at studying the structure of Cu(II) ions in the cavities of zeolites by EPR spectroscopy (20-22). For a paramagnetic cation

TABLE III.4

Magnetic and optical spectral data of the metal ion-exchanged zeolites

Sample	Absorption (cm^{-1})	Tentative assignment	μ_{eff} (B.M)
MnY	33550	Charge transfer band	5.8
	8300	d-d transition	
FeY	35000	Charge transfer band	5.8
	22200	d-d transition	
CoY	42550	Charge transfer band	4.3
	18500	d-d transition	
	16150	"	
	5600	"	
NiY	40000	Charge transfer band	3.1
	28600	Charge transfer band	
	24450	${}^3T_{1g}(P) \leftarrow {}^3A_{2g}(F)$	
	14300	${}^3T_{1g}(F) \leftarrow {}^3A_{2g}(F)$	
	8210	${}^3T_{2g}(F) \leftarrow {}^3A_{2g}(F)$	
CuY	40000	Charge transfer band	1.9
	13500	d-d transition	

Note: The bands at 6897cm^{-1} and 5128cm^{-1} which are observed in all the samples and are characteristic of the zeolite lattice are not included in the table.

TABLE III.5

Magnetic and electronic spectral data of the zeolite encapsulated complexes of embelin

Sample	Absorption (cm ⁻¹)	Tentative assignment	μ_{eff} (B.M)
YMnEm	28600	Charge transfer band	6.1
	26300	"	
	21750	${}^4A_{1g} \leftarrow {}^6A_{1g}$	
	19000	${}^4T_{2g} \leftarrow {}^6A_{1g}$	
	17850	${}^4T_{1g} \leftarrow {}^6A_{1g}$	
YFeEm	35350	Charge transfer band	5.9
	26600	"	
	16300	d-d transition	
YCoEm	28200	Charge transfer band	5.5
	23530	${}^4T_{1g}(P) \leftarrow {}^4T_{1g}(F)$	
	18850	${}^4A_{2g}(F) \leftarrow {}^4T_{1g}(F)$	
	8150	${}^4T_{2g}(F) \leftarrow {}^4T_{1g}(F)$	
YNiEm	28490	Charge transfer band	3.4
	17450	${}^3T_{1g}(F) \leftarrow {}^3A_{2g}(F)$	
	8500	${}^3T_{2g}(F) \leftarrow {}^3A_{2g}(F)$	
YCuEm	40000	Charge transfer band	1.9
	25000	Charge transfer band	
	17250	d-d transition	
	12800	d-d transition	

Note: The bands at 6897 cm⁻¹ and 5128cm⁻¹ which are common to all the samples have not been included in the table.

exchanged zeolite, the EPR technique enables us to determine the electronic state and symmetry of the ligand field which provides information on the immediate environment of the metal ion. Naccache and Ben Taarit (23) have reported the EPR studies of the dehydration and adsorption of different ligands by Cu-Y zeolites; and the migration of Cu(II) ions through the lattice.

The dehydration process of the copper containing zeolites results in transition from a distorted octahedral to a square planar geometry for the Cu²⁺ ions (23). The distortion has been thought to arise from the constraints imposed by the zeolite cavity and its participation in the coordination sphere (20). More information about the structure could be obtained using simultaneous EPR and diffuse reflectance measurements at variable temperature or EPR studies at variable temperatures. Due to the lack of facilities, we could not do a detailed EPR study. The EPR spectra of the complexes were recorded at the liquid nitrogen temperature and room temperature. A somewhat informative spectrum is obtained only in the case of the copper(II) complexes. The EPR parameters were found out without computer simulation and hence the values determined are not accurate.

The change in EPR parameters of the Cu(II) ions in the metal exchanged zeolite (Cu-Y) with the addition of the ligand is an evidence in favor of the change in environment of the ion and hence supports the encapsulation of the complex in the zeolite cavities. The EPR spectrum of the complex YCuEm recorded at liquid nitrogen temperature is shown in Figure III.9. The following parameters have been calculated from the spectrum.

$$g_{\parallel} = 2.3487; \quad A_{\parallel} = 154 \times 10^{-4} \text{ cm}^{-1}$$

$$g_{\perp} = 2.07; \quad A_{\perp} = 110 \times 10^{-4} \text{ cm}^{-1}$$

The g_{\parallel} value is somewhat higher than that usually reported for Cu(II) complexes. Sakaguchi and Addison (24) have given the following reasons for such unexpected values.

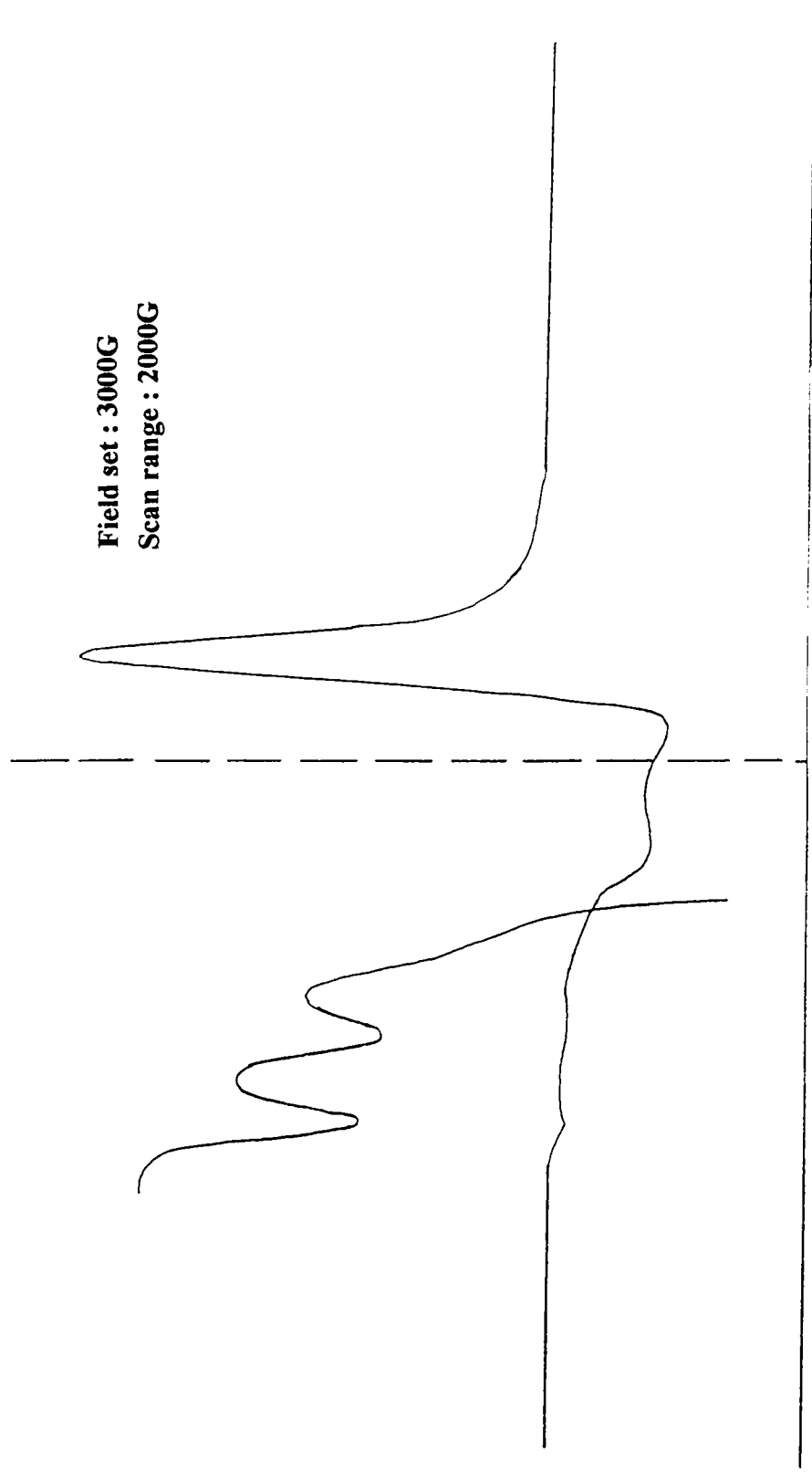


Fig III.9: EPR Spectrum of YCuEm recorded at LNT

- (i) Tetrahedral distortion of a square planar chromophore with any of the biomimetic (N, O, S) donors reduces $|A_{II}|$ and increases g_{II} .
- (ii) Hard donor atoms tend to shift g_{II} towards higher values which could be due to increased delocalization of spin density at the copper nucleus and often interpreted in terms of decreased covalence in the metal – ligand bond and
- (iii) Increasing the positive charge on donor atom set can reduce A_{II} and increase g_{II} .

The higher g_{II} value may be due to the effect of oxygen donor atoms. The increased value also could be due to distortion caused by the ligands and the zeolite framework. According to Sakaguchi and Addison the quotient g_{II}/A_{II} may be taken a convenient empirical index of tetrahedral distortion. This quotient ranges from ca. 105 to 135 cm for square planar structures. The ratio obtained for YCuEm is 152 cm. Such higher values have been reported (25-27) in the case of copper (II) complexes with rather flattened tetrahedral structures formed, when Cu(II) ion is doped into the dipiperidylthiouramdisulphide (152 cm); and zinc dialkyl dithiophosphate (154 cm); and bis(N-t-butyl salicylaldimino)Cu(II) (157 cm). Therefore, YCuEm might also have a similar structure. On the basis of the g_{II} and A_{II} values the complex can be assumed to have a square pyramidal structure (28). Conclusion arrived from electronic spectral results are also in agreement with this observation.

For the Cu(II) complexes with the unpaired electron in the B_{1g} orbital, the density of the unpaired electron at the central atom can be computed (29) from the following equation:

$$\alpha^2 = (A_{II}/P) + (g_{II}-2) + 3/7(g_{\perp}-2) + 0.04$$

where $1-\alpha^2$ measures the covalence associated with the bonding of the Cu^{2+} ions to the ligands and $P = 0.036 \text{ cm}^{-1}$. The α^2 value for YCuEm is 0.84 which indicates the Cu^{2+} ion to be in an ionic environment.

Magnetic moment values can also be determined from the EPR spectrum (30) by substituting g , $g_{||}$ and g_{\perp} values for monomeric complexes in the following equation

$$\mu_{\text{eff}}^2 = g_{||}^2/4 + g_{\perp}^2/2 + (3kT/\lambda_o)(g-2)$$

where λ_o is the spin orbit coupling constant for the free ion and for Cu^{2+} it is -828 cm^{-1} . Using this equation a μ_{eff} value of $\sim 1.9 \text{ B.M}$ was obtained for the copper complex, which is in agreement with the value obtained from the room temperature magnetic susceptibility measurements.

The ESR spectrum of the dehydrated Cu-Y recorded at LNT is given in Fig III.10 The spectra gives the following parameters

$$g_{||} = 2.4 ; A_{||} = 169.8 \times 10^{-4} \text{ cm}^{-1}$$

$$g_{\perp} = 2.07; A_{\perp} = 40 \times 10^{-4} \text{ cm}^{-1}$$

The large value of $g_{||}$ can also be explained on the basis of the above mentioned factors. A $g_{||}/A_{||}$ ratio of 141 cm is obtained which is close to the value for a square planar complex and is also in agreement with the reported values for dehydrated CuY, in which Cu^{2+} ion is in a square planar geometry. A magnetic moment value (1.89 B.M) calculated from the epr data agrees with that obtained from susceptibility measurements. The value of α^2 for this case is 0.866, which indicates the large ionic nature of the metal-ligand bond. The Cu-Y in the dehydrated state in the hexagonal prisms is coordinated to the lattice oxygen.

3.1.2.7 X - Ray diffraction:

Powder X-ray diffraction patterns were obtained for NaY, metal exchanged zeolite and the zeolite encapsulated complexes of embelin. The diffraction patterns of the different samples are given in Fig. III.11. No variation was observed in the diffraction pattern as a result of the metal exchange and encapsulation procedures, which suggests that there is little or only negligible loss in crystallinity of the zeolite. Therefore, the reduction in surface area observed in the case of the encapsulated complexes (vide page 37) is not due to collapse of the crystalline structure.

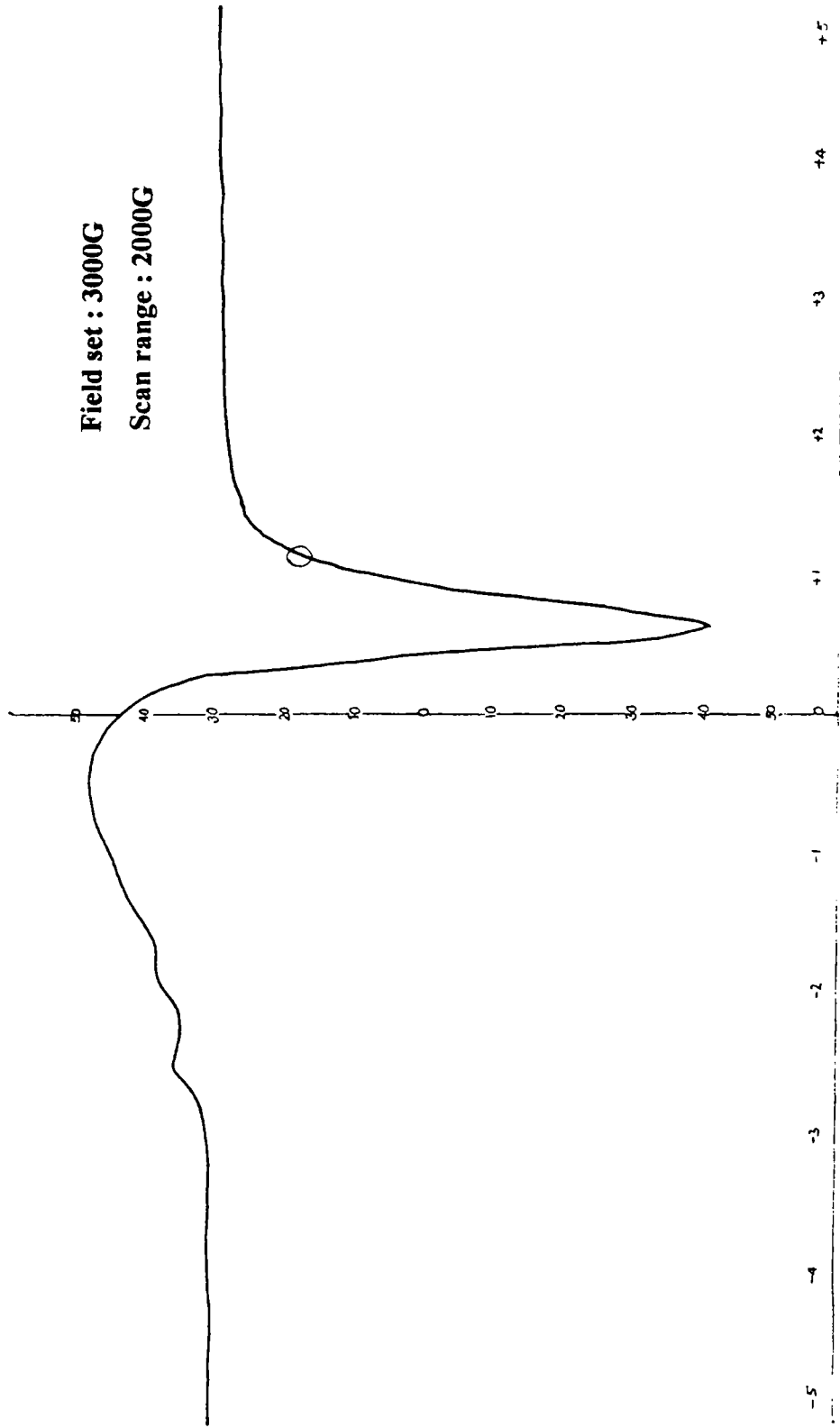
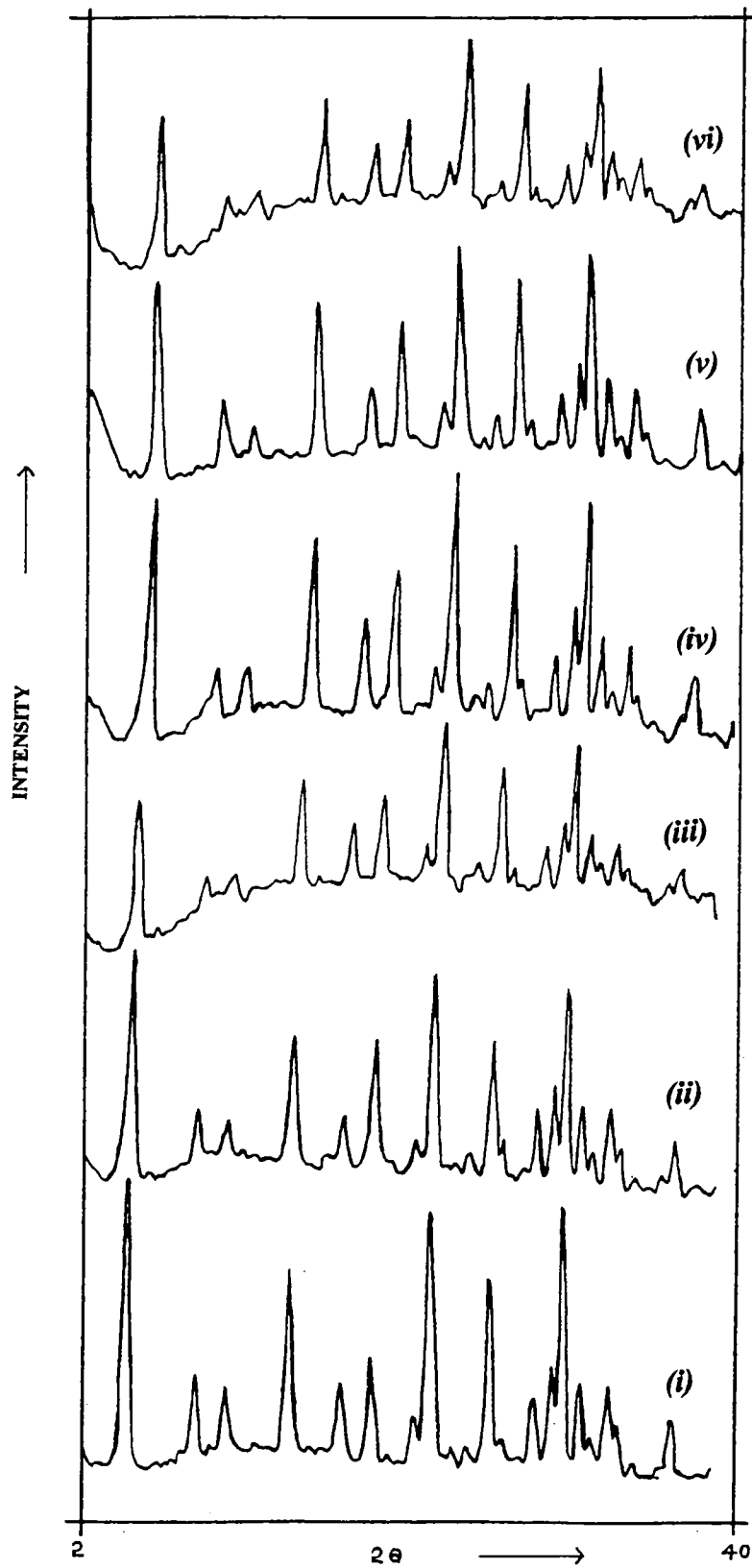


Fig III.10: EPR Spectrum of CuY recorded at LNT



**FigIII.11: XRD pattern of (i) NaY (ii) YMnEm (iii) YCoEm (iv) YNiEm (v) YCuEm
(vi) YFeEm**

3.1.2.8 Thermal behaviour

TG curves of the ligand and the zeolite samples have been recorded under an inert atmosphere from ambient temperature to 800⁰C. The ligand embelin, is found to decompose in three stages between 150⁰C and 740⁰C. The TG curve for parent zeolite, NaY, reveals that the weight loss starts at ~50⁰C and ends at ~345⁰C. The weight loss of 21.9% observed in this case can be attributed to the loss of intrazeolite water molecules.

The TG curves of the metal ion-exchanged zeolites were also recorded under the same conditions. A comparison of the TG curves of NaY with that of the metal ion-exchanged zeolites (Fig. III.12) reveal that the properties of the parent zeolite have been modified by ion exchange. The water molecules are more strongly bonded in the ion-exchanged zeolites, which is evident from the percentage water loss and the temperature at which the dehydration process is completed.

The TG/DTG curves for the encapsulated complexes are given in Fig III.13. The pattern of thermal decomposition is the same for all the encapsulated complexes. The thermal analysis data of the zeolite encapsulated complexes are given in Table III.6. There are three stages of weight loss for all the complexes except for the manganese complex in which the last two stages merge into one. The first stage in all the cases is due to the loss of intrazeolite and coordinated water molecules. Decomposition of the complexes at this stage is ruled out since the IR spectra taken at this stage reveals all the functional groups to be intact. The second and third stages of decomposition could be attributed to the decomposition of the complex inside the cavities. The percentage mass loss after decomposition of the complexes is found to agree with the compositions deduced from elemental analyses.

Procedural decomposition temperatures for the encapsulated metal complexes were taken as those temperatures at which the decomposition of the ligand portion of

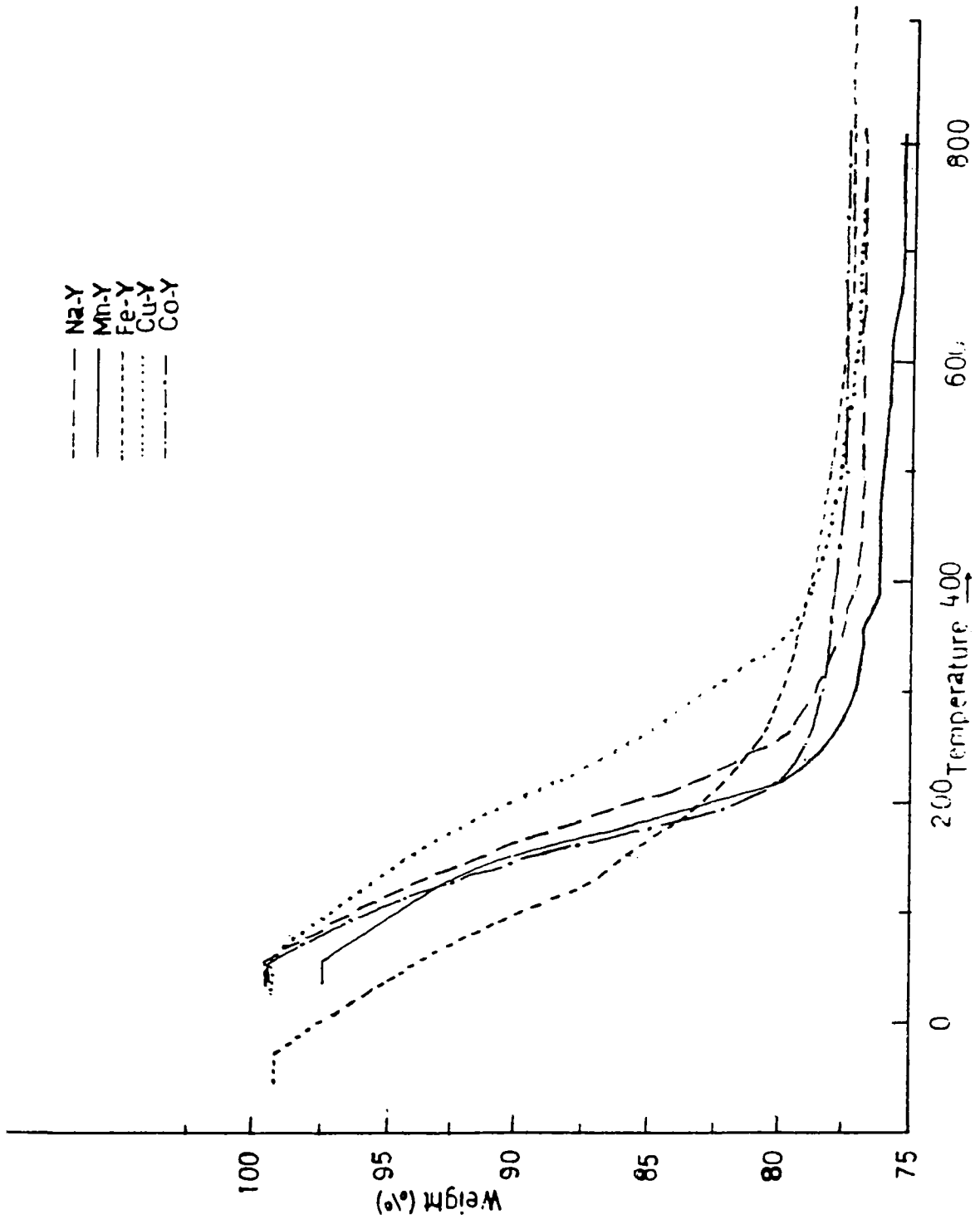


Fig III.12 TG curves of Zeolite Y and metal ion exchanged zeolites.

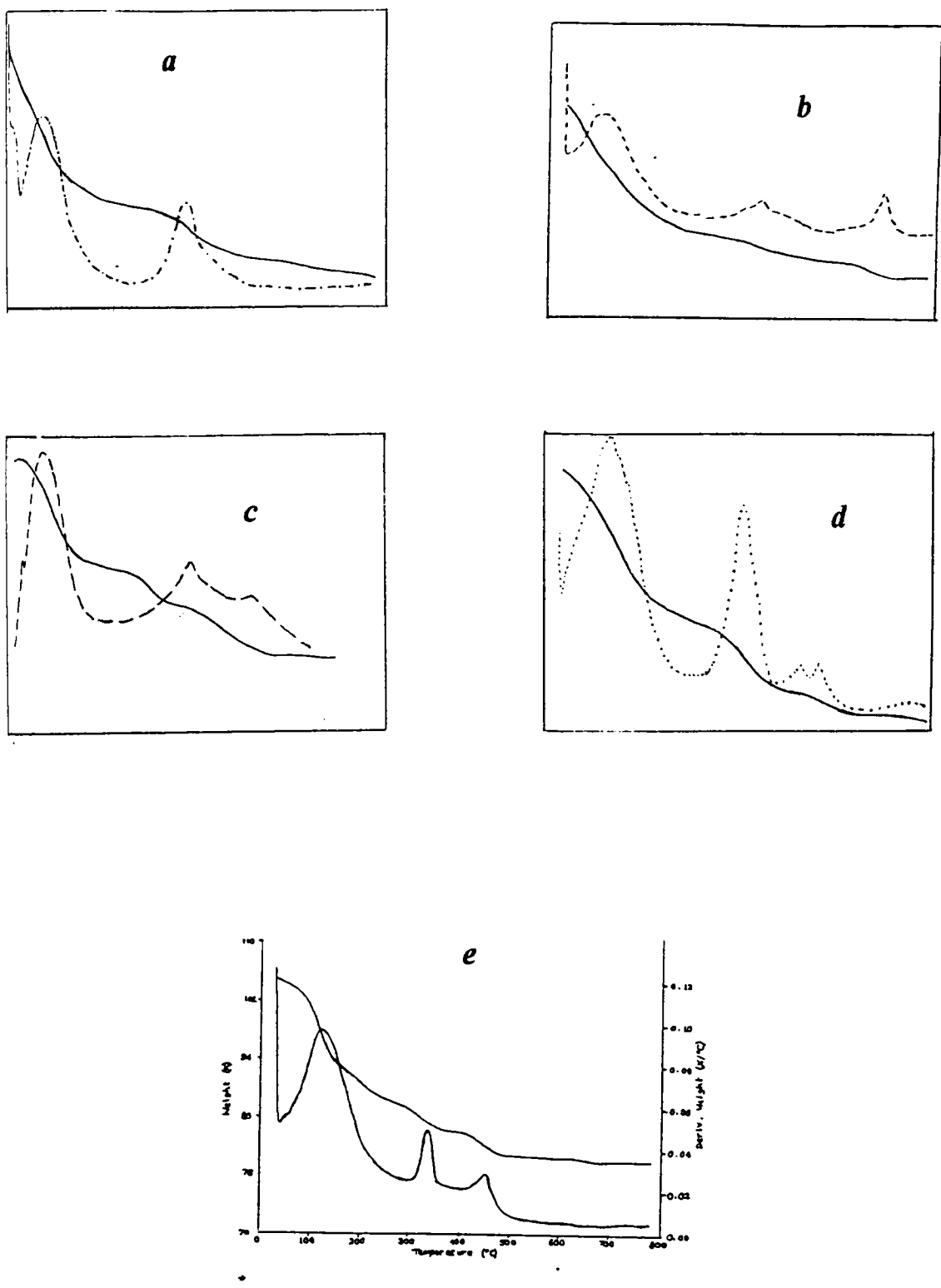


Fig III.13 TG/DTG patterns of (a) YMnEm (b) YFeEm (c) YCoEm (d) YNiEm (e) YCuEm.

the complex started after the dehydration stages. On the basis of the procedural decomposition temperatures, the complexes have the following irregular stability sequence: Co>Mn>Fe>Ni>Cu. However, the order of thermal stability is not similar to that exhibited by the simple metal complexes of embelin. Irregular thermal stability pattern have been reported for the metal complexes of hydroxyquininoid ligands (31).

Among the encapsulated complexes, the copper complex of embelin exhibits the lowest thermal stability as indicated by the procedural decomposition temperature. An IR spectrum (Fig.III.14) of the residue after heating the complex to 275⁰C shows that all the relevant peaks remain intact endorsing the fact that the ligand portion does not decompose before 275⁰C. However, just after the dehydration stage ie, after 230⁰C, there is some change in the structure of the complex. Removal of a coordinated water molecule might occur above this temperature; imparting catalytic activity to the complex (the details of which are described in page 96 of chapter V). Further, there is a possibility of dissociation of C=O bonds during heating as indicated by the decreased value of the C=O stretching frequency. Lower thermal stability has been reported for the simple copper(II) complex of embelin, 2,5-dihydroxy-1,4-benzoquinone and 5,8-dihydroxynaphthaquinone (13,15).

The procedural decomposition temperatures of all the encapsulated metal complexes are higher than their respective unencapsulated analogues. In the case of the manganese(II) complex the procedural decomposition temperature is increased by 80 C , by 50⁰C in the case of cobalt(II) and nickel(II) complexes, by 125⁰C in the case the iron(III) complex and by 25 ⁰C in the case of the copper(II) complex. The increase in the procedural decomposition temperature points to the increased thermal stability as a result of encapsulation of the complexes inside the zeolite cages.

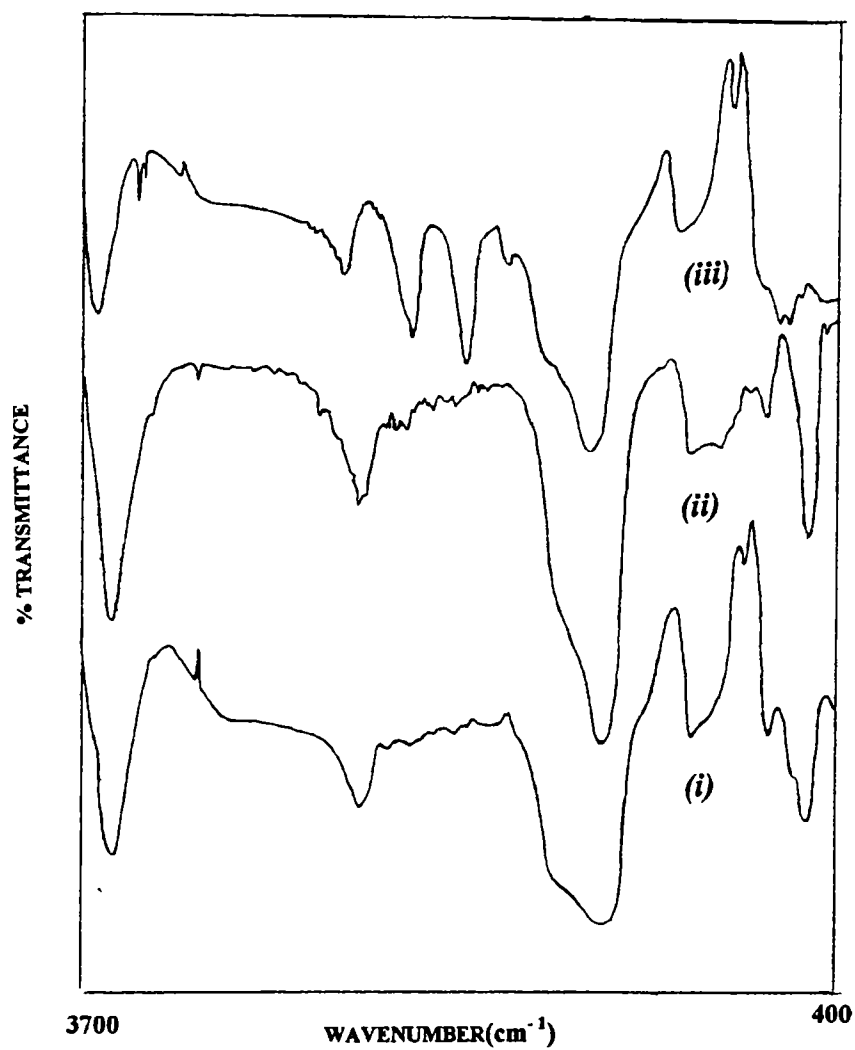


Fig III.14 FTIR spectrum of YCuEm isolated after TG upto (i) 270^oC (ii) 365^oC
(iii) 470^oC.

TABLE III.6*TG/DTG data of the zeolite encapsulated complexes of embelin*

Sample	Peak temperature in DTG	Temp. Range in DTG	Temperature range in TG	Percentage Weight loss
YMnEm	129.5	76-156	69-112	9
			156-270	5.4
	426.6	369-533	331-533	5.5
YFeEm	115	50-300	50-300	17
	431	350-450	350-450	3.8
	685	650-710	645-710	1.0
YCoEm	145	100-210	100-245	11.0
	445	425-460	320-375	2.5
	560	530-595	425-595	7.0
YNiEm	121.8	34.2-1923	34-274	12.1
	396	339-449.5	339-450	6.1
		495-580	495-580	1.8
YCuEm	120	80-175	60-235	12.7
	340	300-350	275-365	3.50
	460	405-465	405-475	3.50

3.2 . STUDIES ON THE TRANSITION METAL COMPLEXES OF 2-AMINOBENZIMIDAZOLE IN ZEOLITE Y

Complexes of Mn(II), Co(II), Ni(II) and Cu(II) with the ligand 2-aminobenzimidazole were encapsulated in the cavities of zeolite Y and characterised. The details of this study are presented in this section.

3.2.1 EXPERIMENTAL

3.2.1.1 *Materials:*

Details regarding metal ions used for the preparation of the complexes are given in Chapter II. The ligand, 2-aminobenzimidazole, obtained from E. Merck was recrystallised from ethanol prior to preparation of the complexes

3.2.1.2 *Preparation of the complexes in NaY:*

The transition metal complexes of the ligand 2-aminobenzimidazole were encapsulated inside the zeolite cavities by refluxing a mixture of the metal exchanged zeolite (1.0g) and the ligand (0.25g) for 4-6 hrs in methanol. The purification procedures adopted in the case of the complexes of embelin were employed in this case also.

3.2.1.3 *Preparation of a reaction blank:*

The encapsulation of the aminobenzimidazole ligand in the cavities was attempted by sealed heating of a mixture of the ligand and the zeolite, NaY. The spectral studies of the material obtained after purification gave no evidence of the ligand which implies that no ligand can remain in the cavities without binding to the metal ions.

3.2.2. PHYSICOCHEMICAL CHARACTERIZATION

3.2.2.1 Elemental analysis:

Details regarding the elemental analyses are given in Chapter II. The results of the elemental analyses are presented Table III.7. The microanalysis of carbon and nitrogen suggest that only a small amount of Mn(II), Co(II), and Ni(II) complexes are encapsulated in the cavities of the zeolite.

3.2.2.2 Surface area analyses:

The results of the surface area measurement of the encapsulated complexes are given in Table III.8. A decrease in surface area of the zeolite is observed for the encapsulated complexes (2). However, the decrease is not very large when compared with the encapsulated complexes of embelin. This could probably be due to the lower concentration of complexes in the cavities.

3.2.2.3 Magnetic Susceptibility measurements:

Magnetic moments of the complexes were calculated by the method adopted earlier in the case of the encapsulated complexes of embelin (vide page 37) and the values are presented in Table III.10. The magnetic moment values (6.2 B.M, 4.9 B.M, and 3.2 B.M were obtained for the Mn(II), Co(II) and Ni(II) complexes respectively) indicate an octahedral or near octahedral arrangement of ligands around the metal ions. The value obtained for the Cu(II) complex (YCuAb) indicates a somewhat distorted tetrahedral geometry (8,9,11).

3.2.2.4 Infrared spectra:

The ligand molecule, the metal ion-exchanged zeolites and the zeolite encapsulated complexes were subjected to FTIR spectral analyses. An examination

TABLE III.7

Analytical data of the Zeolite encapsulated complexes of Aminobenzimidazole

Sample	Elements in percentage by weight					
	Si	Al	Na	Metal	C	N
YMnAb	20.45	8.1	6.05	0.7	1.0	0.77
YCoAb	20.4	8.0	6.2	0.5	0.7	0.4
YNiAb	20.5	8.1	5.0	1.2	1.7	0.86
YCuAb	20.3	8.02	3.9	3.92	2.4	1.2

TABLE III.8

Surface area of the ion exchanged zeolites and zeolite encapsulated complexes of 2-aminobenzimidazole

Sample	BET Surface area (m ² /g)
NaY	507
MnY	480
YMnAb	400
CoY	482
YCoAb	430
NiY	478
YNiAb	410
CuY	492
YCuAb	403

of the spectral data (Table III.9) reveal the encapsulation of the complexes in the pores of the zeolite. Simple complexes of 2-aminobenzimidazole were not prepared and hence a comparison of the encapsulated complexes and their unencapsulated analogues were not possible.

The appearance of the infrared spectra of aminobenzimidazoles is very complex. However, almost all the bands present in the spectra of the ligand are present in the spectra of the encapsulated complexes also (see Fig III.15-Fig III.18). This points to the presence of ligand in the cavities. The region 1660 cm^{-1} - 1550 cm^{-1} is very important for benzimidazoles (33). Strong bands are observed at 1660 cm^{-1} and 1550 cm^{-1} . The band at 1660 cm^{-1} could probably be the N-H bending of the nitrogen on the ring, while that at 1560 cm^{-1} could be the N-H bending of the amino group at 2-position. The benzimidazoles are known to be associated through intermolecular hydrogen bonding. The band at 3375 cm^{-1} indicates polymeric association through hydrogen bonding. The bands at 3125 cm^{-1} and 3042 cm^{-1} could probably be the N-H stretching vibrations coupled with the C-H stretching vibrations..

The band at 1669 cm^{-1} in the spectra of the ligand is shifted to 1652 cm^{-1} in the manganese complex (YMnAb), to 1652 cm^{-1} in the cobalt complex (YCoAb), to 1655 cm^{-1} in the nickel complex (YNiAb) and to 1680 cm^{-1} in the copper complex (YCuAb). The shift in frequency indicates coordination of the ring nitrogen. The band at 1568 cm^{-1} is also seen to shift to lower frequencies in the complexes suggesting coordination of the amino group also. Thus benzimidazole ligand can coordinate to the metal ions either through the ring nitrogens or through the amino group at position 2.

3.2.2.5 Electronic spectra:

As in the case of the encapsulated complexes of embelin the electronic spectra of the encapsulated complexes of aminobenzimidazole were also recorded in the diffuse reflectance mode. The results are presented in Table III.10. Representative spectra are also given in Fig III.19.

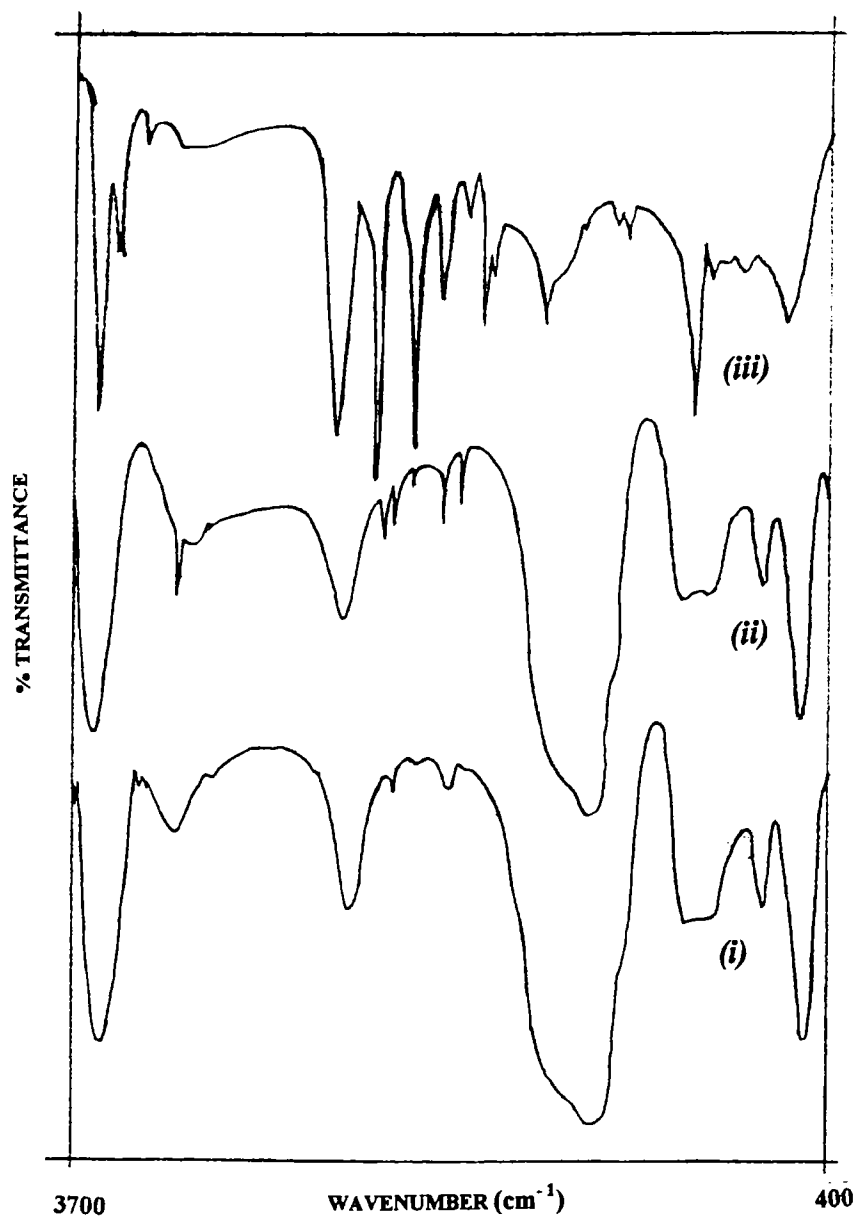


Fig III.15: FTIR Spectrum of (i) MnY (ii) YMnAb (iii) 2-Aminobenzimidazole

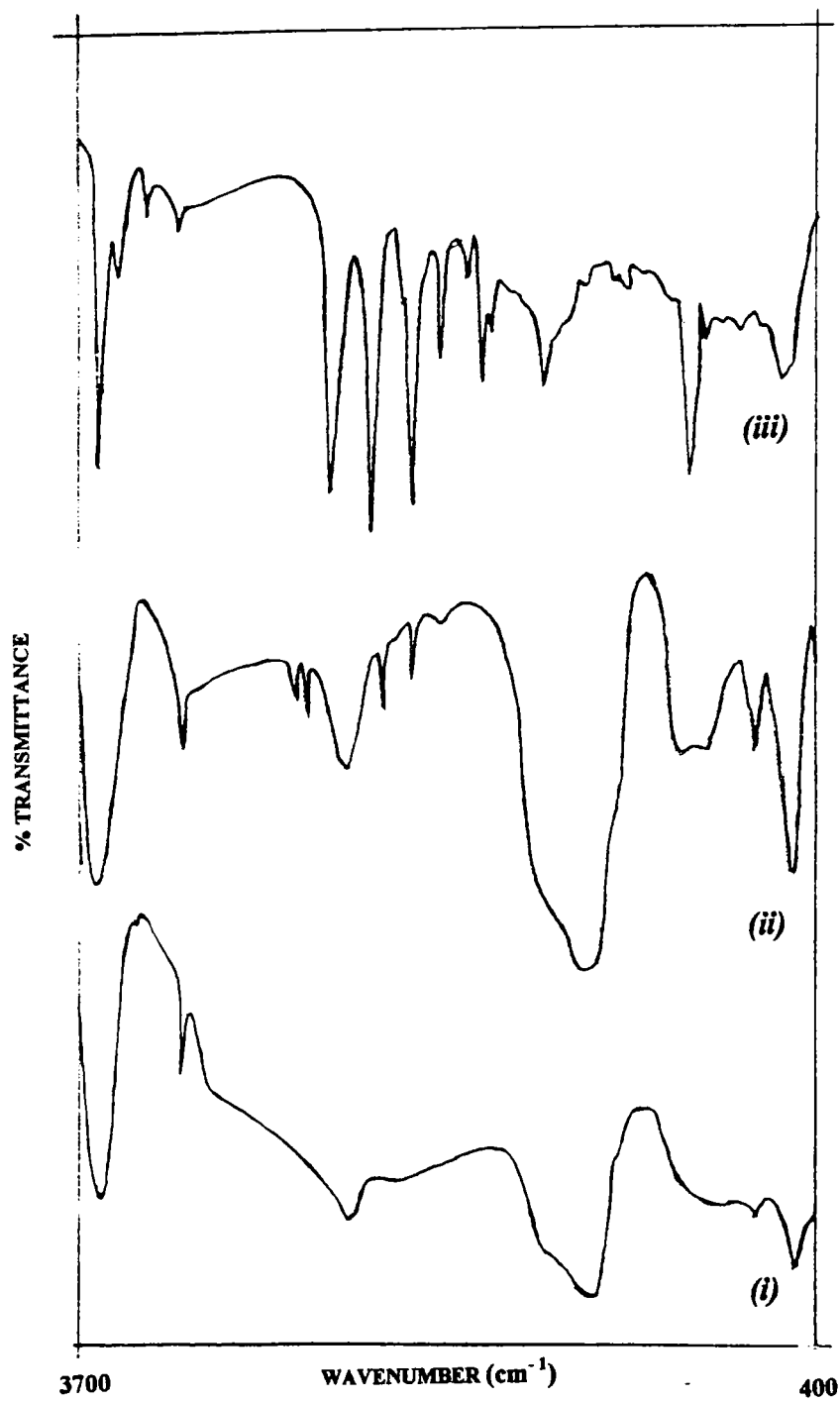


Fig III.16: FTIR Spectrum of (i) CoY (ii) YCoAb (iii) 2-Aminobenzimidazole

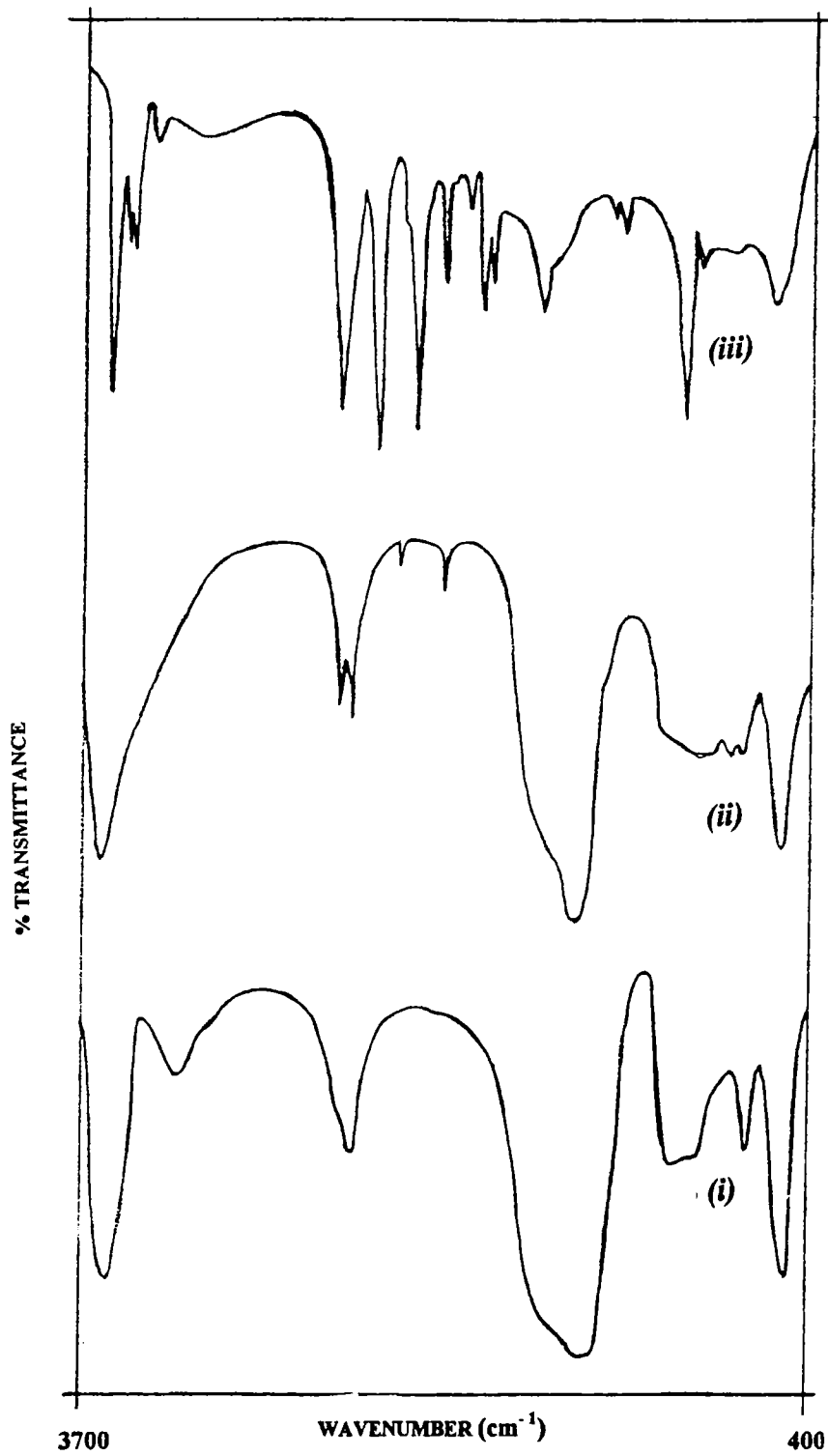


Fig III.17: FTIR Spectrum of (i) NiY (ii) YNiAb (iii) 2-Aminobenzimidazole

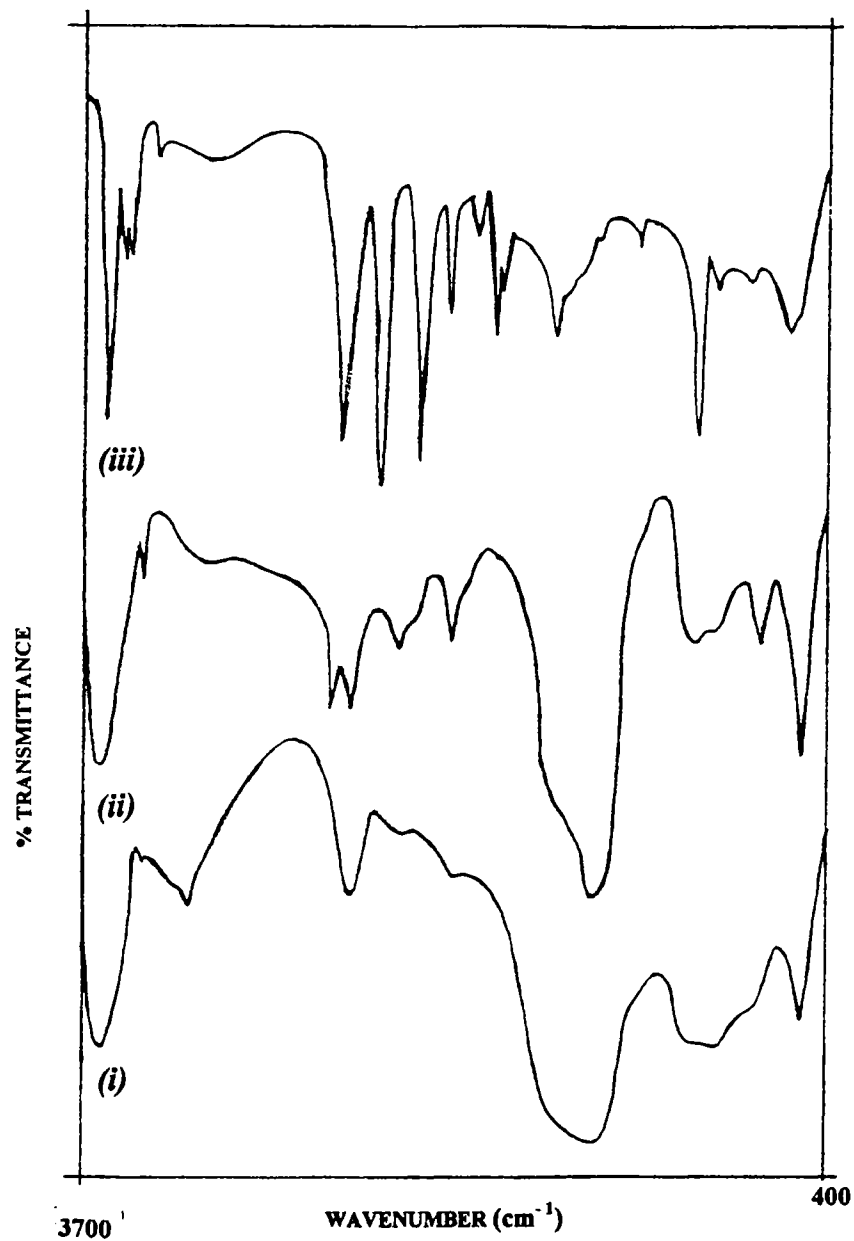
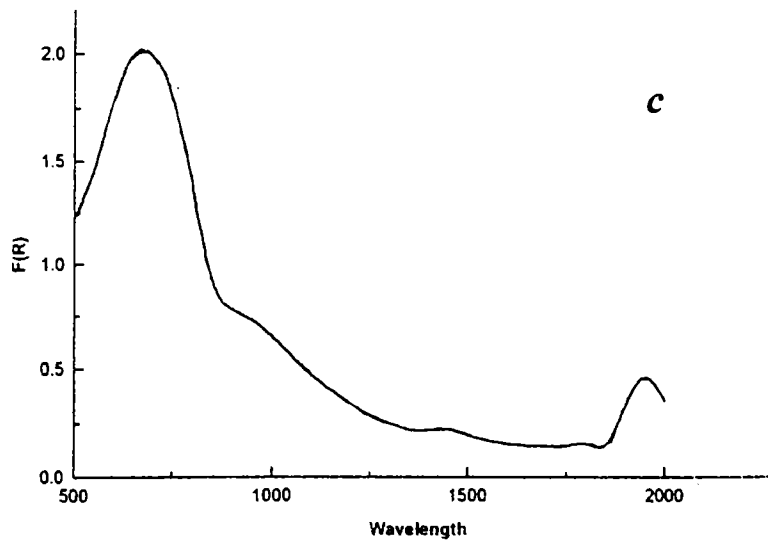
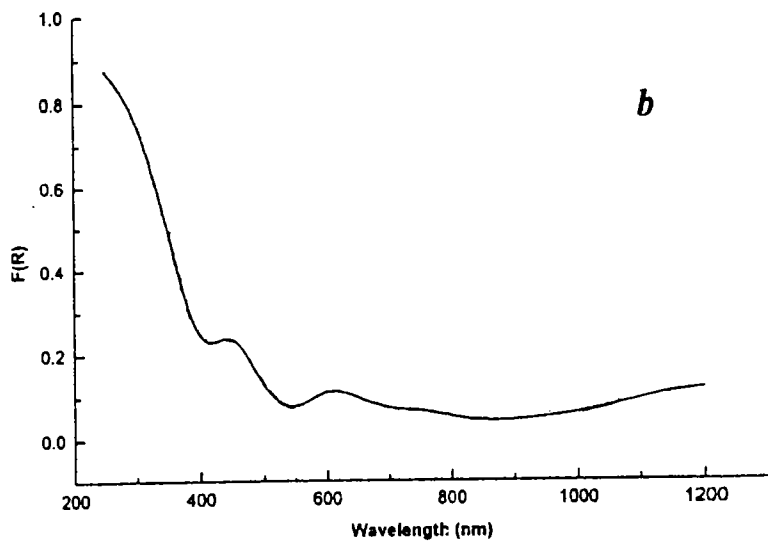
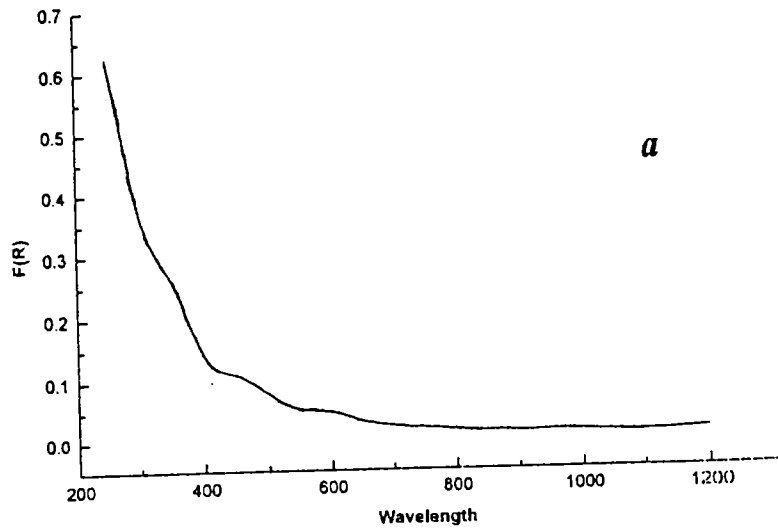


Fig.III.18: FTIR Spectrum of (i) CuY (ii) YCuAb (iii) 2-Aminobezimidazole

TABLE III.9

IR spectral data of 2-aminobenzimidazole, metal ion-exchanged zeolites and encapsulated complexes (cm⁻¹)

Amb	MnY	YMnAb	CoY	YCoAb	NiY	YNiAb	CuY	YCuAb
	3464	3500	3467	3500	3428	3566	3400	3500
3387								
1669		1652		1651		1655		1680
	1644	1638	1640	1638	1644	1644	1638	1646
1568		1545		1543		1543		
				1522		1522		1518
1458		1458		1474		1473		1458
1383		1385		1385		1385		1381
1269								
1246								
1111								
	997	997	1005	1003	1007	1007	1007	1007
	757	760	767		767	765	752	742
735								
	694	695	696	689	702	694	693	696.4
690								
607								
	575	569	565	567	569	575	569	569
493								
	470	461	463	459	463	465	465	463



FigIII.19: Diffuse Reflectance Spectrum of (a) YMnAb (b) YNiAb (c) YCuAb

Manganese (II) complex:

The bands seen at 23810 cm^{-1} and 16950 cm^{-1} might be d-d transitions. However they cannot be assigned with confidence.

Cobalt (II) complex:

The bands seen at 20500 cm^{-1} , 16650 cm^{-1} and 8100 cm^{-1} can be interpreted as the ${}^4T_{1g}(P) \leftarrow {}^4T_{1g}(F)$, ${}^4A_{2g}(F) \leftarrow {}^4T_{1g}(F)$ and ${}^4T_{2g}(F) \leftarrow {}^4T_{1g}(F)$ transitions respectively of a Co(II) ion in the octahedral geometry (17).

Nickel(II) complex:

The analysis of the spectra of the nickel(II) complex reveals an octahedral geometry for the metal ion. Bands at 22220 cm^{-1} , 16260 cm^{-1} and 8330 cm^{-1} could be attributed to the ${}^3T_{1g}(P) \leftarrow {}^3A_{2g}(F)$, ${}^3T_{1g}(F) \leftarrow {}^3A_{2g}$, and ${}^3T_{2g} \leftarrow {}^3A_{2g}$ transitions respectively (17).

Copper (II) complex

Bands are observed at 14800 cm^{-1} and 11200 cm^{-1} for the the copper(II) complex, YCuAb. The values and position of the bands points to a somewhat distorted octahedral geometry (17).

3.2.2.6 EPR spectra:

The EPR spectrum of YCuAb was recorded at liquid nitrogen temperature. The hyperfine splittings possibly due to nitrogen implies coordination of nitrogen to the metal ion. The following EPR parameters were obtained from the spectrum (Fig. III.20)

TABLE III.10

Electronic spectral and magnetic data of the Zeolite encapsulated complexes of 2-aminobenzimidazole

Compound	Absorption (cm ⁻¹)	Tentative assignment	μ_{eff} (B.M)
YMnAb	31050	Charge transfer	6.2
	23810	d-d transition	
	16950	d-d transition	
YCoAb	35000	Charge transfer	4.9
	20500	${}^4T_{1g}(P) \leftarrow {}^4T_{1g}(F)$	
	16650	${}^4A_{2g}(F) \leftarrow {}^4T_{1g}(F)$	
	8100	${}^4T_{2g}(F) \leftarrow {}^4T_{1g}(F)$	
YNiAb	34600	Charge transfer band	3.2
	22220	${}^3T_{1g}(P) \leftarrow {}^3A_{2g}(F)$	
	16260	${}^3T_{1g}(F) \leftarrow {}^3A_{2g}(F)$	
	8330	${}^3T_{2g}(F) \leftarrow {}^3A_{2g}(F)$	
YCuAb	31250	Charge transfer band	1.9
	14800	d-d band	
	11200	d-d band	

Field set : 3000G
Scan range : 2000G

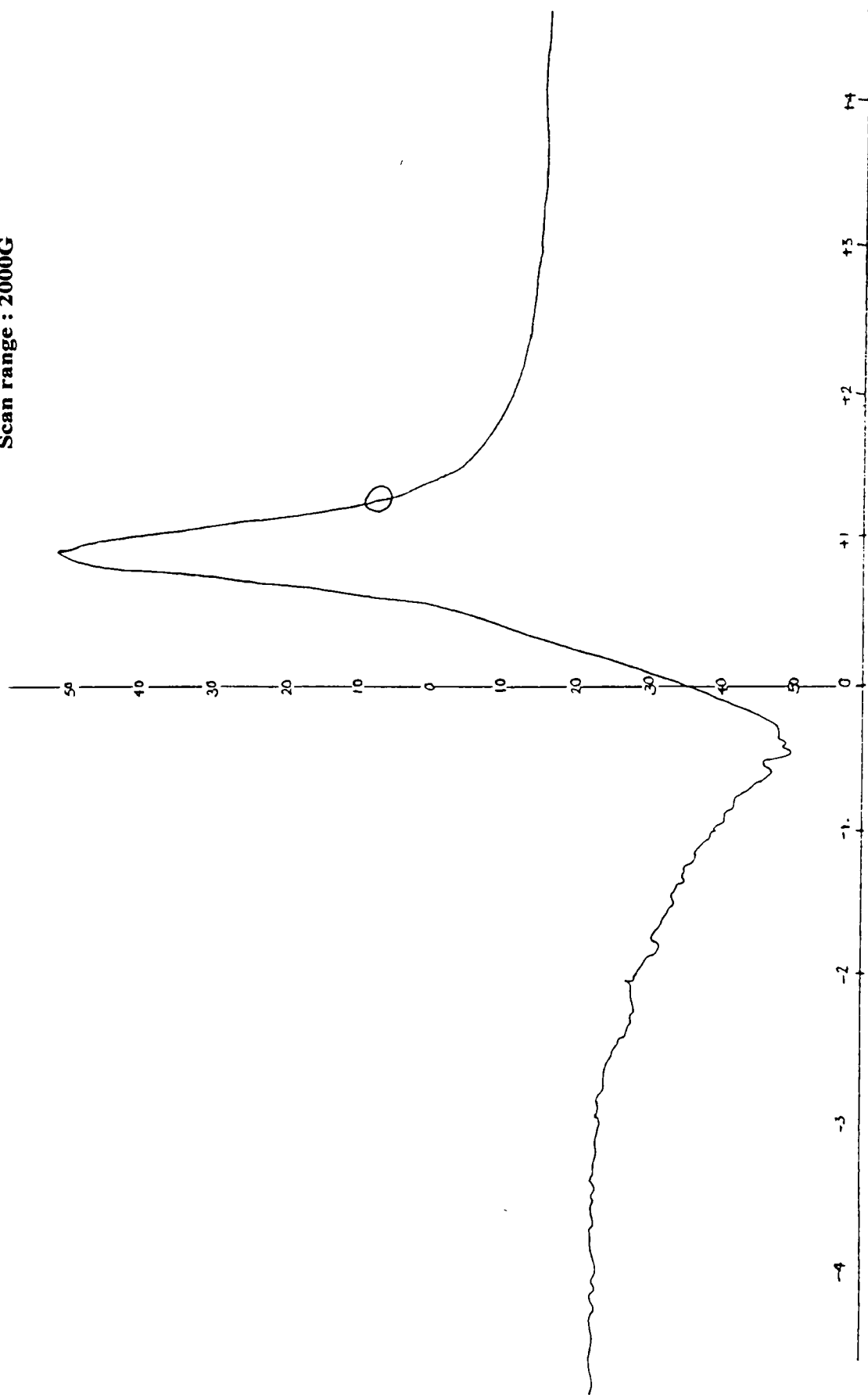


Fig III.20: EPR Spectrum of YCuAb recorded at LNT

$$g_{11} = 2.4; A_{11} = 188 \times 10^{-4} \text{ cm}^{-1}$$

$$g_{\perp} = 2.08; A_{\perp} = 58 \times 10^{-4} \text{ cm}^{-1}$$

The large value of g_{11} could be due to the ionic environment about the metal ion. The ratio of g_{11}/A_{11} is 130 cm^{-1} . This value is rather close to that for a square planar complex (24). Probably, this might be the reason for the complex exhibiting higher catalytic activity in the decomposition of hydrogen peroxide (described in page 107 of Chapter VI) as compared to YCuEm or CuY. A magnetic moment value (1.94 B.M) calculated using the epr parameters also indicates a square planar geometry for the metal complex in the zeolite. The value of in-plane covalence parameter (α^2) is around 0.9, which indicates the ionic nature of the metal-ligand bond.

3.2.2.7 XRD:

A comparison of the the powder XRD patterns of the encapsulated complexes and that of the parent zeolite (Fig.III.21) reveal that the crystallinity has been retained after the encapsulation procedure.

3.2.2.8 Thermal behaviour:

The TG data of the encapsulated complexes are given in Table III.11.

TABLE III.11

TG data of the Zeolite encapsulated complexes of 2-aminobenzimidazole

Sample	Temp. Range in TG	Weight loss (%)
YMnAb	50-330	23.45
YCoAb	30-500	23.5
YNiAb	50-600	24
YCuAb	50-260	20
	280-475	5.88

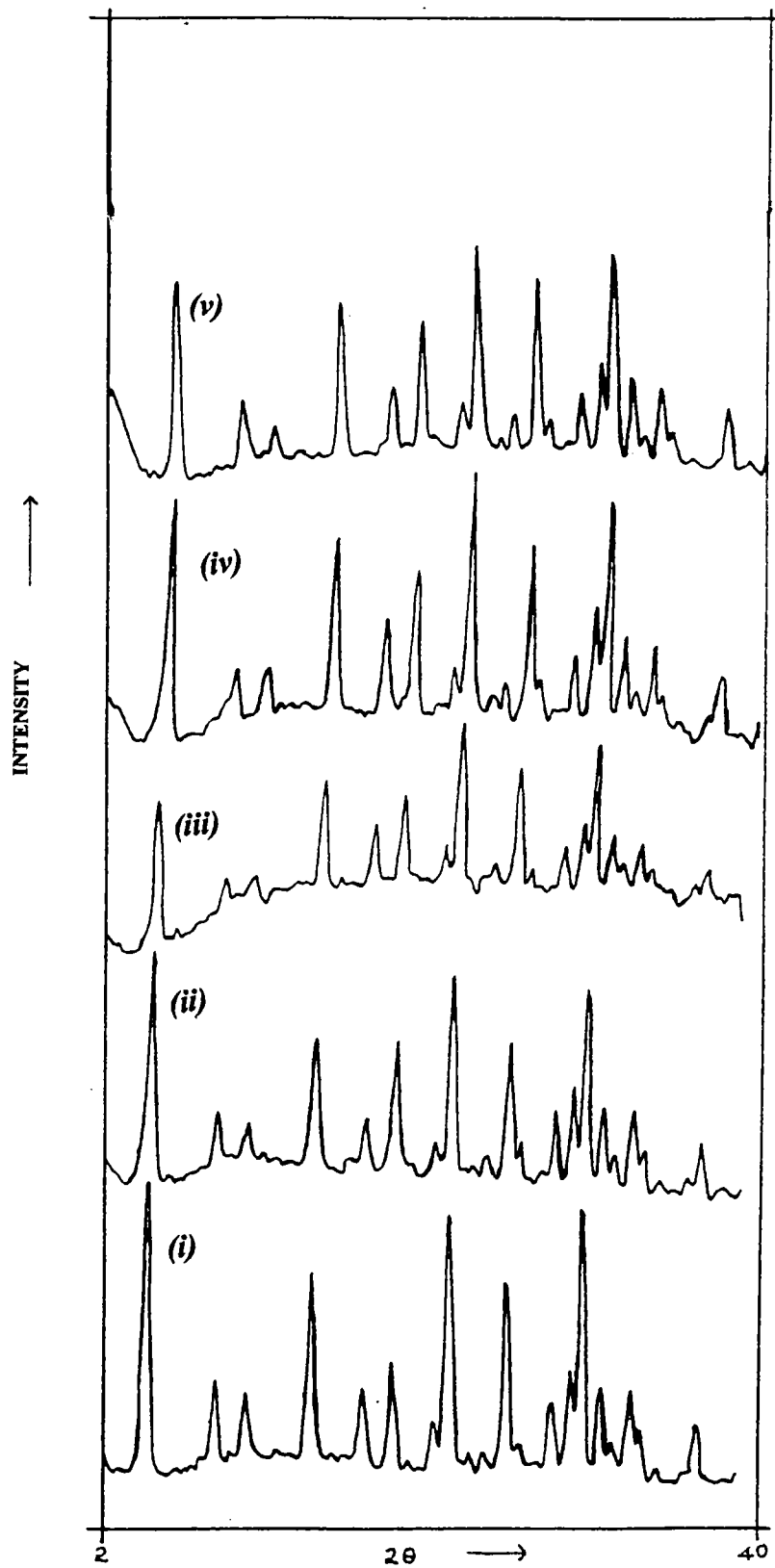


Fig III.21: XRD Patterns of (i) NaY (ii) YMnAb (iii) YCoAb (iv) YNiAb (v) YCuAb

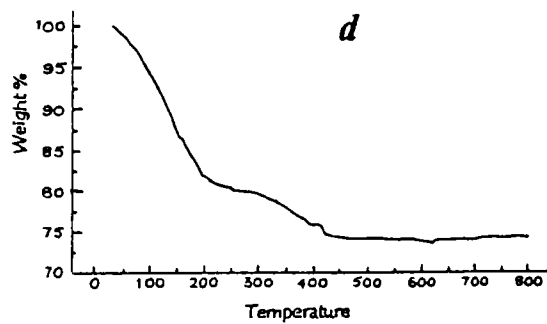
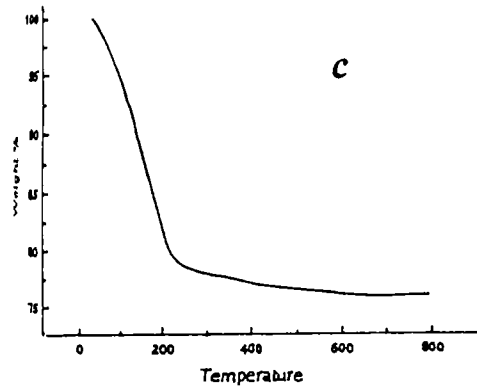
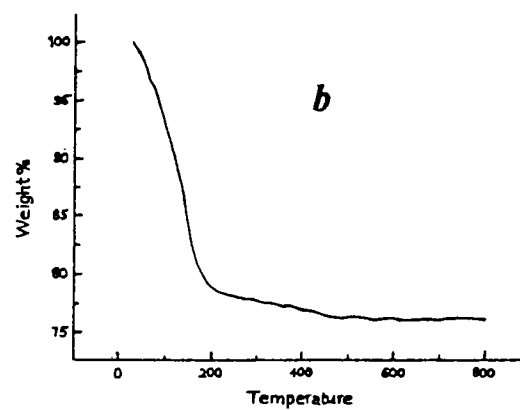
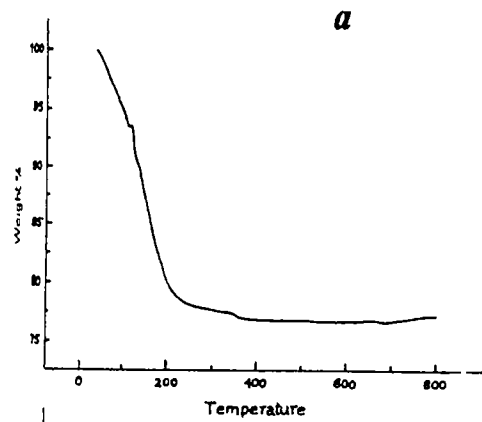


Fig III.22: TG pattern of (a) YMnAb (b) YCoAb (c) YNiAb (d) YCuAb.

The thermogravimetric analyses of the complexes were performed in an inert atmosphere at a heating rate of 20⁰C per minute. With the exception of YCuAb, the complexes exhibit a one step decomposition (Fig III.22). This could be due to the simultaneous removal of water and the complex. In the case of the copper complex it is to be noted that the weight loss due to decomposition of the ligand part and that due to the loss of water can be discriminated. A comparison of the thermal stabilities of these complexes with that of the complexes of embelin in zeolite indicates that the latter group of complexes are superior in terms of thermal stability.

REFERENCES

- [1] C.R. Chang and T.G. Taylor, *J. Am. Chem. Soc.*, **1973**, *95*, 8475.
- [2] K.J. Balkus Jr and A.G. Gabrielov, *J. Inclusion Phenom. Mol. Recogn. Chem.*, **1995**, *21*, 159.
- [3] C. Tollman and N. Herron, *Symposium on Hydroc. Oxidation*, 194th National Meeting of the American Chemical Society, New Orleans, LA, Aug. 30-Sept. 4, 1987.
- [4] P.M. Edgardo; G. Nyole; L. Fabio; D.D. Acosta; P. Pasquale; L.G. Aldo; R. Patricio and D. Bernard, *J. Phys. Chem*, **1993**, *97*, 12819.
- [5] S.P. Varkey and C.R. Jacob, *Ind. J. Chem*, **1998**, *37A*, 407.
- [6] S. K. Tiwary and S. Vasudevan, *Inorg. Chem.* **1998**, *37*, 5239.
- [7] A.K. Mukherjee and P.Ray, *J. Ind. Chem. Soc.*, **1955**, *32*, 581, 604.
- [8] Alan Earnshaw, *Introduction to Magnetochemistry*, Academic Press, London, 1968.
- [9] N.N. Greenwood and A. Earnshaw, *Chemistry of the Elements*, Pergamon Press, 1984
- [10] T.A. Egerton; A. Hagan; F.S. Stone and J.C. Vickerman, *J. Chem. Soc. Faraday Trans. I*, **1972**, *68*, 723.
- [11] B.N. Figgis and J. Lewis, *Progress in Inorganic Chemistry*, F.A. Cotton Ed.; Interscience Publishers, New York, Vol. VI, 1964.
- [12] L.J. Bellamy, *The Infrared Spectra of Complex Molecules*, Vol.I, III Ed.; Chapman and Hall, London
- [13] K.K.A. Rashid; J. Chacko and P.N.K. Nambisan, *Polyhedron*, **1983**, *2(4)*, 293.
- [14] R.S. Bottei and J.T. Fangman, *J. Inorg. Nucl. Chem.*, 1966, *28*, 1259.
- [15] H.D. Coble and H.F. Holtzclaw Jr, *J. Inorg. Nucl. Chem.*, **1974**, *36*, 1049.
- [16] K. Klier; R. Kellerman and P.J. Hutta, *J. Chem. Phys.*, **1974**, *61*, 4224.
- [17] A.B.P. Lever, *Inorganic Electronic Spectroscopy*, Elsevier, Amsterdam, 1968.
- [18] P.J. Hutta and J.H. Lunsford, *J. Chem. Phys.*, **1977**, *66*, 4716.

- [19] V.J. Patel and M.N. Patel, *Ind. J. Chem.*, **1989**, 28A, 428.
- [20] J.H. Lunsford, *ACS Symp. Ser.*, **1977**, 40, 473.
- [21] C.C. Chao and J.H. Lunsford, *J. Chem. Phys.*, **1972**, 57, 2890.
- [22] C.J. Vedrine *In Characterisation of Heterogeneous catalysts*, F. Delanny Ed.; Marcel Dekker, New York, 1984.
- [23] C. Naccache and Y. Ben Taarit, *Chem. Phys. Letters*, **1971**, 11, 11.
- [24] U. Sakaguchi and A.W. Addison, *J. Chem. Soc. Dalton Trans.*, **1979**, 600.
- [25] R.A. Palmer; W.C. Tennant; M.F. Dix; and A.D. Rae, *J.C.S. Dalton*, **1976**, 2345.
- [26] H.J. Stoklosa; G.L. Seebach and J.R. Wasson, *J. Phys. Chem.*, **1974**, 78, 962.
- [27] H. Yokoi, *Bull. Chem. Soc. Jpn.*, **1974**, 47, 3037.
- [28] A. Bencini and D. Gatteschi, *In Transition Metal Chemistry*, G.A. Melson and B.N. Figgis Ed.; Marcel Dekker Inc., New York, 8, 1965.
- [29] D. Kivelson and R. Neiman, *J. Chem. Phys.*, **1961**, 35, 149.
- [30] B.V. Agarwala, *Inorg. Chim. Acta.*, **1979**, 36, 209.
- [31] B.P. Block, *Inorganic Polymers*, F.G.A. Stone and W.A.G. Graham Ed.; Academic Press, London, 1962.
- [32] R.S. Bottei and D.L. Greene, *J. Inorg. Nucl. Chem.*, **1968**, 30, 1469.
- [33] K.J. Morgan, *J. Chem. Soc.*, **1961**, 2343.

CHAPTER IV

TRANSITION METAL COMPLEXES OF POLYMER BOUND SCHIFF BASES

INTRODUCTION

The compounds embelin and 2-aminobenzimidazole were each reacted with a functionalised polystyrene support to prepare the respective polymer bound Schiff bases. These polymer bound Schiff bases were then treated with metal salts in order to study the heterogenization of metal complexes by employing an organic support and to compare the properties of these complexes with those of the complexes heterogenized using an inorganic support like zeolite. Chloromethylpolystyrene was used as the supporting polymer matrix. This was converted to aminomethylpolystyrene for the condensation with embelin. For reaction with aminobenzimidazole the initial step was the conversion of chloromethylpolystyrene to polystyrene aldehyde. Eventhough a complete characterization of polymer bound complexes is not possible, an attempt has been made to gather information about the environment surrounding the metal ion using the following analytical techniques: FTIR, electronic and EPR spectroscopy; magnetic susceptibility measurements, TG and surface area analyses. A knowledge of the environment around the metal, which is necessary for the proper understanding of their involvement in catalytic reactions and other useful technological applications, may be obtained from such studies.

This chapter is divided into two parts. The first part deals with studies on the complexes of the polymer anchored Schiff base of embelin while the second part deals with the studies of the complexes of the polymer anchored Schiff base of 2-aminobenzimidazole.

4.1. TRANSITION METAL COMPLEXES OF THE SCHIFF BASE DERIVED FROM POLYMER BOUND AMINE AND EMBELIN

Manganese(II), cobalt(II), nickel(II) and copper(II) complexes of the polymer bound Schiff base derived from embelin and aminomethyl polystyrene were prepared and characterised. The details of these studies are presented in this section.

4.1.1 EXPERIMENTAL

4.1.1.1 Materials:

Details regarding the materials used are given in Chapter II. Preparation of the polymer bound amine and polymer bound Schiff base are also described therein.

4.1.1.2 Preparation of the complexes:

The polymer bound complexes of Mn(II), Co(II), Ni(II) and Cu(II) ions were prepared by the same general procedure. Chloromethylpolystyrene was first converted to the polymer bound amine and then to polymer bound embelin. The polymer bound embelin was suspended in methanol for two hours. After two hours an excess of metal chloride in methanol was added to this in one portion and the vessel was sealed. It was then shaken for six hours using a mechanical shaker. After shaking, the mixture was allowed to stand for another six hours. It was then filtered, washed with methanol, ethanol, chloroform and acetone and dried in vacuum over anhydrous calcium chloride.

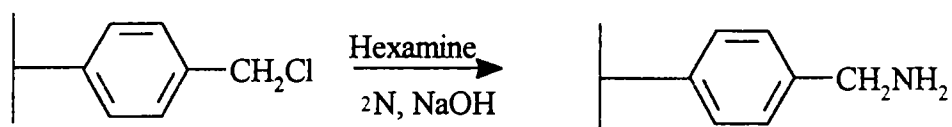
4.1.1.3 Analytical methods:

Details about the analytical methods and other characterization techniques are given in Chapter II.

4.1.2 RESULTS AND DISCUSSION:

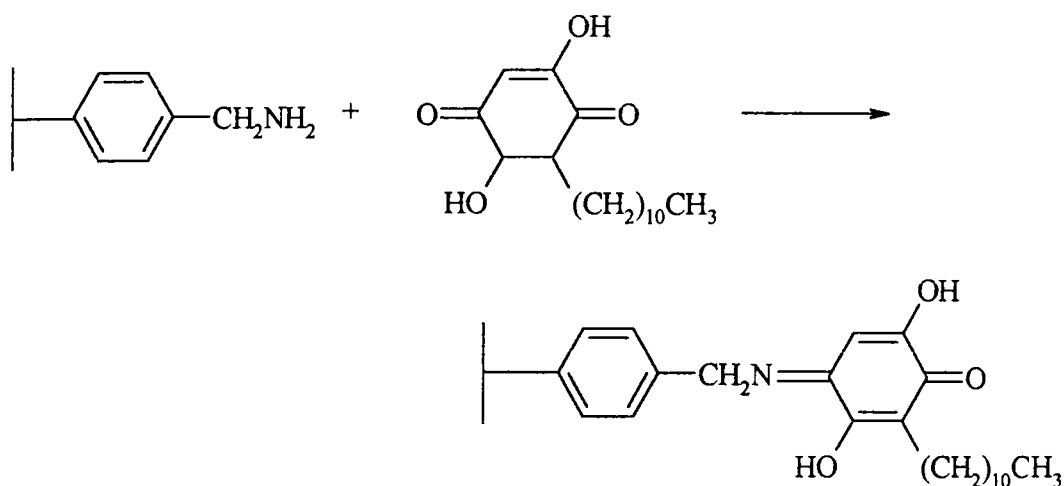
A few remarks regarding the structure of polymer bound complexes must necessarily precede the discussion of the present investigation. Detailed information on the structure of polymer bound complex is very difficult to obtain. Elemental analysis of the complexes provides only small amount of information. Most often, the identifications have been based on comparisons between the spectra of the unsupported metal complexes and those of analogous attached species. If the complex species on the polymer is of very low concentration, the analysis of the spectrum becomes difficult. Problems also arise when there is no analogous unsupported species. Even if the comparisons are possible detailed information about the micro and macroenvironment of the metal ion, the nature of the ligands present and structural changes of the polymer support during complexation is usually not known.

Chloromethylated polystyrene (crosslinked with 2% divinylbenzene, 3.7 meq. of chlorine /g) as macroporous beads of surface area $154\text{m}^2/\text{g}$ was used as the starting material in the present investigation. The chloromethyl groups in the resin were converted to amino groups by treatment with hexamethylene tetramine and potassium iodide. This reaction is a polymer analogous extension of the Delepine reaction. Activated halides react with hexamethylenetetramine in a non-aqueous medium to form an iminium salt, which is hydrolyzed by hydrochloric acid to produce the corresponding amine hydrochloride (1). The reaction is depicted in the following scheme



Scheme I. Preparation of Aminomethylpolystyrene

The amino resin gave a deep blue colour with ninhydrin reagent characteristic of the amino group. The amino capacity of the resin was determined by treatment of the resin with excess standard hydrochloric acid and back titration of the excess acid. The amino capacity determined was found to agree with the percentage nitrogen obtained from microanalysis. The aminomethylpolystyrene was condensed with embelin to give the polymer bound ligand, PEm, as shown in the following scheme.



Scheme II. Preparation of Schiff base

Using this ligand, complexes of Mn(II), Co(II), Ni(II) and Cu(II) were prepared. The analytical data for these complexes are given in Table IV.1. In arriving at probable structures, the percentage nitrogen obtained from elemental analysis of the ligand has been taken as the standard. Nitrogen present in the polymer bound Schiff base, PEm, was found out to be 3.57 mmols on analysis. It is assumed that two polymer bound Schiff base units are coordinated to a metal ion.

TABLE IV-1*Analytical data of the metal complexes of the PEm*

Compound/ colour	Elements (%) found / (calc.)					Metal binding capacity of the resin ^a
	Metal	Cl	C	H	N	
PEmMn/ Brownish yellow	1.70/ (1.68)	3.00/ (2.67)	79.90/ (80.80)	7.50/ (7.65)	2.56/ (2.60)	30.9
PEmCo/ Beige	1.89/ (1.90)	9.60/ (9.53)	75.00/ (76.30)	6.90/ (7.00)	2.82/ (2.84)	32.0
PEmNi/ Light green	1.63/ (1.65)	2.10/ (2.03)	78.50/ (79.90)	7.20/ (7.33)	2.40/ (2.36)	28.0
PEmCu/ Beige	2.90/ (2.88)	-	78.10/ (78.50)	7.03/ (7.20)	3.24/ (3.17)	45.6

^a Calculated from the observed value of metal ion percentage in the resin using the formula

$$\text{Binding capacity} = \frac{\text{Metal\% (observed)} \times 1000}{\text{Atomic weight of metal}}$$

4.1.2.1 Magnetic Susceptibility Measurements:

Magnetic susceptibilities were measured at room temperature by the Gouy method. Magnetic moment values calculated for polymer supported complexes are often taken as a qualitative rather than a quantitative guide, as the molecular weight and empirical formulae calculated are only approximate. χ_M values were calculated using the empirical formula weight for the anchored simple complexes. The diamagnetic correction for the whole polymeric complex has been calculated and was subtracted from the χ_M values to get χ_M' values. In the present study we have

employed the procedure developed by Syamal and Singh (2) for calculating the diamagnetic susceptibility in polystyrene supported complexes. The magnetic moment values are given in Table IV.4.

Magnetic moment values of 5.9 B.M, 4.7 B.M and 3.00 B.M observed respectively for the manganese(II), cobalt(II) and nickel(II) complexes indicate octahedral geometries for these complexes. The μ_{eff} value for the Cu(II) complex, PEmCu is 1.9 B.M which indicates a planar arrangement of ligands around the metal ion (3)

4.1.2.2 Surface Area Analyses:

The surface area of the polymer support as well as that of the polymer supported complexes are given in Table IV.2. A decrease in surface area was observed after loading the metal ions on the polymer support. This may be due to blocking of pores of the polymer support after introduction of the ligand as well as the metal ion. Similar results have been reported for the polymer supported complexes (4).

TABLE IV-2

Surface analyses of the polymer support and metal complexes of PEm

Sample	Surface area (m ² /g)
Aminomethyl polystyrene	154
PEmMn	49.6
PEmCo	48.8
PEmNi	55
PEmCu	37.8

TABLE IV-3

IR Spectral data of PEm and the transition metal complexes of PEm (cm⁻¹)

PEm	PEmMn	PEmCo	PEmNi	PEmCu
3375(w)	3376(w)	3375(w)	3376(w)	3375(w)
3036(w)	3036(w)	3032(w)	3035(w)	3036(w)
2923(s)	2923(s)	2923(s)	2924(s)	2924(s)
2852(s)	2854(s)	2853(s)	2855(s)	2853(s)
1700 (vs)	1690 (s)	1685 (s)	1680 (s)	1696 (s)
	1674 (s)	1674 (s)	1674 (s)	1674 (s)
1657 (s)	1647 (s)	1648 (s)	1648 (s)	1647 (s)
1610 (s)	1610 (s)	1610 (s)	1610 (s)	1610 (s)
1522 (s)	1524 (s)	1517 (s)	1527 (s)	1523 (s)
1501 (s)	1501 (s)	1500 (s)	1499 (s)	1501 (s)
1459 (s)	1459 (s)	1459 (s)	1459 (s)	1459 (s)
1435 (s)	1435 (s)	1435 (s)	1435 (s)	1435 (s)
1399 (s)	1398 (s)	1399 (s)	1390 (s)	1390 (s)

(cont....)

PEm	PEmMn	PEmCo	PEmNi	PEmCu
1366 (s)				
	1311 (m)	1311 (m)	1311 (m)	1311 (m)
1217 (s)	1216 (s)	1216 (s)	1214 (s)	1216 (s)
1172 (m)	1174 (m)	1173 (m)	1171 (m)	1172 (m)
1117 (m)	1115 (m)	1117 (m)	1117 (m)	1116 (m)
1072 (w)	1068 (w)	1068 (w)	1068 (w)	1072 (w)
1026 (w)	1018 (w)	1019 (w)	1020 (w)	1023 (w)
982 (w)	983 (w)	983 (w)	986 (w)	986 (w)
910 (w)	910 (w)	906 (w)	910 (w)	900 (w)
835 (m)	830 (m)	830 (m)	835 (m)	837 (m)
762 (w)				
703 (w)				
606 (w)	606 (w)	606 (w)	608 (w)	603 (w)
459 (w)				

4.1.2.3 Infrared spectra:

The FTIR spectral data of the polymer support, ligand, polymer anchored ligand and polymer supported complexes is given in Table IV.3. A strong band seen at 1700 cm^{-1} could be due to the C=O stretching of the free carbonyl group of the anchored ligand. This band is seen to shift to 1674 cm^{-1} (fig.IV.1) in the complexes which indicates coordination of the carbonyl group. The C=N stretching of the azomethine group is observed at 1657 cm^{-1} in the polymer bound embelin. This band is seen at $\sim 1647\text{ cm}^{-1}$ in the spectra of the complexes which suggests participation of the azomethine nitrogen in coordination. Weak bands are observed 3375 cm^{-1} and 3036 cm^{-1} in the spectra of the complexes and the polymer bound ligand, due to the presence of unreacted amino groups in the polymer chain (5,6).

4.1.2.4 Electronic spectra

The electronic spectral data of the complexes are given in Table IV.4. The interpretation of these data gives an idea of the structure of the metal complexes.

Manganese(II) complex:

Bands observed around 21850 cm^{-1} and 19600 cm^{-1} could be assigned to ${}^4A_{1g} \leftarrow {}^6A_{1g}$ and ${}^4T_{2g} \leftarrow {}^6A_{1g}$ respectively. The transition ${}^4E_g(G) \leftarrow {}^6A_{1g}$ expected around 25000 cm^{-1} is probably obscured by the strong ligand/charge transfer absorption at 28000 cm^{-1} . The above spectral bands along with the the magnetic moment of 5.89 B.M suggests an octahedral geometry for PEmMn (7).

Cobalt(II) complex:

The cobalt (II) complex, PEmCo, exhibits bands at 20360 cm^{-1} and 9200 cm^{-1} which can be assigned to ${}^4T_{1g}(P) \leftarrow {}^4T_{1g}(F)$ and ${}^4T_{2g}(F) \leftarrow {}^4T_{1g}(F)$ transitions.

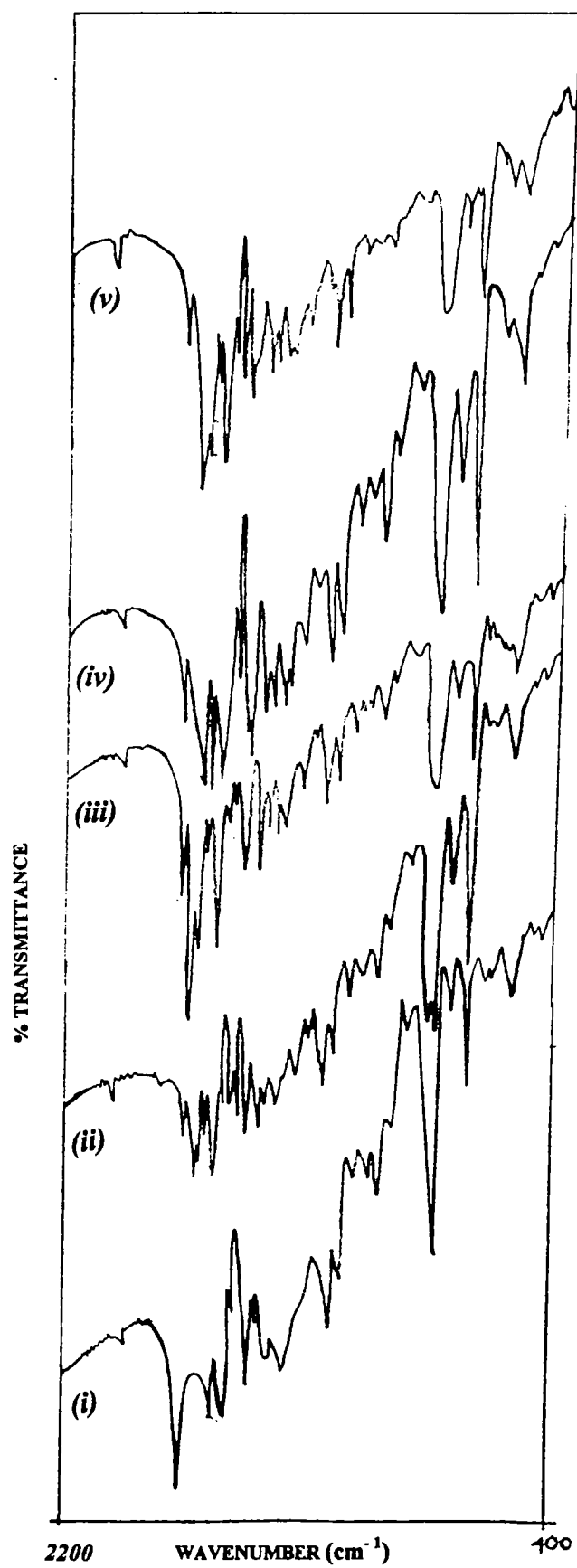


Fig IV. 1 FTIR spectrum of (i) PEm (ii) PEmMn (iii) PEmCo (iv) PEmNi (v) PEmCu.

These transitions coupled with the magnetic moment of 4.7 B.M indicate a somewhat distorted octahedral geometry around the Co (II) ion. The intense bands observed at 33300 cm⁻¹ and 25000 cm⁻¹ can be assigned to charge transfer or intra ligand transitions (7).

Nickel (II) complex:

, The Ni(II) complex, PEmNi, exhibits bands at 9620 cm⁻¹, 14120 cm⁻¹ and 22300 cm⁻¹. These bands can be assigned to the transitions ${}^3T_{2g}(F) \leftarrow {}^3A_{2g}(F)$, ${}^3T_{1g}(F) \leftarrow {}^3A_{2g}$ and ${}^3T_{1g}(P) \leftarrow {}^3A_{2g}(F)$ respectively which are in accordance with a Ni(II) complex having an octahedral geometry (7).

Copper (II) complex:

The copper(II) complex, PEmCu, exhibits a broad band in the region 12800-13000 cm⁻¹ characteristic of a Cu(II) ion in a tetrahedrally distorted planar structure (7).

4.1.2.5 EPR Spectra

The EPR spectrum (Fig IV.2) of the polymer anchored Cu(II) complex gives the following parameters:

$$g_{\parallel} = 2.3 ; A_{\parallel} = 148 \times 10^{-4} \text{ cm}^{-1}$$

$$g_{\perp} = 2.08 ; A_{\perp} = 44.5 \times 10^{-4} \text{ cm}^{-1}.$$

As expected, the esr data indicates that $g_{\parallel} > g_{\perp}$ and $A_{\parallel} > A_{\perp}$. Kivelson and Neiman (8) have demonstrated that for ionic environments around the metal ion g_{\perp} is normally ≥ 2.3 and for covalent environment g_{\parallel} is less than 2.3. Our polymer anchored complex, PEmCu belongs to the latter category.

For tetragonal Cu(II) complexes, G is given by (9)

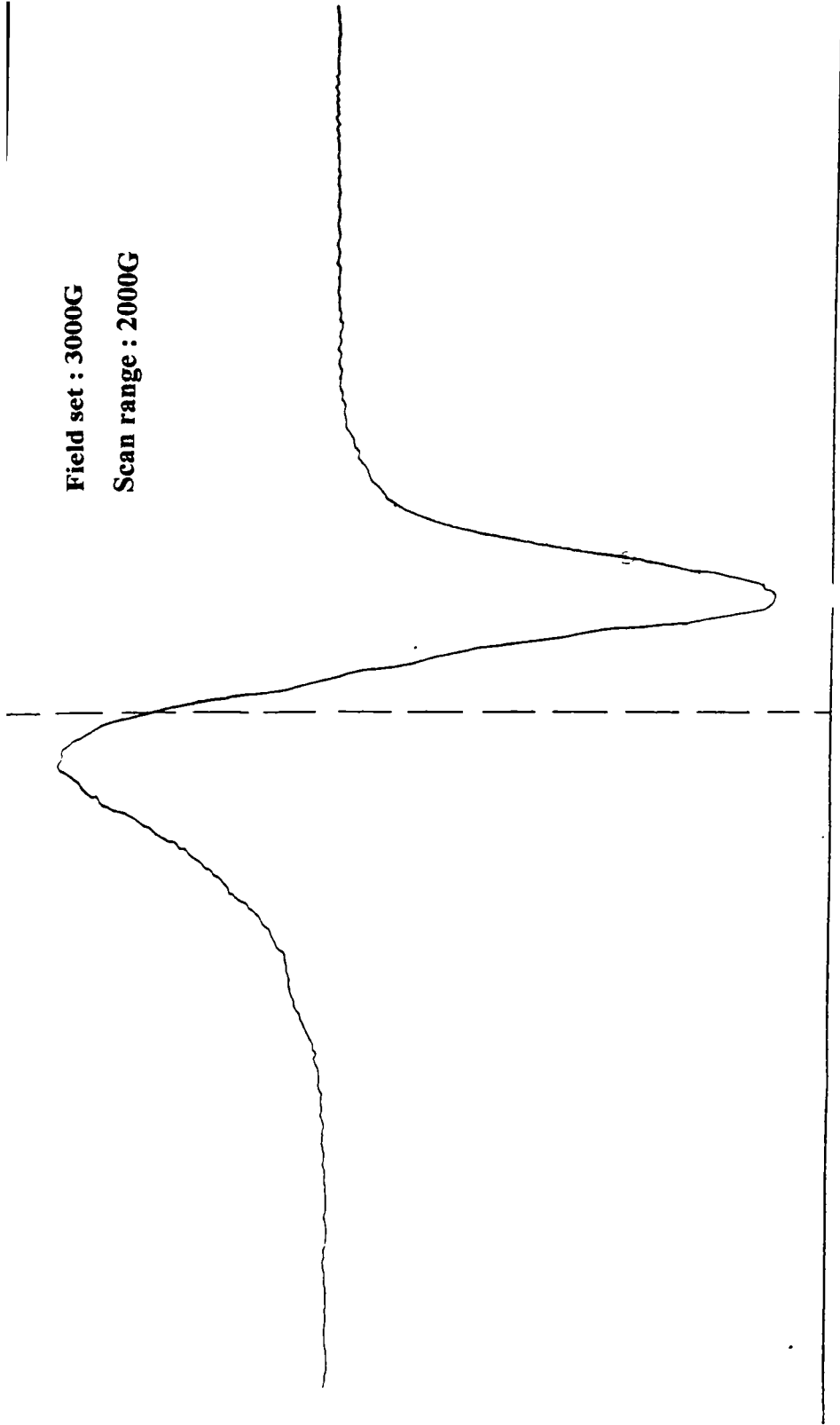


Fig IV.2: EPR Spectrum of PEmCu recorded at LNT

TABLE IV-4

Magnetic and electronic spectral data of the transition metal complexes of PEm.

Complex	Absorbance (cm ⁻¹)	Assignment	μ_{eff} (B M)
PEmMn	28000	charge transfer band	5.9
	21850	${}^4A_{1g} \leftarrow {}^6A_{1g}$	
	19600	${}^4T_{2g} \leftarrow {}^6A_{1g}$	
PEmCo	33300, 25000	charge transfer bands	4.7
	20360	${}^4T_{1g}(P) \leftarrow {}^4T_{1g}(F)$	
	9200	${}^4T_{2g}(F) \leftarrow {}^4T_{1g}(F)$	
PEmNi	27500	Charge transfer band	3.0
	22300	${}^3T_{1g}(P) \leftarrow {}^3A_{2g}(F)$	
	14120	${}^3T_{1g}(F) \leftarrow {}^3A_{2g}(F)$	
	9620	${}^3T_{2g}(F) \leftarrow {}^3A_{2g}(F)$	
PEmCu	39370	charge transfer band	1.9
	26250	charge transfer band	
	12800	d-d transition.	

$$G = (g_{\parallel} - 2.002) / (g_{\perp} - 2.002)$$

Assour et al. (10) have indicated that when G is less than 4.0, the ligand forming the Cu(II) complex can be considered as a strong field ligand. The value of $G = 3.82$ obtained for the complex indicates the strong field nature of the polymer anchored ligand. The in plane covalence parameter α_{Cu}^2 was calculated (8) and was found to be 0.78 which indicates the covalent nature of the complex. Further the value of $g_{\parallel}/A_{\parallel}$ is found to be 155 cm^{-1} which indicate tetrahedral distortion from the expected square planar structure resulting in a flattened tetrahedra (11)

The value of μ_{eff} calculated from the epr spectra is found to be 1.87 B.M and is close to the value calculated using the Guoy method.

4.1.2.6 Thermal behaviour

Thermal stability of polymer supported complexes is one of the most important criteria for high temperature applications. Thermogravimetric analyses of the polymer support and supported complexes were carried out from ambient temperature to 1000°C at a heating rate of $20^{\circ}\text{C min}^{-1}$. The TG/DTG data is given in Table IV.5.

Chloromethylpolystyrene decomposes in in four stages between 300°C and 700°C . The <2% weight loss below this temperature could be attributed to loss of moisture. The 96% weight loss at 700°C indicates a somewhat complete decomposition of the polymer. In the case of aminomethyl polystyrene the decomposition starts at the same temperature but is complete at $\sim 670^{\circ}\text{C}$. The polymer supported complexes starts decomposing after 50°C (Fig VI.3). This thermal instability seriously hinders the use of these systems in high temperature applications.

4.1.2.7 SEM

The SEM of PEmCu which shows the presence of metal complexes in the pores of the polymer support is given in Fig. IV.7.

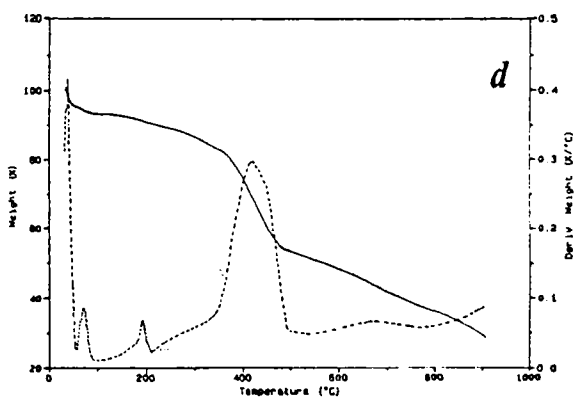
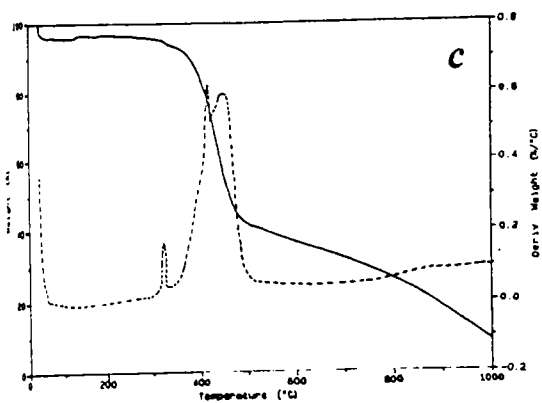
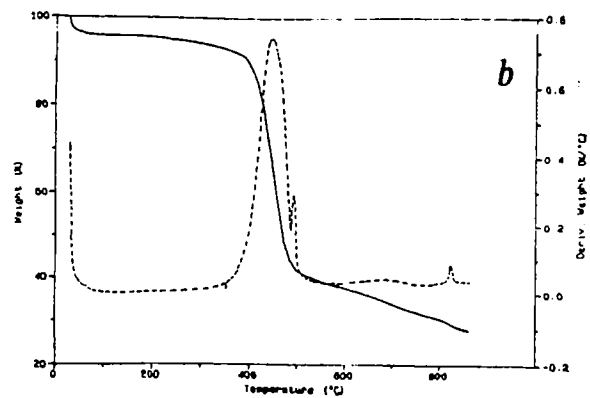
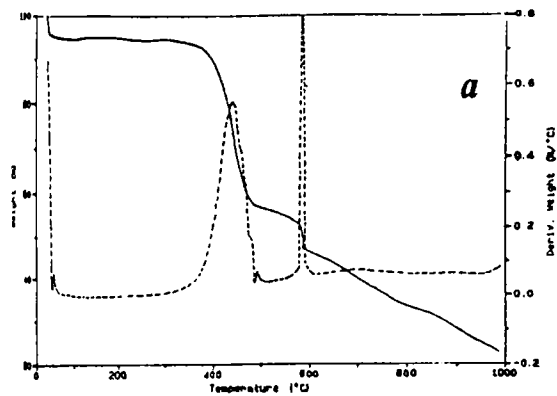


Fig IV.3: TG/DTG pattern of (a) PEmMn (b) PEmCo (c) PEmNi (d) PEmCu.

TABLE IV-5*TG/DTG data of the transition metal complexes of PEm.*

Sample	Peak temperature in DTG	Temperature range in DTG	Temperature range in TG	Percentage weight loss.
PEmMn	433	362-476	below 100°C	5
	577	576-581	362-476	38.7
			476-576	4.24
			576-581	6.39
PEmCo			590-990	23.47
	455	365-490	<360	6
	492	490-495	360-490	50
			490-495	2.5
PEmNi			495-860	13.5
	420	340-480	<340	6
	480	490-995	340-485	50
			485-1000	35
PEmCu				
	445	365-495	<370	21
			370-495	52.5
			495-865	13.5

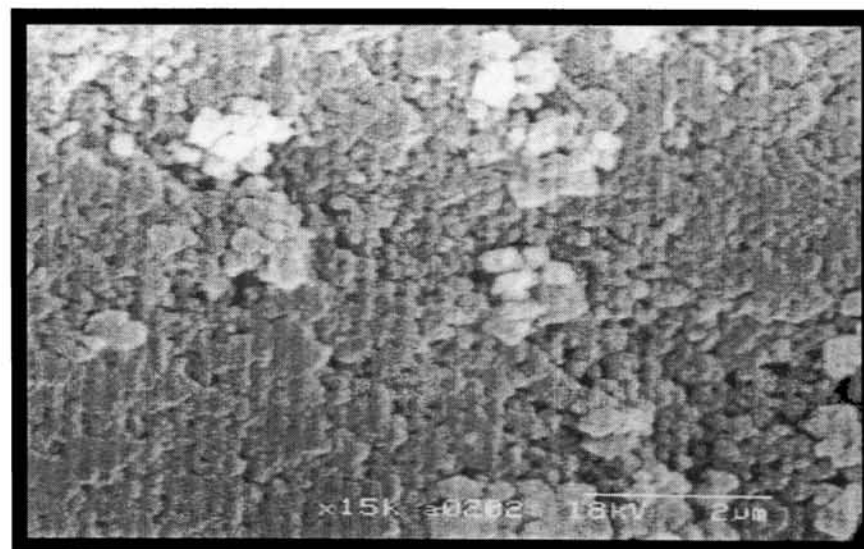
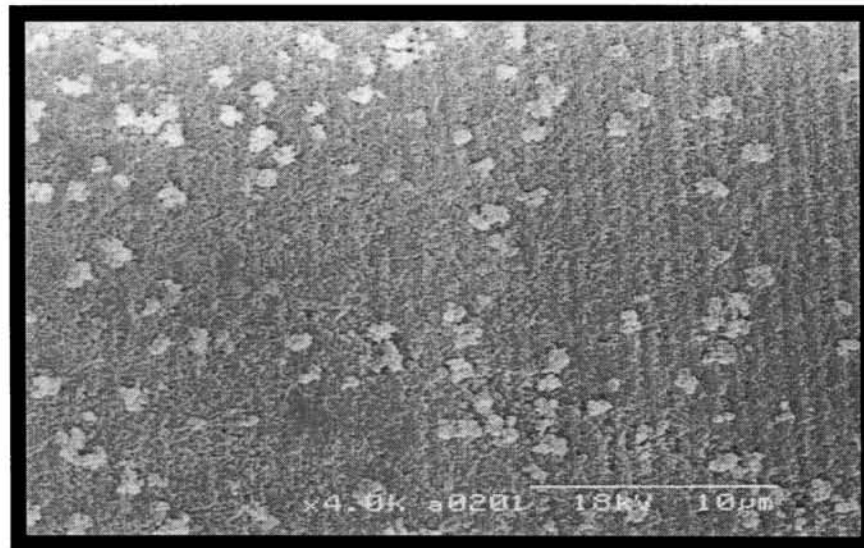
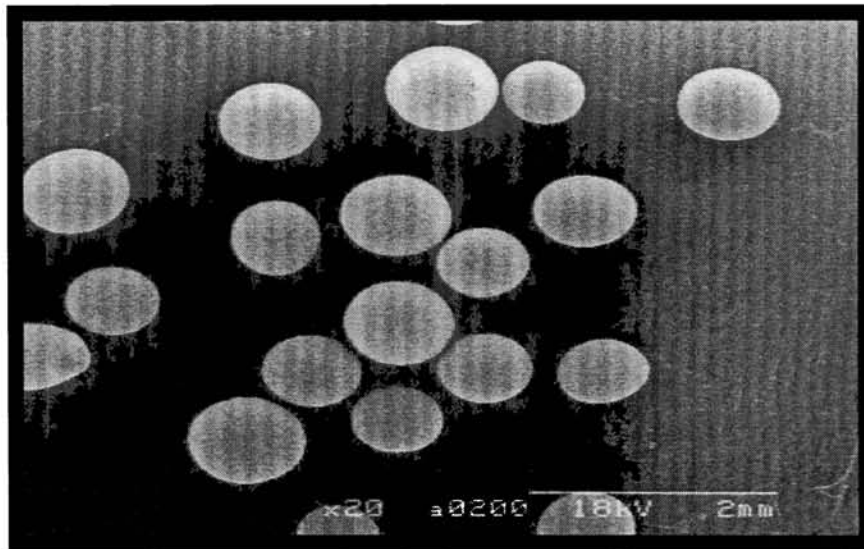


Fig. IV. 7 SEM of PEmCu at different magnifications

4.2. TRANSITION METAL COMPLEXES OF THE SCHIFF BASE DERIVED FROM POLYMER BOUND ALDEHYDE AND 2-AMINOBENZIMIDAZOLE

We have synthesized the Co(II) and Cu(II) complexes of the polymer bound Schiff bases formed by the condensation of polystyrene bound benzaldehyde and 2-aminobenzimidazole.

4.2.1 EXPERIMENTAL

4.2.1.1 Materials

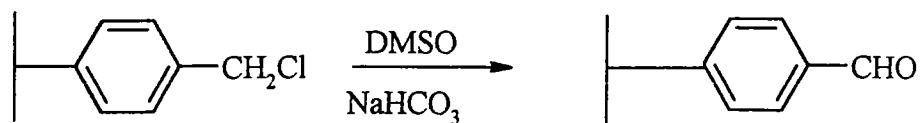
Details regarding the preparation of the polymer bound benzaldehyde from chloromethyl polystyrene and the conversion of polymer bound aldehyde to the Schiff base are given in Chapter II.

4.2.1.2 Synthesis of the complexes .

Polymer bound Schiff base (2.0g) was swollen in ethanol for 2 hours. An excess (0.1g) of the respective metal chloride was added and the reaction vessel was sealed. The mixture was shaken for five hours on a mechanical shaker. The resulting polymer bound metal complexes were filtered, washed with ethanol, methanol, chloroform, etc., and dried in vacuo over anhydrous calcium chloride.

4.2.2 RESULTS AND DISCUSSION

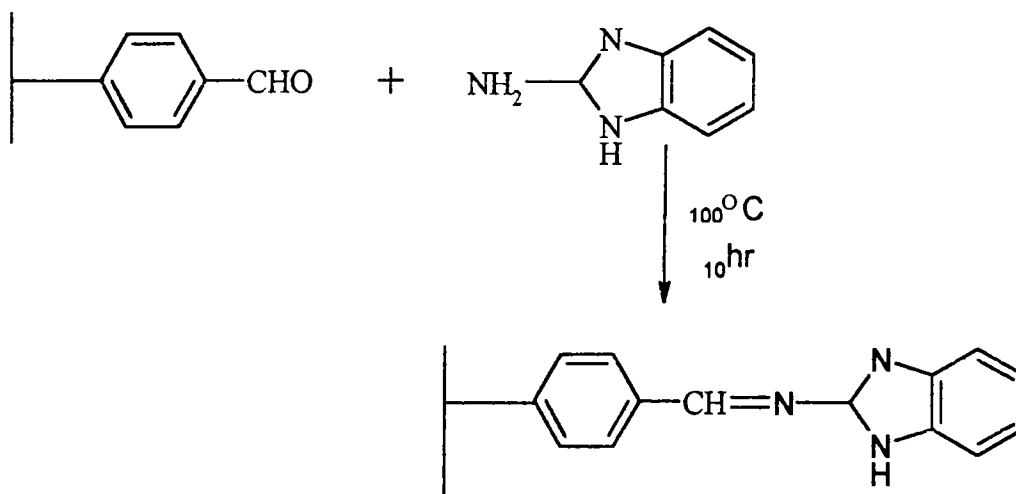
The chloromethylated polystyrene beads on treatment with DMSO and NaHCO₃ yield polymer bound benzaldehyde. The reaction is depicted in the following scheme



Scheme III. Preparation of Aldehyde resin

This is evidenced by a positive test with Borsche's reagent. The loading of aldehyde groups on the support was estimated by estimating the chlorine content of the beads. The chlorine content in the polymer bound aldehyde was found to be 0.2% which shows that almost all chloromethylene groups have been converted into the aldehyde. The formation of the aldehyde resin was further supported by the IR spectrum which showed a peak at 1698 cm^{-1} characteristic of the aldehydic ($\nu_{\text{C=O}}$) stretch (12).

The polymer bound benzaldehyde was then condensed with 2-amino benzimidazole to give the polymer bound Schiff base, PAb, as shown in Scheme IV. The nitrogen analysis of this sample indicates that 14% of the aldehyde groups have been converted to Schiff base units. This low conversion might be due to the large size of the benzimidazole molecule.



Scheme IV. Preparation of Schiff base

Treatment of this polymer bound Schiff base with the metal salt solutions yield the complexes. The cobalt complex is bright blue in colour while the copper complex is of bright green colour. The analytical data of the complexes are given in Table IV.6.

4.2.2.1 Magnetic measurements:

The magnetic measurements done at room temperature by the Gouy method yields a μ_{eff} value of 4.3 B.M for the cobalt complex, PAbCo and a value of 1.80 B.M for the copper complex, PAbCu. The magnetic moment of PAbCo lies in the range expected for tetrahedral complexes while that of PAbCu hints at a distorted planar structure (3).

4.2.2.2 Surface area analysis

The surface area of the polystyrene beads were measured before and after anchoring the ligands and complexes. A low surface area is observed for the complexes (Table IV.7). This could be due to the occupation of the complexes in the pores of the polymer(4).

4.2.2.3 Infrared spectra

The FTIR spectral frequencies are given in Table.IV.8. The infrared absorption observed at 1697 cm^{-1} in the aldehyde is shifted to 1680 cm^{-1} ($\nu_{\text{C=N}}$) indicating the formation of the polymer bound Schiff base. This band is shifted to 1675 cm^{-1} in the cobalt complex and to 1673 cm^{-1} in the copper complex (Fig IV.4) The shifting of this band clearly indicates coordination of the azomethine nitrogen (5,6). The band at 1512 cm^{-1} due to the ring nitrogen is also shifted to 1518 cm^{-1} in the complexes indicating coordination of the ring nitrogen.

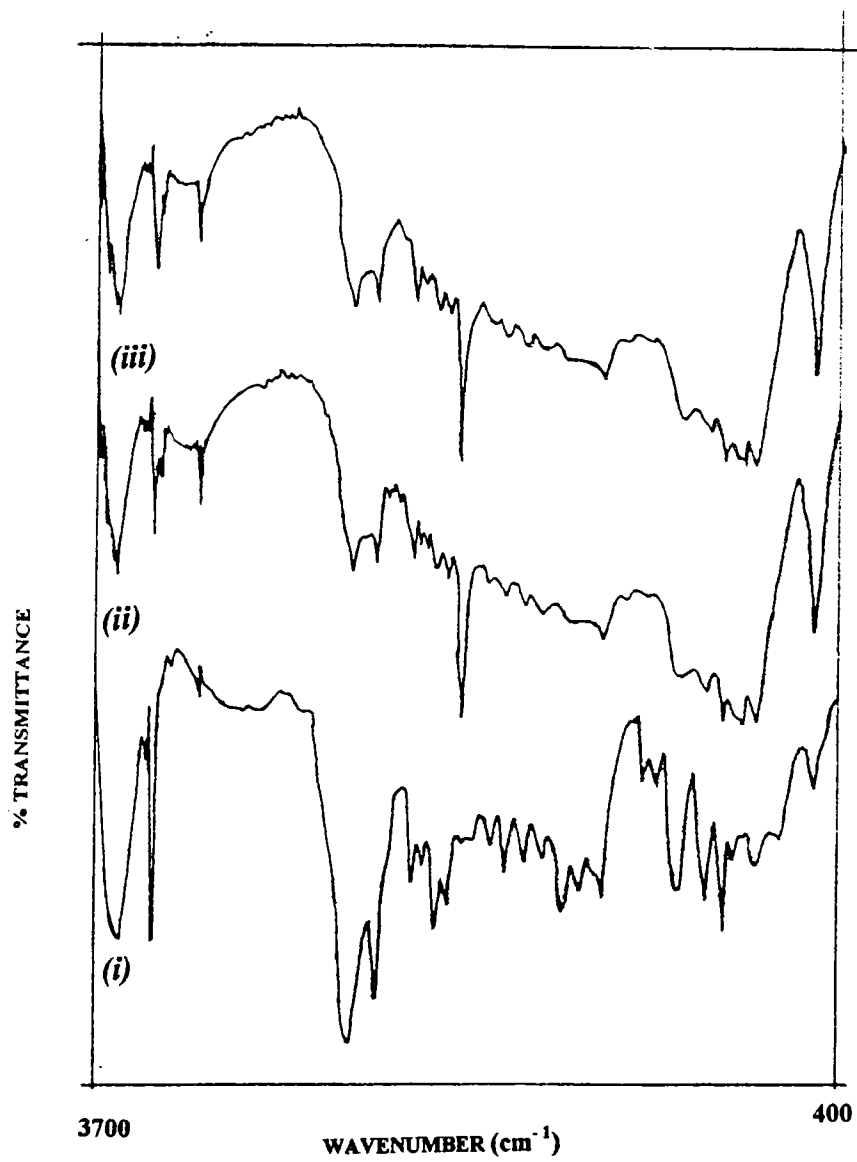


Fig IV.4 FTIR spectrum of (i) PAb (ii) PAbCu (iii) PAbCo.

TABLE IV-6*Analytical data of the transition metal complexes of PAb*

Sample	Element (%) found/(calc)				Metal binding capacity of resin
	M	C	H	N	
PAbCo	1.95/ (2.00)	73.40/ (72.80)	6.37/ (6.40)	2.80/ (2.87)	33
PAbCu	2.93/ (12.90)	81.00/ (80.30)	6.23/ (6.40)	3.80/ (3.86)	46

TABLE IV-7*Surface area of the support and transition metal complexes of PAb*

Sample	Surface area (m ² /g)
Polystyrene aldehyde	145
PAbCo	42
PAbCu	35

TABLE IV-8

IR spectral data of PAb and transition metal complexes of PAb (cm⁻¹)

PAb	PAbCo	PAbCu
3420	3432	3430
2926	2926	2926
2857	2857	2857
1680	1673	1673
1605	1605	1607
1512	1518	1518
1485	1485	1485
		1475
1451	1451	1451
1422	1422	1422
	1385	1385
1310	1310	1310
1266	1266	1266

(Cont.....)

PAb	PAbCo	PAbCu
1213	1213	1214
1171	-	1171
	1150	
1126	-	-
1080	1080	
1020.6	1020	1019
911	-	-
880	-	-
826	826	821
747	747	747
702	702	702
673	675	673
	648	648
615	615	613
553.6	-	-
459	463	459

4.2.2.4 Electronic Spectra

The electronic spectra was taken in the absorption mode . The spectral data are given in Table IV.9. Bands are observed at 22300 cm^{-1} and at 18850 cm^{-1} for the anchored complex PAbCo. These transitions might have originated from a tetragonal distortion of an octahedral structure. However, it would be erroneous to assign the transitions with only these two spectral bands. The copper complex PAbCu exhibits bands at 15800 cm^{-1} characteristic of a four-coordinated geometry with planar arrangement of ligands (7).

4.2.2.5 EPR Spectra

The EPR spectrum of PAbCu is given in Fig.IV.5. The following parameters were obtained from the spectrum;

$$g_{\parallel} = 2.27 ; A_{\parallel} = 97 \times 10^{-4} \text{ cm}^{-1}$$

$$g_{\perp} = 2.06 ; A_{\perp} = 40 \times 10^{-4} \text{ cm}^{-1}$$

The g_{\parallel} value of 2.27 indicate a covalent environment for the metal ion. The value of G was calculated and found to be 4.18 which indicates that this polymer anchored ligand is not a strong field one like the polymer anchored embelin discussed in the previous section. The in- plane covalence parameter α^2_{Cu} was obtained as 0.6 which indicates more covalence in the metal -ligand bond of the polymer bound complexes of aminobenzimidazole compared to polymer supported complexes of embelin. The quotient $g_{\parallel}/A_{\parallel}$ was found to be 234 cm^{-1} which suggests a tetragonal distortion of the square planar structure.

The μ_{eff} value calculated for the Cu(II) complex from the esr parameters is about 1.846 B.M. This value is close to 1.80 B.M calculated by the room temperature Guoy method.

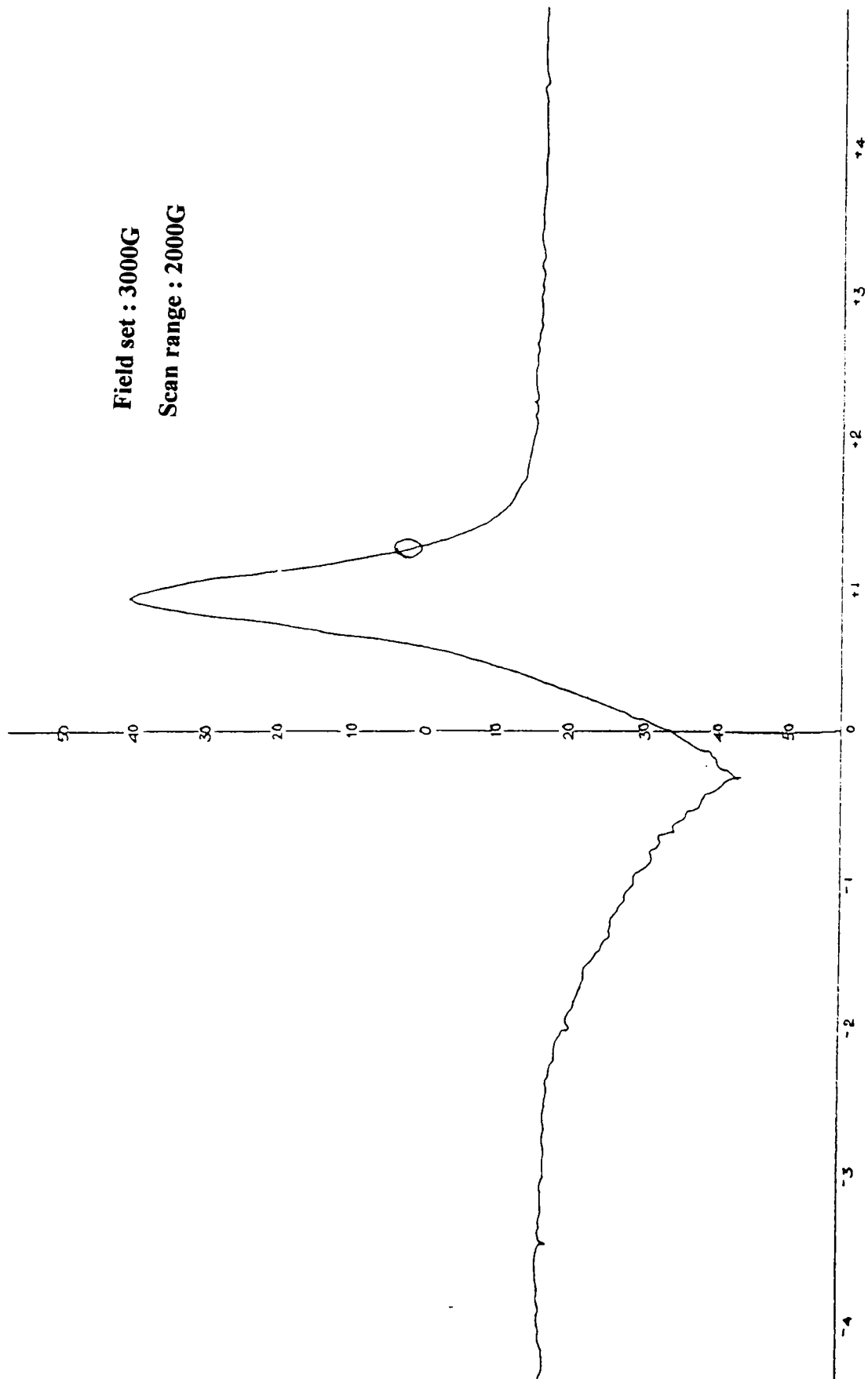


Fig IV.5: EPR Spectrum of PAbCu recorded at LNT

TABLE IV-9

Magnetic and Electronic Spectral data of the transition metal complexes of PAb

Sample	Absorption maxima (cm ⁻¹)	Tentative assignment	μ_{eff} (BM)
PAbCo	28000	Charge transfer band	4.3
	22300	d-d transition	
	18850	d-d transition	
PAbCu	25000	Charge transfer band	1.8
	15800	d-d transition	

TABLE IV.10

TG data of the the transition metal complexes of PAb

Sample	Temperature range in TG	Weight loss (%)
PAbCo	30-190	2
	190-590	96
PAbCu	30-90	2.9
	90-555	93

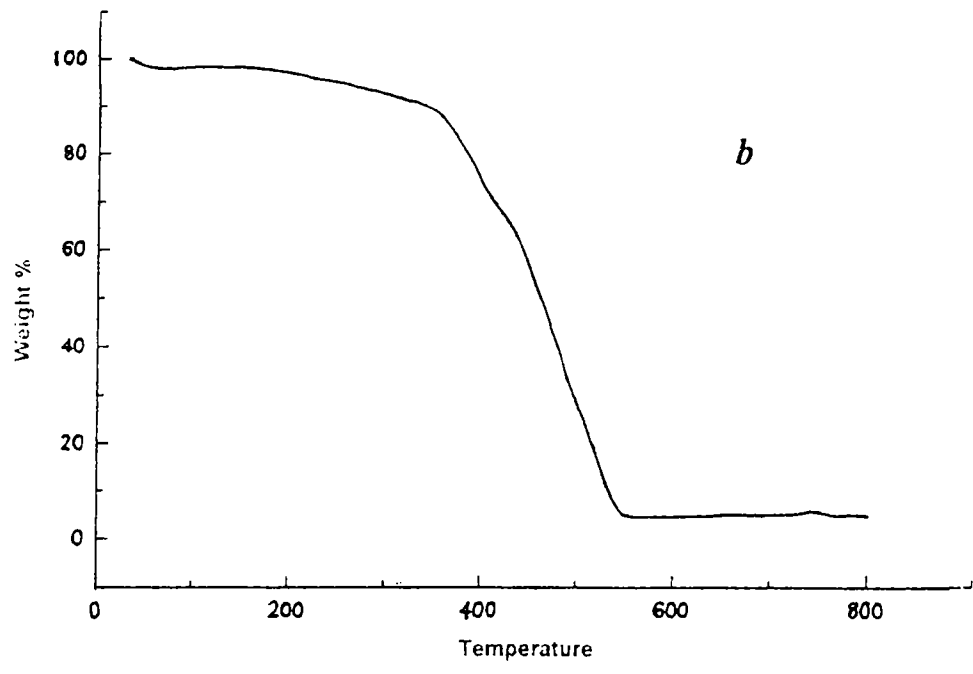
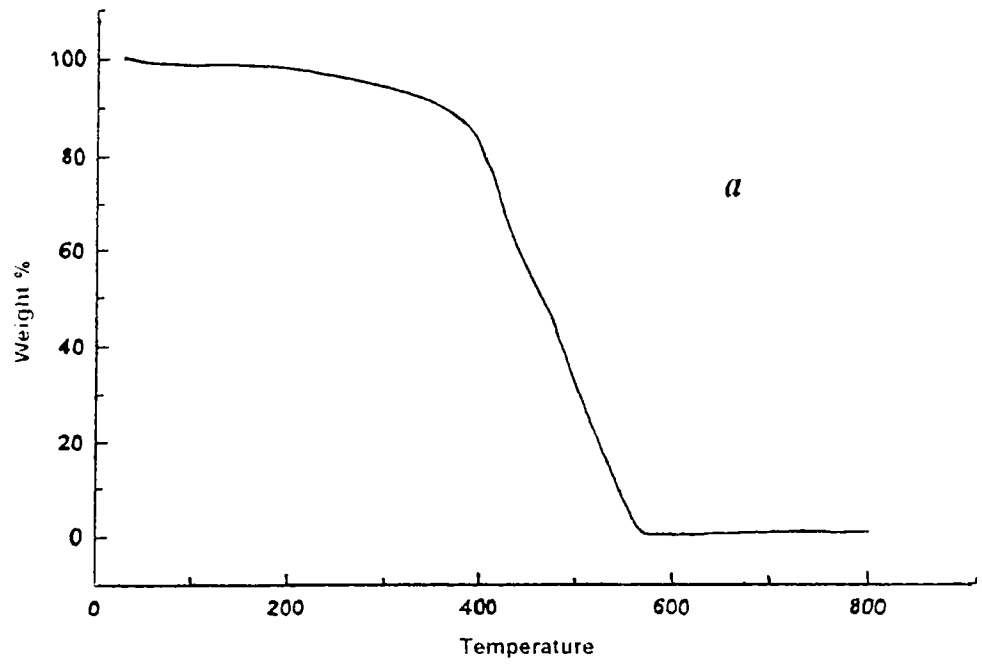


Fig IV.6: TG pattern of (a) PAbCo (b) PAbCu.

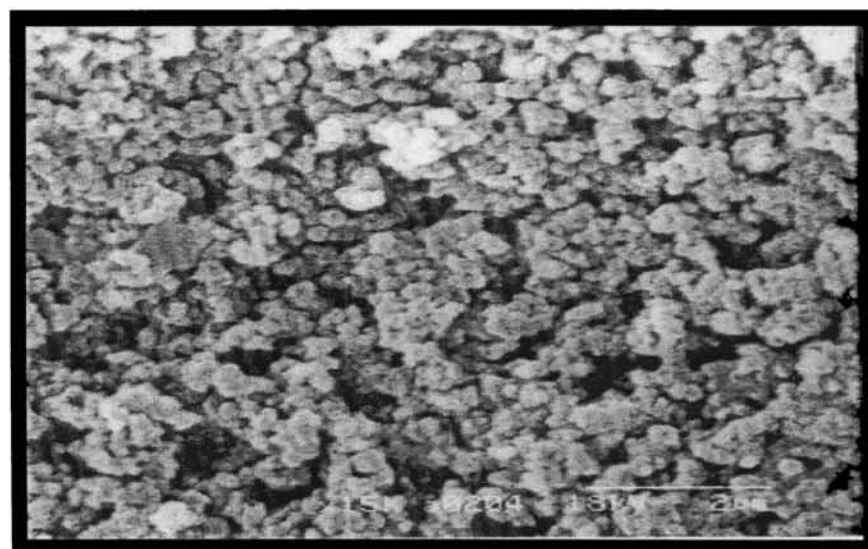
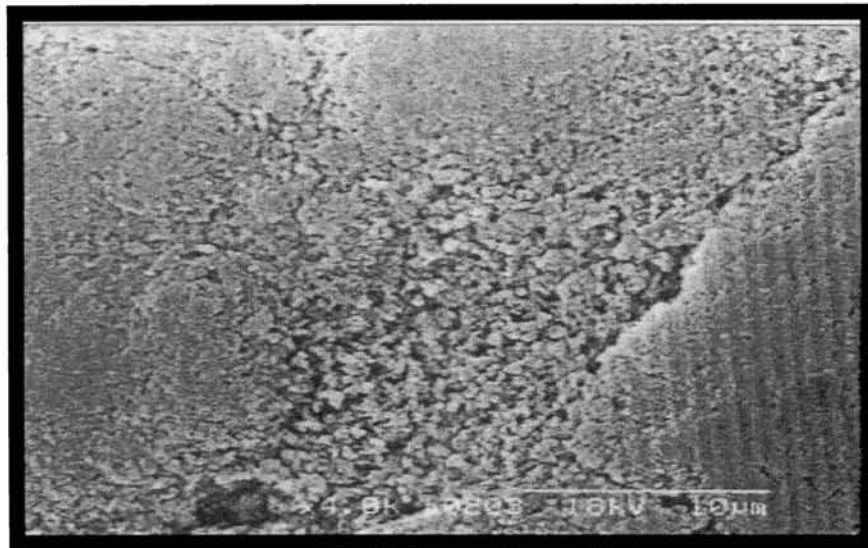
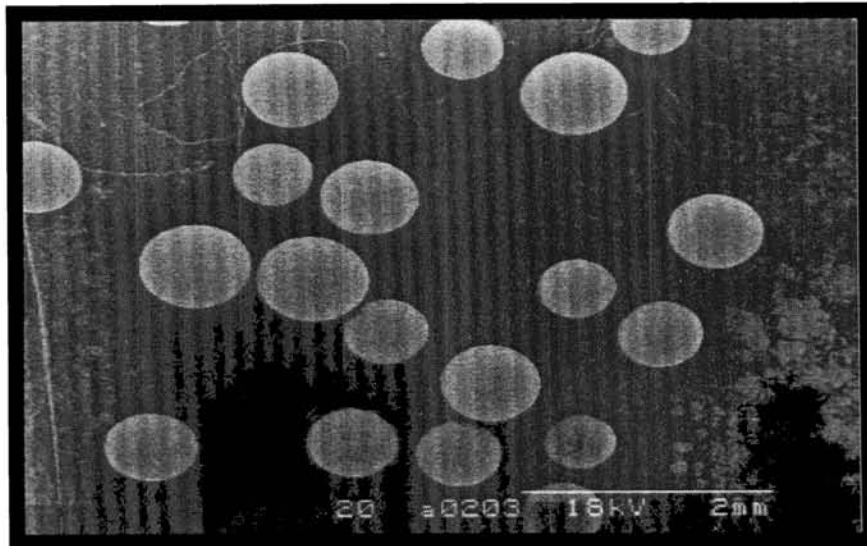


Fig. IV. 8 SEM of PAbCo at different magnifications

4.2.2.6 Thermal behaviour:

Thermogravimetric analyses of the complexes were carried out from room temperature to 800^oC to investigate their thermal stability. The TG data is given in table IV.10 and the patterns are given in Fig.IV.6. The polymer support is stable upto a temperature of 300^oC. Below this temperature, there is only a weight loss of 2%, which can be attributed to the loss of moisture. However, the polymer bound aldehyde reveal a weight loss of 5.6% below 200^oC which suggests the removal of the aldehyde group at this stage. The polymer bound complexes also decompose in this temperature range. The decomposition of the cobalt complex starts at 195^oC, while the copper complex start decomposing at a lower temperature suggesting it to be less stable than the cobalt complex.

4.2.2.7 SEM

The SEM of PAbCo which indicates the presence of the metal complexes in the pores of the polymer is given in Fig IV.8.

REFERENCES

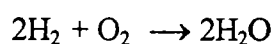
- [1] K.S. Devaki and V.N.R. Pillai, *Eur. Polym. J.*, **1988**, 24, 209.
- [2] A. Syamal and M.M.Singh, *Ind. J. Chem.*, **1994**, 33A, 58.
- [3] B.N. Figgis and J. Lewis, *Progress in Inorganic Chemistry*, Vol. VI, F.A. Cotton Ed., Interscience Publishers, New York, 1964.
- [4] J.N. Shah; D.T. Gokak and R.N. Ram, *J. Mol. Catal*, **1990**, 60, 141.
- [5] K. Nakamoto, *Infrared and Raman Spectra of Inorganic and Coordination Compounds*, V Ed.; 1997, John Wiley and Sons Inc., New York
- [6] L.J. Bellamy, *The Infrared Spectra of Complex Molecules*, Vol I, III Ed.; Chapman and Hall, London.
- [7] A.B.P. Lever, *Inorganic Electronic Spectroscopy*, Elsevier, Amsterdam.
- [8] D. Kivelson and R. Neiman, *J. Chem. Phys.*, **1961**, 35, 149.
- [9] I.M. Proctor; B.J. Hathaway and P. Nicholls, *J. Chem. Soc. A*, **1968**, 1678.
- [10] J.M. Assour, *J. Chem. Phys*, **1965**, 43, 2477.
- [11] U. Sakaguchi and A.W. Addison, *J. Chem. Soc. Dalton Trans.*, **1979**, 600.
- [12] R.M. Silverstein; G.C. Bassler and T.C. Morrill, *Spectroscopic Identification of Organic Compounds*, V Ed.; John Wiley and Sons Inc, New York.

CHAPTER V

ACTIVITY OF THE SUPPORTED TRANSITION METAL COMPLEXES IN CATALYSING THE HYDROGEN-OXYGEN REACTION

Introduction

The reaction between hydrogen and oxygen, once referred (1) to as the Mona Lisa of all reactions by Hinshelwood, can be represented as



The reaction referred to as oxidation of hydrogen or reduction of oxygen, can take place with the aid of a catalyst or at very high temperatures ($\sim 1300^\circ\text{C}$). This type of catalytic oxidations, which involve small molecules like H_2 , O_2 , CO , etc. and occur without the formation of side products, were applied by numerous research workers (2) as catalytic test reactions for characterization of various catalysts, metallic as well as non-metallic.

The catalytic oxidation of hydrogen was discovered in 1822 by Döberner who showed that at ambient temperatures Pt sponge can induce spontaneous combustion of hydrogen in oxygen. This was one of the processes, which prompted Berzelius to formulate his ideas of catalysis. Studies on this reaction have been carried out with the contemporary methods of surface science, and this has contributed appreciably to the understanding of mechanism of the reaction especially, those which occur on the surface of Pt group metals.

From a practical point of view, this reaction has lot of applications (3). Trace amounts of oxygen present as impurities in several systems are removed using this

reaction which is referred to as deoxo reaction. The deoxo reaction is used in the refining of petroleum and also in corrosion control.

During catalytic reforming of crude petroleum oil, the feed is treated with a Pt catalyst which is adversely affected by nitrogen, oxygen and sulfur compounds. These elements are removed by pretreating the reforming feed over a Ni-Mo or Co-Mo catalyst in the presence of hydrogen.

The removal of oxygen is important in preventing corrosion in piping and storage systems. The rate of oxygen reduction is increased by adding a cobalt compound. In industries, removal of oxygen from the feed water to high pressure boilers is necessary. The bulk of oxygen is removed by passing through a deaerator. But, this equipment cannot remove the last traces of oxygen; and hence, it becomes necessary to add a chemical oxygen scavenger to produce oxygen free feed water.

The main application of this reaction is in the removal of trace impurities of oxygen present in gas streams. Hydrogen from coke oven gas and from an electrolysis very often contains oxygen in concentrations upto 1%. This oxygen is removed in deoxo reactors. The Pt group metals exemplified by Pt, Pd, Pd supported on alumina are largely used for this reaction (4-6). Several transition metal complexes were also found to be active in catalysing the removal of oxygen by coordinating to it. The recent advances in kinetics of oxygen reduction by transition metal complexes (7) have been reviewed by Adzic Radoslav. Cobalt complexes bind oxygen reversibly and can even separate oxygen from nitrogen from dry air (8). Several model metal complexes containing porphyrin and Schiff base ligands have been synthesized and studied for their oxygen uptake (9). However, such complexes decompose slowly due to the attack of oxygen on the ligands or due to the dimerisation of the complexes.

The use of supported metal complexes could overcome this difficulty. Several attempts with zeolite encapsulated complexes have been reported. The zeolite framework prevents dimerisation and degradation of the complexes and thus makes the complexes more efficient than the free complexes (which degrade in solution). The use of Co (salen) in zeolite Y as a catalyst for this reaction was reported by Herron et al. (10). An anionic cobalt cyanide complex in zeolite Y has been reported to be an effective oxygen carrier (11). The metal complexes of bipyridine and terpyridine in zeolite Y were found to be very efficient for separation of oxygen from nitrogen in dry air (12).

Another interesting example is provided by Park Sang et al (13). They prepared a catalyst by encapsulating 2-ethylanthraquinone (2-EAQ) together with Pd species in zeolite Y and found out that it could catalyse the production of H_2O_2 in aqueous solution. The production is synergistically enhanced with the aid of the encapsulated 2-EAQ in faujasite pores. The catalysis of oxygen reduction using pyrolyzed metal complexes have been reported (14). The influence of pyrolysis temperature on the oxygen reduction activity of pyrolyzed metal macrocyclic complexes were studied. Several Fe and Co porphyrin complexes deposited on carbon were most effectively pyrolyzed at $800^{\circ}C$. Pyrolysis not only enhanced the oxygen reduction activity but also improved the swelling behaviour of the metal complexes in an acid.

The examples given above clearly indicate the potential of supported complexes for gas separation and purification and warrant further studies on the development of new catalysts. Hence, we have made an endeavor to explore the capability of our complexes in effecting the above reaction.

5.1 EXPERIMENTAL

5.1.1 Materials:

Gamma alumina in the form of tablets of 4.7mm dia and 3.2mm height obtained from United Catalysts India Limited, were used. The gases used were hydrogen of Sterling Gases, Kochi, nitrogen and oxygen from West Coast Industrial Gases Limited, Kochi.

5.1.2 Preparation of the catalysts:

The zeolite encapsulated metal complexes described in Chapter III were processed as follows: The zeolite complex and pseudoboehmite in the ratio 3:7 were mixed together, and made into a paste with a few drops of 2% acetic acid this mixture was pelletized with a hand press. These pellets were dried in an air oven before use. The polymer supported complexes which are in the form of macroporous beads were used as such without further processing.

5.1.3 Analysis of the complexes:

The metal content in the catalyst samples before and after the reaction was determined by the procedures described in Chapter II. The infrared spectra of the samples prior to and subsequent to the reaction were recorded to examine whether any changes have occurred to the catalyst.

5.1.4 Reaction set up:

A schematic representation of the experimental set up for the catalytic activity studies is given in Fig.V.I. A microcatalytic reactor loaded with ~0.2g of catalyst is connected to a gas chromatograph through a gas sampling valve. Hydrogen is passed

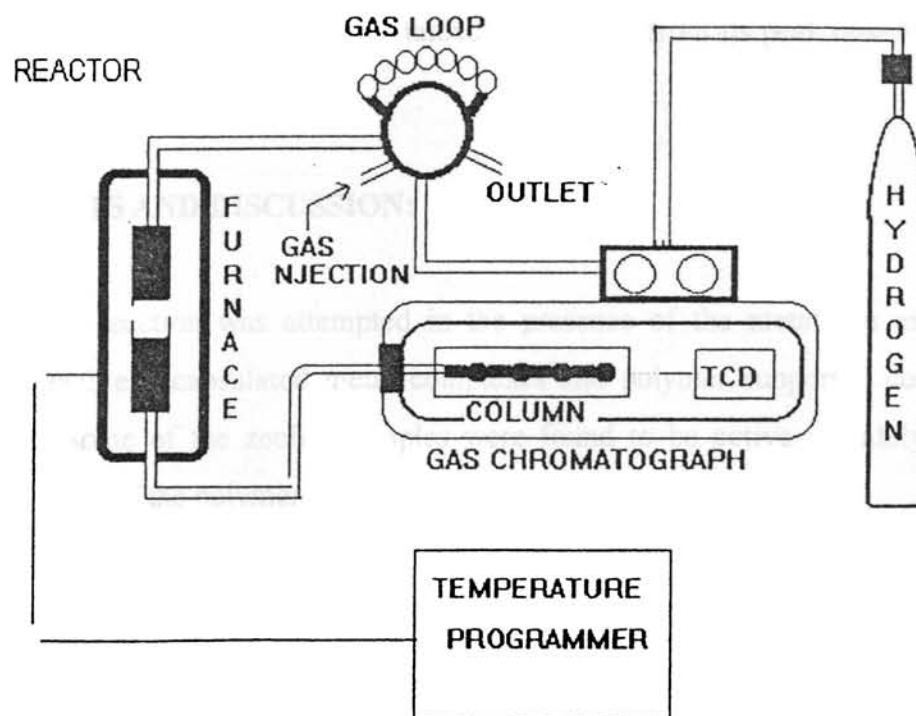


Fig V.1: EXPERIMENTAL SETUP FOR CATALYTIC ACTIVITY STUDY

through the reactor at a flow rate of 30ml per minute. Oxygen gas is injected through the precalibrated loop of the auto gas sampling valve. The oxygen thus admitted into the reactor is reduced by the hydrogen and the unreacted oxygen is carried into the thermal conductivity detector of the GC for analysis. The output signal is recorded and the concentration of oxygen was measured with reference to the calibration for a known quantity of oxygen. The percentage conversion was calculated from the concentration of the unreacted oxygen obtained from the chromatogram. Further, the product of the reaction was ascertained to be water from its peak observed in the chromatogram after reaction.

5.2 RESULTS AND DISCUSSION:

The reaction was attempted in the presence of the metal ion exchanged zeolites, zeolite encapsulated metal complexes and polymer supported complexes. While the some of the zeolite samples were found to be active in catalysing the reaction, none of the polymer supported samples exhibited any activity.

The reaction in presence of the polymer supported complexes were attempted at a temperature below 50 °C as the thermogravimetric analysis of the complexes indicated that they were not stable at higher temperatures. On injecting oxygen into the reactor containing the polymer samples, at room temperature there was a decrease in the area of the oxygen peak, but with a slight increase (by a few degrees from room temperature) in temperature the peak with an area corresponding to the residual oxygen appeared. This suggests a possible adsorption of the oxygen in the pores of the macroporous polymer beads initially and desorption when temperature is increased. From the above observations it was concluded that our polymer supported complexes could not catalyze the reaction to even a small extent.

In the case of the zeolite samples, the encapsulated metal complexes exhibited an activity in the range 200-240°C. However, none of the complexes were active at

TABLE V.1*Percentage conversion of oxygen in presence of different catalysts*

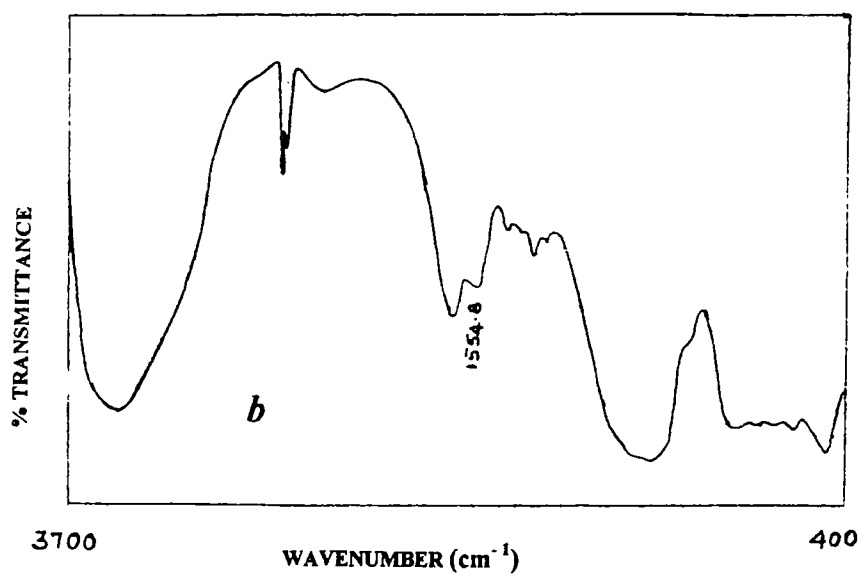
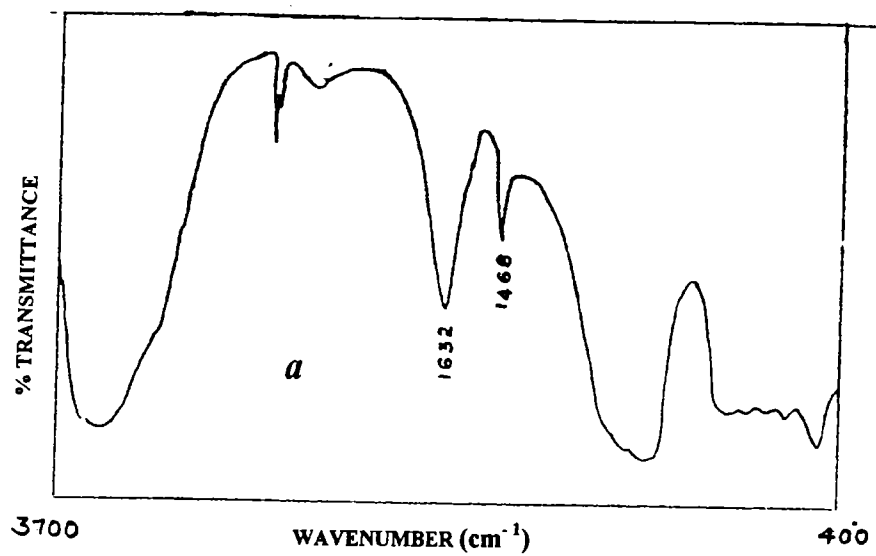
Sample	Vol. of O ₂ injected = 0.2 ml					Vol. of O ₂ injected = 1.5 ml			
	conversion (%) at					conversion (%) at			
	RT	100 ^o C	200 ^o C	230 ^o C	240 ^o C	RT	100 ^o C	200 ^o C	230 ^o C
NaY	nil	nil	nil	nil	nil	nil	nil	nil	nil
MnY	nil	5	40	58	70	nil	nil	5	8
YMnEm	nil	10	73	75.4	75.4	nil	nil	9	12
CoY	15	15	15	58	83	nil	nil	8	13
NiY	nil	-	-	48	54	nil	nil	nil	4
YNiEm	nil	nil	33	54	62	nil	nil	nil	6
CuY	nil	20	39	49	50	3	3	7	8
YCuEm	nil	20	54	93	95	nil	nil	5.2	55
YCuAb	nil	10	38	82		nil	nil	5	40

room temperature. In most of the cases the maximum conversion was effected at $\sim 230^{\circ}\text{C}$. In some cases even though an increase in temperature by a few degrees resulted in a slight increase of activity, the catalyst became deactivated very quickly. The activities of the different catalysts in the above temperature range are given in table V.1.

The metal ion exchanged zeolites exhibited a slight activity at lower temperatures. However, with increase in temperature the increase in activity was not that significant as that of the encapsulated complexes. The enhanced activity exhibited by the encapsulated complexes in comparison to the ion exchanged zeolites could be only due to the influence of the ligand. The ligand could induce changes in the structure as well as in the redox potential of the metal ions.

Among the encapsulated complexes the maximum activity was displayed by the complexes of copper(II). In spite of effecting comparable conversions, the copper-embelin complex, YCuEm, turned out to be far more superior than the copper-aminobenzimidazole complex, YCuAb, because the latter got deactivated after one or two runs.

A plausible justification for the complex exhibiting maximal activity at $\sim 230^{\circ}\text{C}$ is that at this temperature there might be a removal of the coordinated water. The thermogravimetric analysis of the complexes indicates that the dehydration is almost complete at this temperature (vide page 54) and an IR spectral analysis indicates the presence of the ligand portion of the complex. So just after the loss of intrazeolite water molecules the coordinated water molecules could be removed. The loss of the coordinated water molecules could result in a different arrangement of ligands around the metal ion. Thus a change in structure along with the tuning of the redox potentials of the metal ion could be attributed to the sudden rise in the catalytic activity of the complexes at these temperatures. The FTIR spectrum of the catalyst pellets before and after the reaction is given in Fig. V.2. It is seen that the $\nu_{\text{C=O}}$ peak



**FigV.2: FTIR Spectrum of YCuEm catalyst a) prior to reaction
b) after reaction**

at 1468 cm^{-1} in the catalyst before reaction disappears while a new peak appears at 1555 cm^{-1} . This could be due to the strengthening of the C-O bond and consequent weakening of the M-O bond, when dioxygen molecule coordinates to the metal.

The effect of various parameters affecting the conversion has been studied in the case of YCuEm, the most efficient catalyst in the group. The details of these studies are presented below.

5.2.1 Influence of oxygen concentration:

The percentage conversion rate for two different concentrations of oxygen injected is presented in Table V.1. The percentage conversion is higher for 0.2ml of oxygen injected at same catalyst weight. This indicates that the conversion is dependent on the concentration of the oxygen gas.

5.2.2 Influence of catalyst weight:

When oxygen (1.5ml) was injected into the reactor containing YCuEm (0.2g) the conversion rate was found to 59%; and when the same volume of oxygen was injected into the reactor containing 0.1g of catalyst at the same temperature, conversion turned out to be only 10% suggesting a dependence of the reaction on the quantity of catalyst employed.

5.2.3 Influence of temperature:

The influence of temperature in this reaction has already been discussed. Table V.2 gives the conversion of oxygen to water at different temperatures starting from room temperature.

TABLE V.2

*Effect of temperature on the reduction of oxygen
in presence of YCuEm catalyst*

For 0.2 ml of Oxygen		For 1.5 ml of oxygen	
Temperature	Conversion (%)	Temperature	Conversion (%)
175	18.4	175	nil
200	54	200	5.24
225	65	225	27
229	70	229	27
230	95	230	55

R
5.11.302
RAN



TABLE V.3

Life cycle study for YCuEm catalyst (0.2g) at 230°C

Time (min)	conversion (%)	Time (min)	conversion (%)	Time (min)	conversion (%)
0	51	75	52	150	52
5	52	80	52	155	51
10	55	85	53	160	52
15	55	90	53	165	52
20	55	95	53	170	51
25	59	100	53	175	51
30	57	105	53	180	51
35	55.3	110	52	185	48
40	55.3	115	52.4	190	47
45	54	120	52	195	47
50	54	125	51	200	48
55	54	130	50	205	46
60	52	135	52	210	47
65	53	140	51		
70	53	145	52		

Note: The reaction was carried out by injecting 1.5 ml of oxygen at intervals of 2.5 minutes.

5.2.4 Life cycle of the catalyst:

One of the ways in which the zeolite encapsulated complex can lose its activity is by loss of metal ions, which is brought about by leaching of the metal complex or reduction to free metal. The recycling efficiency of the catalyst was studied in the following way; the experiment was carried out at 230⁰C by injecting a known volume (1.5 ml) of oxygen gas at intervals of 2.5 minutes and the conversion was monitored. The results are summarized in Table V.3. It can be seen that the maximum conversion was maintained for 2 to 2.5 hrs., after which a slight decrease in activity was observed. An estimation of the catalyst at the end of the reaction revealed that no metal leaching takes place during the reaction. This also suggests that the metal complexes are intact within the cavities and the structural features of the zeolite are not changed during the reaction.

REFERENCES

- [1] E.K. Rideal, *Advances in Catalysis*, 9, 1957, 8.
- [2] B. Adams and H. Jerzy, *Oxygen in Catalysis*, Marcell Deker Inc., New York, 1991
- [3] Kirk Othmer, *Encyclopedia of Chemical Technology*, Vol. 12, III Ed.; John Wiley and Sons Inc., New York.
- [4] M.G. Jones and T.G. Nevell, *J. Catal.*, 1990, 122, 219.
- [5] G.K. Boreskov; V.V. Popovskii and V.A. Sazonov, *Proc. Int. Congr.*, IV, 1968, I, 439.
- [6] I. Kozlov; V.S. Pavelko; K.S. Anatoly, Russian Patent, 1996 (CA. 125: 333276c).
- [7] Adzic Radoslov, *Electrocatalysis*, 1998, 197.
- [8] K. Mizono; S. Imamura and J.H. Lunsford, *Inorg. Chem.*, 1984, 23, 3510; *Langmuir* 1985, 1, 326.
- [9] (a) G.M. Lendon and A.E. Martell, *Coord. Chem. Rev.*, 1976, 19, 1
(b) E.L. Neiderhoffer; J.H. Tommins and A.E. Martell, 1984, 84, 137.
- [10] N. Herron, *Inorg. Chem.*, 1986, 25, 4714.
- [11] R.S. Drago; I. Bresinka; J.E. George; K.J. Balkus Jr ; and J. Taylor, *J. Am. Chem. Soc.*, 1988, 110, 304.
- [12] G.A. Ozin and C. Gil, *Chem. Rev.*, 1989, 1749.
- [13] E.Y. Park Sang; Jung Whan; L.W. Jin and L.C. Wee, *Bull. Korean Chem. Soc.*, 1999, 20(1), 21.

CHAPTER VI

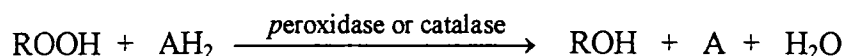
CATALYTIC DECOMPOSITION OF HYDROGEN PEROXIDE - A KINETIC AND MECHANISTIC STUDY

6.1 INTRODUCTION

Knowledge of a reaction rate is of great importance to both laboratory and industrial practice. Reaction that takes years to become sensibly complete is not particularly useful in making its product; but, reactions that are complete in fraction of a second are also not useful and may include hazardous explosions. It is clearly necessary to understand the factors controlling the rate at least to some extent before a reaction becomes useful on any scale. An understanding of reaction mechanism allows a more informed extension of the reaction to new but mechanistically related cases and the understanding of mechanisms of related reactions is a useful way to classify the hosts of known reactions and to remember them. As an area of pure science in itself, the study of kinetics and mechanisms is one of rich variety, concerned with the chemistry of every element and full of experimental challenge. The importance of studying mechanisms prompted us to endeavor into this field to get ourselves acquainted with the means and methods of kinetics.

The reactions of hydrogen peroxide are among the most widely studied from mechanistic point of view. Hydrogen peroxide participates in a variety of chemical reactions and that many of the earlier reactions investigated still provide matter for further studies. This has attracted the attention of chemical kineticists towards its reactions for more than hundred years. Further, the decomposition reaction of hydrogen peroxide (which may be expressed as $2\text{H}_2\text{O}_2 \rightarrow 2\text{H}_2\text{O} + \text{O}_2$)

is often employed as a standard reaction (1) to determine the catalytic activity of metal complexes. This is because the catalytic action is always observed regardless of the metal ion species and the ligand species due to the capability of hydrogen peroxide to undergo oxidation as well as reduction reaction. Moreover, the reaction takes place even if the catalyst is insoluble in the reaction solvent and the experimental technique is not difficult to employ. Catalysis of this reaction by metal complexes is similar to the action of the enzymes, catalase and peroxidase (2) and this is yet another reason why this is being pursued by workers. The proper function of the enzymes involves the disproportionation of hydrogen peroxide to liberate oxygen which can then be used to oxidize a variety of compounds (3). This process can be represented as,



where, ROOH is H_2O_2 , A is O_2 and in peroxidase catalysis AH_2 is either H_2O_2 or pyrogallol, p- cresol, mesitol, aniline, NADH, ferrocyanide, or dihydroxy fumarate and in case of catalysis by catalase, it is pyrogallol, p- cresol, p-phenylene diamine, methanol, ethanol.

An unwanted product in many redox reactions involving oxygen is H_2O_2 . A convenient method for removing the unwanted H_2O_2 is to add catalase, which catalyses its disproportionation to H_2O and O_2 (3).

H_2O_2 is used as the source of oxygen in many oxidation and epoxidation reactions. The kinetics of the decomposition reaction as well as the reaction utilizing H_2O_2 as redox agent have been reported to be catalysed by zeolite encapsulated complexes (4-8) and polymer supported complexes (9-11).

In view of the importance of catalytic decomposition of hydrogen peroxide, we have screened our supported metal complexes to assess their catalytic activity

towards this reaction. These studies indicated that copper and cobalt species are highly active. We have also studied the kinetics of decomposition of hydrogen peroxide in the presence of YCuEm to understand the mechanism of the reaction. The results of these studies are presented in this chapter.

6.2 EXPERIMENTAL

6.2.1 *Materials:*

The preparation of the complexes has already been described in chapters III and IV. Hydrogen peroxide solution (30%, Merck) was used without further purification. The required concentration of hydrogen peroxide was obtained by dilution with deionised water and it was standardized by titration against standard potassium permanganate solution prior to each set of kinetic runs. All other chemicals used were of analytical grade purity.

6.2.2 *Experimental setup:*

The experimental set up employed is shown in figure VI.1. The decomposition reaction in the presence of the complexes was followed by measuring the volume of oxygen evolved. To monitor the reaction, required volume of hydrogen peroxide (~0.27 M) was taken in a flask containing a magnetic paddle and diluted with deionised water to 20 ml. A plastic float containing the catalyst was placed over the solution and the reaction vessel was placed in water maintained at room temperature. The vessel was then connected to the gas burette containing 20-25% sodium chloride solution acidified with dilute hydrochloric acid and coloured with methyl orange. After 30 minutes the levels in the two arms of the burette were made equal and the reading was noted. The catalyst is introduced into the solution by means magnetic stirring. As the reaction proceeds the level in the right arm lowers due to the evolution of oxygen. The levels in the two arms were equalized at regular

intervals of time and the reading on the right arm was noted to give the volume of oxygen evolved.

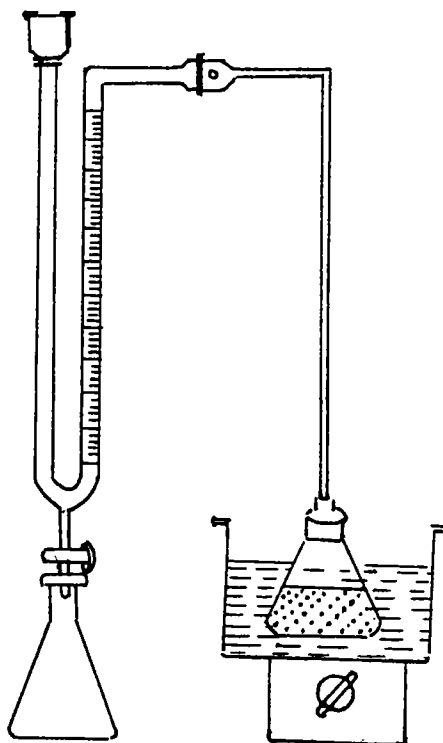


Fig VI.1: Experimental set up for the study of hydrogen peroxide decomposition.

The kinetics of the reaction was studied by the initial rate method. This method involves constructing a plot of concentration, 'c' versus time, 't' and determining the slope of the tangent to this curve at $t = 0$, which gives the initial rate. In the present study we constructed these plots by fitting the concentration versus time data into a polynomial of the form,

$$c = a_0 + a_1t + a_2t^2 + \dots$$

using polynomial regression method (12). This was achieved by employing a software called "AXUM" (Trimetrix, 1989). All the kinetic results were found to be reproducible within an error of $\pm 6\%$.

6.3 SCREENING STUDIES:

The screening studies were made by carrying out kinetic runs in the presence of the different catalysts prepared, maintaining the same concentration of hydrogen peroxide in each. The initial rates thus obtained showed different activities for the different supported metals and their complexes. An attempt is made to correlate this to the nature of the metal ion and its coordination environment which is discussed in this section.

6.3.1 Catalysis by Zeolite encapsulated complexes:

The activities of the different zeolite samples are given in Table VI.1. Among the metal exchanged zeolites, the cobalt(II) and copper(II) exchanged ones are found to exhibit excellent activity. Catalytic activities of metals and their complexes are usually explained in terms of either their redox potentials or structures (11,13). Redox potential of a metal ion has been considered as one of the critical factors in determining the catalytic activity of the catalyst containing the metal ion towards redox reactions, because the reaction appears to involve a change in the oxidation state of the metal ion during the redox steps. It has also been reported (2) that complexes of metal ions favor the decomposition of hydrogen peroxide only if they are coordinately unsaturated or, if they have coordinated water molecules at one or more sites which are available for substitution by H_2O_2 or HOO^- . Such sites are considered as "free" sites.

TABLE VI.1

Activities of the metal exchanged zeolites and their complexes for the decomposition of H_2O_2

Metal ion employed	Activity per unit weight of the catalyst, ml/min g.		
	Metal exchanged zeolite	Embelin complex in zeolite Y	Aminobenzimidazole complex in zeolite Y
Mn(II)	1.92	2.29	2.00
Fe(III)	3.04	3.48	-
Co(II)	9.65	6.63	7.00
Ni(II)	0.55	1.46	1.00
Cu(II)	14.20	10.20	12.04

The Co(II) and Cu(II) exchanged zeolites, whether they have appropriate redox potentials or not, do possess a four coordinate structure, facilitating further coordination of the reactive species when introduced into the reaction medium. They are thus expected to be considerably active, as observed to be the case. The activity of the Fe(III) and Mn(II) exchanged zeolites are less than that of the Co(II) and Cu(II) exchanged ones. These two complexes are six coordinated and are not expected to have considerable catalytic activity. The activity observed for the Fe(III) and Mn(II) complexes is probably due to favorable redox potentials.

A similar trend in activities is observed for the metal encapsulated complexes also. However, a decreased rate has been observed in the case of the encapsulated copper(II) and cobalt(II) complexes of embelin and an increased rate in the case of their 2-aminobenzimidazole complexes, in comparison to their respective metal exchanged zeolites. This may be partially due to the tuning of the redox potentials of the metal ions by the ligand and partially due to the change in structure. The encapsulated complexes, YCoEm and YCuEm are likely to have six coordinated and five coordinated structures respectively, while YCuAb is expected to have a nearly planar structure. This is supported by the observation that YCoEm and YCuEm on

dehydration exhibit enhanced rates. The rates of the reaction involving YMnEm, and YFeEm are more or less similar to that of their uncomplexed counterparts. This may be because ligand field stabilisation energies of Mn(II) and Fe(III) (being d^5 species) complexes are unaffected by the change in the ligand field.

Octahedrally coordinated nickel is usually observed to be inactive towards catalysis. This can be due to both its structure and redox potentials disfavoring its activity. The same observation has been made in the present case also, and Ni-Y and YNiEm are found to be the least active among those studied.

6.3.2. *Catalysis by Polymer supported complexes:*

The H_2O_2 reaction was studied in presence of the polymer supported complexes as catalysts. The values obtained for the activities of the different catalysts are given in table VI.2. The activities obtained indicate that the supported complexes of cobalt and copper are excellent catalysts for the reaction. The trend in the activities of the different metal complexes in polymer matrix is similar to that of the zeolite encapsulated complexes. A comparison of the cobalt and copper complexes indicates that the complexes of the polymer schiff base derived from embelin are superior to the complexes derived from aminobenzimidazole. This is perhaps due to the difference in abilities of the ligands in the two different environments in tuning the redox potentials of the metal ions.

TABLE VI.2

Activities of the polymer supported complexes for the decomposition of H_2O_2

Metal ion employed	Activity per unit weight of the catalyst, ml/min g.	
	Supported complexes of embelin	Supported complexes of aminobenzimidazole.
Mn(II)	5.80	-
Co(II)	26.60	7.12
Ni(II)	0.93	-
Cu(II)	10.30	12.00

6.4 KINETIC STUDY OF THE DECOMPOSITION OF HYDROGEN PEROXIDE IN THE PRESENCE OF THE ZEOLITE ENCAPSULATED COPPER EMBELIN COMPLEX:

In order to gain an insight into the mechanism of the reaction in presence of the catalyst, the kinetics of the reaction were studied by varying different parameters like the concentration of the reactant, catalyst and added ligand, and solvent polarity and pH and studying their effect on the rate of the reaction. The details of the results obtained during these studies are described in this section.

6.4.1 Kinetic Procedure:

Effect of substrate:

To study the effect of $[H_2O_2]$ on the reaction rate, kinetic runs were carried out by varying the volume of H_2O_2 in the range 5-9 ml (0.27 M), keeping catalyst quantity (5×10^{-3} g), the solvent composition and temperature constant.

Effect of catalyst:

Keeping the substrate concentration and solvent composition constant, kinetic runs were carried out by varying the quantity of catalyst in the range $1.0-9.0 \times 10^{-3}$ g at room temperature.

Effect of added embelin ligand:

Ligand solution of concentration, 5×10^{-6} M in methanol (1 to 5 ml) was added at constant catalyst weight, substrate concentration and solvent composition, to study the effect of the ligand on the rate of the reaction.

Effect of solvent:

To study the effect of the solvent polarity on the rate of the reaction, kinetic runs were carried out at constant temperature, catalyst weight and substrate concentration while varying the composition of the solvent by changing the ratio of the volumes of water and methanol and keeping the total volume constant. The dielectric constant of the medium was calculated assuming a linear relationship between the individual dielectric constants and composition of the solvent. Thus if D is the resultant dielectric constant, D_1 and D_2 are the dielectric constants of pure water and methanol and V_1 and V_2 their volumes employed respectively, D may be given as

$$D = \frac{D_1 V_1 + D_2 V_2}{V}$$

where V is the total volume of the reaction mixtures. The values of D_1 and D_2 employed are 78.54 and 32.63 respectively.

Effect of pH:

The pH of the solution was varied in the range 6-8 while keeping all other parameters constant. Phosphate buffers were used for varying the pH. The effect of dihydrogen phosphate ion on the self-decomposition of hydrogen peroxide was monitored prior to this study and confirmed to be absent. However, to be on the safer side, constant concentration of dihydrogen phosphate was maintained throughout the pH variation studies.

6.4.2 Results:Order with respect to substrate:

The initial rates obtained at different concentrations of hydrogen peroxide are given in Table VI.3.

TABLE VI.3

Effect of hydrogen peroxide on initial rate

Weight of catalyst = 5.0×10^{-3} , g

Volume of Hydrogen Peroxide, ml	Initial Rate $\times 10^2$, ml/min
5.0	5.15
6.0	7.41
7.0	8.71
8.0	8.73
9.0	10.73

A plot of $[H_2O_2]$ against initial rate is a straight line passing through origin (figure VI.2) indicating that the order of the reaction is unity in $[H_2O_2]$.

Order with respect to catalyst:

The plot of the initial rates versus catalyst weight was found to be linear (figure VI.3) pointing out the unit order of the reaction with respect to catalyst. The initial rates and their corresponding catalyst quantities are presented in Table VI.4.

TABLE VI.4

Effect of catalyst on initial rate

Volume of hydrogen peroxide = 8.0 ml

Weight of the catalyst $\times 10^3$	Initial Rate $\times 10^2$, ml/min
1.0	4.65
2.0	5.28
3.0	6.30
4.0	7.22
5.0	8.73
9.0	12.53

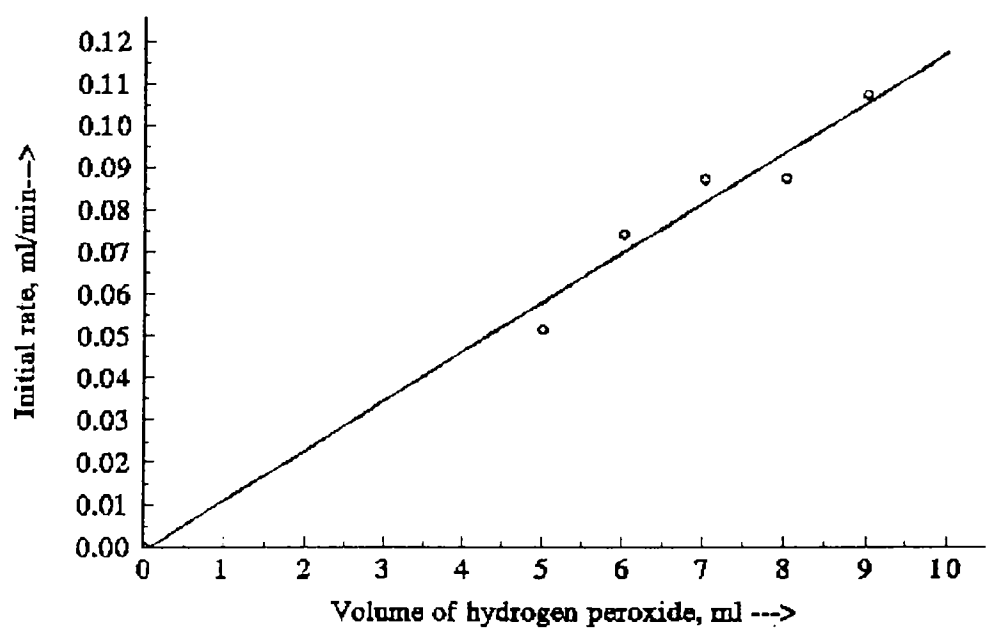


Fig VI.2 Effect of substrate on the initial rate

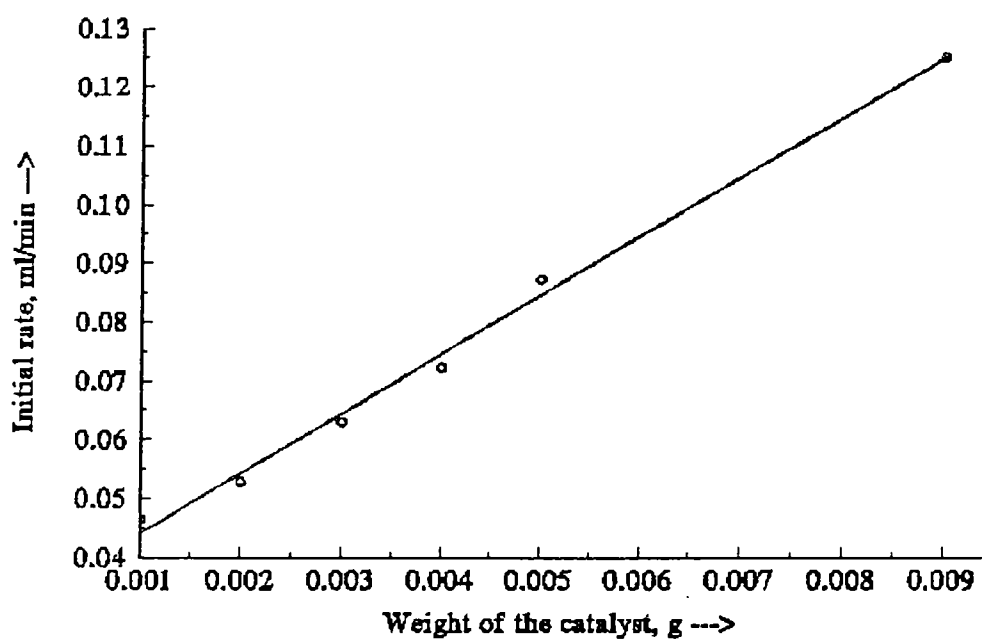


Fig VI.3 Effect of catalyst weight on the initial rate

Effect of added ligand

The added ligand concentrations and their corresponding initial rates are given in Table VI.5. The initial rates obtained from all the plots are reproducible within $\pm 6\%$ error indicating that there is no ligand effect.

TABLE VI.5*Effect of added ligand on initial rate*

Volume of hydrogen peroxide = 8.0 ml

Volume of ligand solution, ml	Initial Rate x 10^2 , ml/min
1.0	2.98
2.0	3.20
3.0	3.20
4.0	2.80

Effect of Solvent:

A plot of (figure VI.4) initial rates against the reciprocal dielectric constant of the medium is a straight line with a positive slope. The values of initial rates obtained in this study are given in table VI.6.

TABLE VI.6*Effect of solvent polarity on initial rate*

Volume of hydrogen peroxide = 5.0 ml

Dielectric constant	Initial Rate x 10^2 , ml/min
78.43	5.10
76.24	7.32
73.95	8.90
71.66	9.85
69.36	17.8

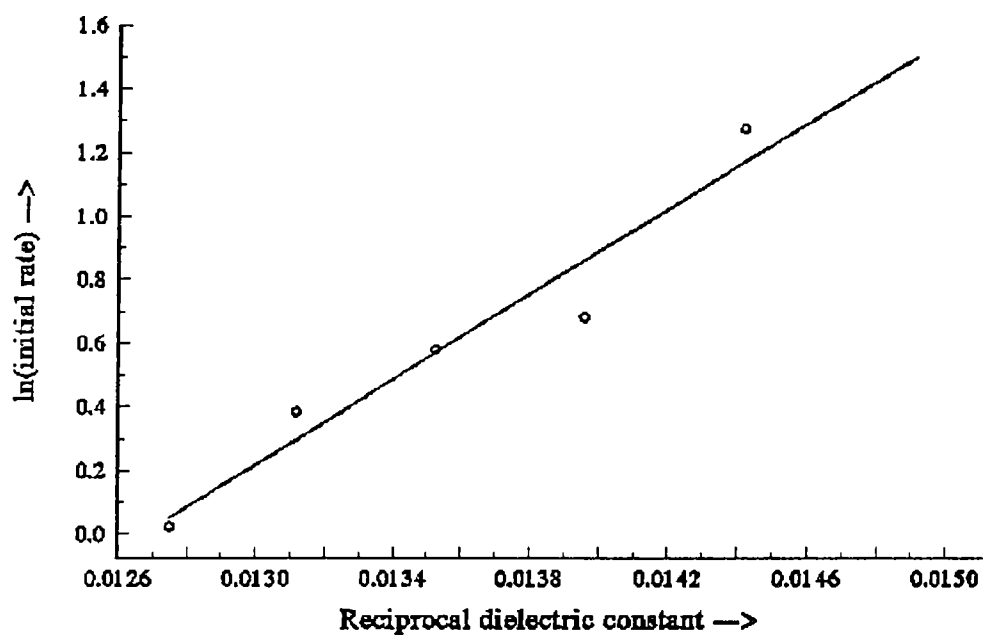


Fig VI.4 Effect of solvent polarity on initial rate

Effect of pH:

The reaction exhibited a complex dependence on pH. It is clear from the results presented in table VI.7 and the plot of pH against initial rates shown in figure VI.5 that the rate increases with pH initially and then decreases.

TABLE VI.7*Effect of pH on initial rate*

Volume of hydrogen peroxide = 5.0 ml

pH	Initial Rate x 10, ml/min
6.0	2.83
6.4	3.78
6.8	4.38
7.2	4.55
7.6	3.37
8.0	2.54

When the reaction was carried out in the absence of added phosphate buffer, the pH of the solution was found to increase from 2.7 before the reaction was initiated, to 4.2 after a reaction for 30 minutes.

6.4.3 Discussion:

Many possible mechanisms for the catalytic decomposition of hydrogen peroxide have been proposed by earlier workers (13). Some of the reactions involve a radical chain mechanism in which the initiation reaction of HOO or OH radical production is catalysed by metal ions, and the others involve a reaction taking place within the coordination sphere of the metal ion.

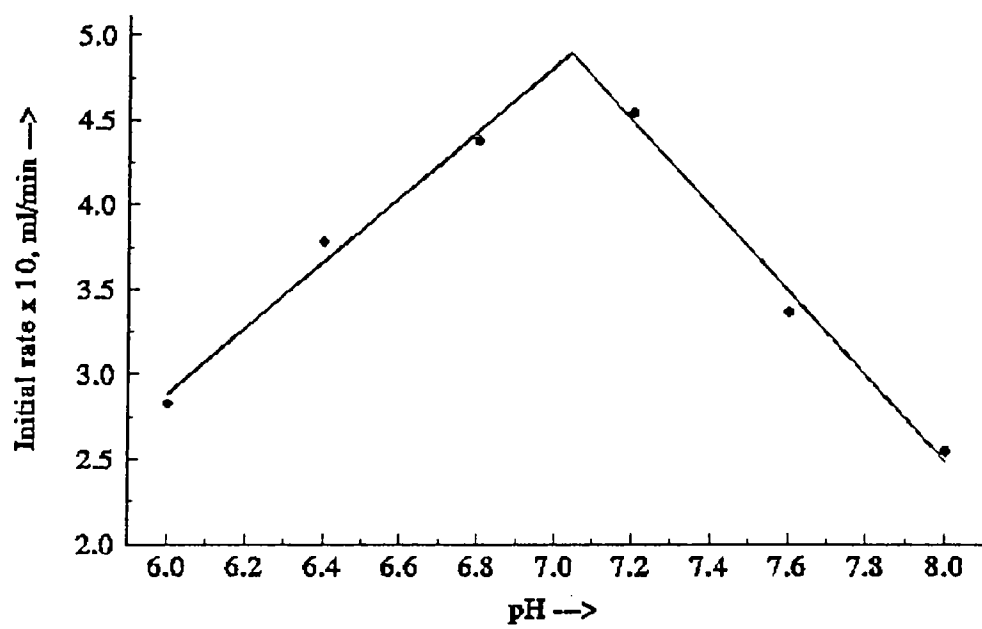
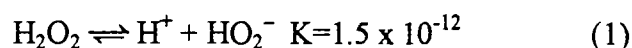


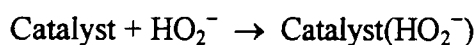
Fig VI. 5 Effect of pH on initial rate

In the present investigation, the order with respect to both hydrogen peroxide and the catalyst were found to be unity, indicating that the two are participating in the rate determining step.

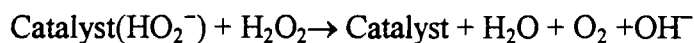
Hydrogen peroxide is a somewhat stronger acid than water and in dilute aqueous solutions it exists in the following equilibrium (14)



In most cases (15) the catalytic decomposition is believed to proceed through coordination of HO_2^- ion to the catalyst which can be represented as

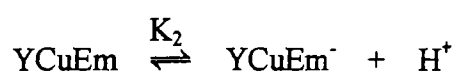


This reaction may then proceed through a step which involves interaction of the coordinated species with another molecule of hydrogen peroxide.



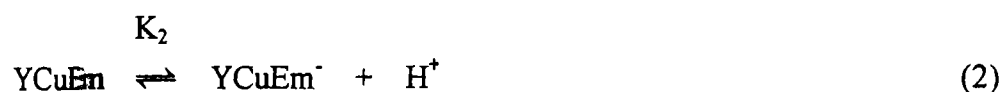
Such a mechanism is similar to the enzyme (catalase) catalysed decomposition of hydrogen peroxide, which is characterized by a rise in pH if the reaction is carried out in unbuffered solutions (15). In our reaction also we have observed that the pH of the reaction mixture which was 2.5 initially, increased to 4.2 after 30 minutes reaction with the catalyst. This increase in pH with progress in the reaction confirms the liberation of OH^- ions as per the above said mechanism which involves HO_2^- ion as the reactive species. Further, in most of the catalytic decompositions of hydrogen peroxide, where HO_2^- is reported to be the reactive species, an increase in rate was observed with an increase in pH and a linear relation is obtained between the reaction rate and hydrogen ion concentration. In the present case the rate of the reaction increased initially with an increase in pH and later decreased with it. In the region of lower values of pH, a plot of reciprocal of the initial rates against $[\text{H}^+]$ was found to

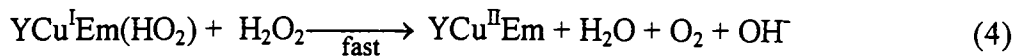
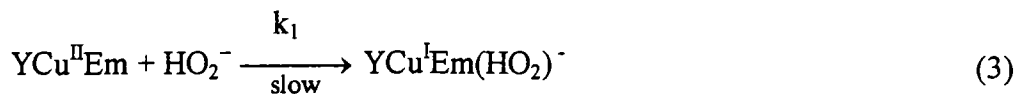
be linear. These results suggest that in the present case also, HO_2^- ion is the reactive species. This is further justified by the solvent effect. A plot of $\log(\text{initial rate})$ against reciprocal of the dielectric constant of the medium was observed to be linear with a positive slope. Since our encapsulated metal complex may be presumed to have a positive dipole, this effect indicates the hydrogen peroxide species to be negatively charged. The decrease in rate at still higher pH values is probably due to change in the species of the complex as per an equilibrium of the type,



Added ligand did not show any effect on the rate of the reaction. This suggests that neither the complex is existing in any equilibrium with the ligand nor hydrogen peroxide species substitute the ligand from the complex during the reaction. The fact that the metal ion in the encapsulated complex is in a penta coordinated environment persuades us to believe that if at all an intermediate is formed between the catalyst and hydrogen peroxide it probably involves an expansion of coordination. Although we have not observed any evidence for complexation of the hydrogen peroxide species with the catalyst, the fact that HO_2^- , which is a better ligand, is more reactive than undissociated hydrogen peroxide suggests some coordination between the catalyst and hydrogen peroxide species. Probably it is formed in the rate determining step and consumed immediately in fast steps to give the products, and thus the order with respect to hydrogen peroxide is observed to be unity.

On the basis of these results the mechanism of our present reaction can be extended as given in the following scheme.





This mechanism leads to the rate expression,

$$\text{Rate} = k_1[\text{YCuEm}]_e[\text{HO}_2^-]_e \quad (5)$$

Assuming $[\text{H}_2\text{O}_2]$ to be the total concentration of all the species of hydrogen peroxide, we can write,

$$[\text{H}_2\text{O}_2] = [\text{H}_2\text{O}_2]_e + [\text{HO}_2^-]_e \quad (6)$$

From equilibrium (1) we have,

$$K_1 = \frac{[\text{HO}_2^-][\text{H}^+]}{[\text{H}_2\text{O}_2]_e} \quad (7)$$

Equations 6 and 7 give rise to the concentration of $[\text{HO}_2^-]_e$ in terms of the total concentration of hydrogen peroxide as,

$$[\text{HO}_2^-]_e = \frac{K_1[\text{H}_2\text{O}_2]}{\{K_1 + [\text{H}^+]\}} \quad (8)$$

Similarly, if $[\text{YCuEm}]$ is assumed to be the total concentration of the complex in the reaction mixture, then it can be written as,

$$[\text{YCuEm}]_t = [\text{YCuEm}]_e + [\text{YCuEm}^-] \quad (9)$$

From equilibrium (3)

$$K_2 = \frac{[\text{YCuEm}^-]_e[\text{H}^+]}{[\text{YCuEm}]_e} \quad (10)$$

From equations (9) and (10) we get,

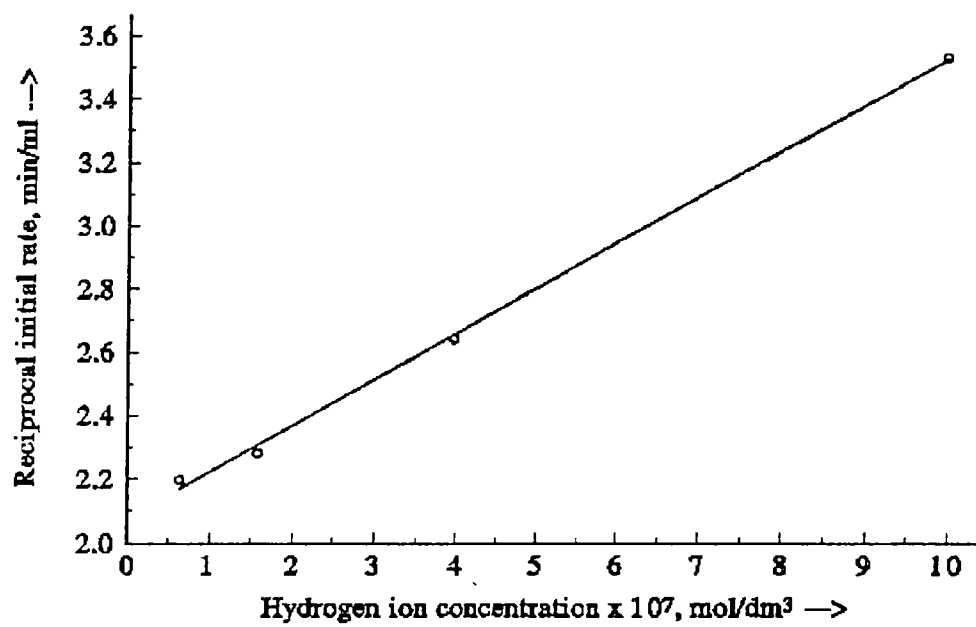


Fig VI.6 Plot of $[H^+]$ versus reciprocal initial rate at high H^+ concentrations

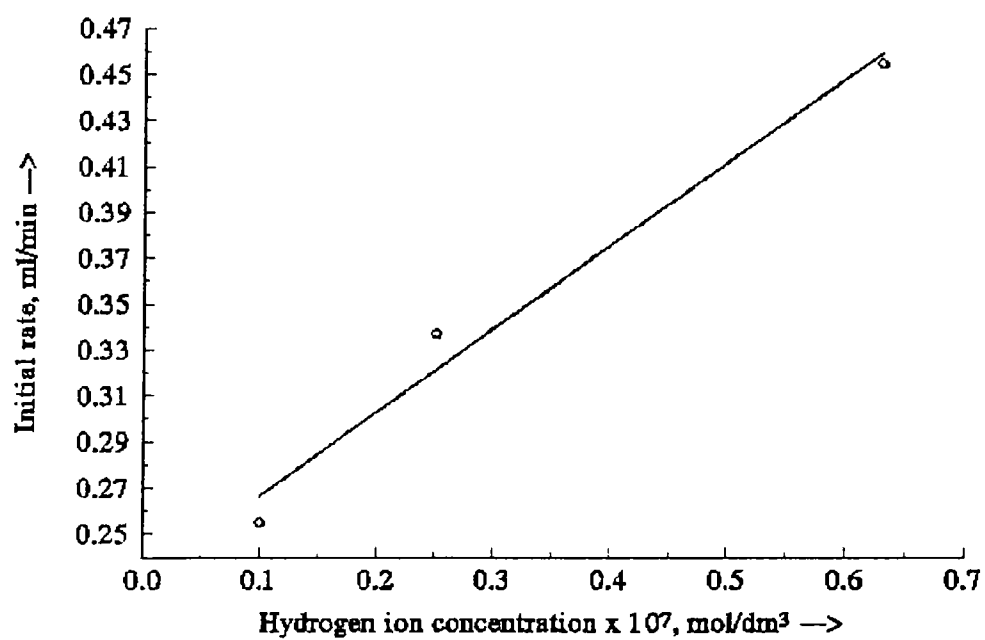


Fig VI.7 Plot of $[H^+]$ versus initial rate at low H^+ concentrations.

$$[\text{YCuEm}]_e = \frac{[\text{YCuEm}]_t[\text{H}^+]}{\{K_2 + [\text{H}^+]\}} \quad (11)$$

Substituting equations (7) and (11) in the rate expression (4) we get

$$\text{Rate} = \frac{k_1 K_1 [\text{H}_2\text{O}_2]_t [\text{YCuEm}]_t [\text{H}^+]}{\{K_1 + [\text{H}^+]\} \{K_2 + [\text{H}^+]\}} \quad (12)$$

The above rate equation is in agreement with the first order observed with respect to both the catalyst and hydrogen peroxide. Further, if at low concentrations of H^+ , it is negligible compared to K_1 and K_2 , the above rate equation reduces to,

$$\text{Rate} = \frac{k_1 [\text{H}_2\text{O}_2]_t [\text{YCuEm}]_t [\text{H}^+]}{K_2} \quad (13)$$

This equation suggests that a plot of initial rate against the corresponding hydrogen ion concentration should be linear. This may be the case in the present reaction and the same is observed at low pH (figure VI. 6)

On the other hand if we rearrange equation 12 we obtain,

$$\frac{1}{\text{Rate}} = \frac{K_1 K_2 + [\text{H}^+][K_1 + K_2] + [\text{H}^+]^2}{k_1 K_1 [\text{H}_2\text{O}_2]_t [\text{YCuEm}]_t [\text{H}^+]} \quad (14)$$

According to this equation, when hydrogen ion concentration is high such that $K_1 K_2$ in the numerator of equation 14 is negligible compared to the other terms, a plot of $[\text{H}^+]$ versus reciprocal of the initial rate is expected to be linear. In order to verify this we have plotted the reciprocal of the initial rate against the corresponding initial rate and obtained a straight line at higher concentrations of hydrogen ion, as shown in figure VI. 7. The equations 11 and 14 explains the variation of rate with pH.

Thus the proposed mechanism explains all the observed experimental results of the present investigation.

REFERENCES

- [1] E. Tsuchida and H. Nishide, *Adv. Polym. Sci.*, **1977**, 24,1.
- [2] H. Sigel, *Angew. Chem. Int. Ed.*; **1969**, 8, 3, 167.
- [3] El-Ichiro Ochiai, *Bioinorganic Chemistry An Introduction*, Allyn and Bacon Inc., London, 1977.
- [4] E. Stefan; A. Weber; and J. Weichert, *Chem Ing. Tech.* **1997**, 71(1/2), 147.
- [5] P.P. Knops-Gerrits; M. L'abbe and P.A. Jacobs, *Stud. Surf. Sci. Catal.*, **1997**, 108,445.
- [6] P.P. Knops-Gerrits and F. Thibault Starzyk, *Stud. Surf. Sci. Catal.*, **1994**, 84, 1411
- [7] R. Robert and P. Ratnasamy, *Stud. Surf. Sci. Catal.*, **1996**, 101.
- [8] K. Nowinska and M. Cejba, *Proc. Pol. Ger. Zeolite Colloq.*, 1995, 42 (CA 124: 260198w).
- [9] I.A. Salem; M.Y. El-Sheikh; A.B. Zaki and N. Ulrich, *Int. J. Chem. Kinet.*, **1994**, 26(9), 955.
- [10] R. Sreekala and K.K.M. Yusuff, *Ind. J. Chem.*, 1995, 34A, 994.
- [11] R. Joshi and S.N. Limiye, *Oxidn. Commun.*, **1998**, 21(3), 337.
- [12] N. Sridevi, *Ph.D Thesis*, Andhra University, Visakhapatnam, India , 1991.
- [13] I. Mochida and K. Takeshita. *J. Phys. Chem.*, **1974**, 78, 16, 1653.
- [14] N.N. Greenwood and A. Earnshaw, *Chemistry of the Elements*, Pergamon Press, 1984.
- [15] R.V. Prasad and N.V. Thakkar, *Ind. J. Chem.*, **1994**, 33A, 861.

SUMMARY AND CONCLUSIONS

The thesis deals with our studies on the synthesis and characterisation of some supported transition metal complexes and their catalytic activity in the deoxo reaction and hydrogen peroxide decomposition. The thesis is divided into six chapters. **Chapter I** of the thesis presents an introduction to the zeolite encapsulated and polymer bound metal complexes which is relevant to the theme of the present investigation. Several references to reports on the synthesis and characterisation using the various physicochemical techniques are included. The application of these compounds are also given.

Chapter II gives an account of the general reagents and the various physicochemical techniques used for characterization of the supported complexes. These techniques include elemental analyses, magnetic susceptibility measurements, surface area analyses (BET method), scanning electron microscopy (SEM), X-ray diffraction studies (XRD), infrared, electronic (diffuse reflectance or absorbance), and EPR spectral studies and thermogravimetric analysis. Procedures for modification of the supports to immobilize the complexes are also given in the chapter.

Chapter III describes our studies on the encapsulation of the transition metal complexes of the ligands, embelin (2, 5-dihydroxy-3-undecyl-2,5-cyclohexadiene-1,4-dione) and 2-aminobenzimidazole, and their characterization. The chapter is divided into two sections. The first section includes the studies on the encapsulated complexes of embelin while the second section includes the studies of the encapsulated complexes of 2-aminobenzimidazole. The characterisation of the complexes based on the various physico chemical techniques (mentioned in chapter II) are discussed. Based on the Si/Al ratio, unit cell formulae were calculated for the zeolites. The elemental analysis data further give an idea of the composition of the

complexes inside the zeolite. Scanning electron microscopy of a representative complex after purification by soxhlet extraction indicates the absence of surface adsorbed species. The formation of the complexes is inferred from FTIR data. The IR bands present in the spectra of the ligand are present in the spectra of the encapsulated complexes also.

In the case of the complexes of embelin in zeolite, coordination of the carbonyl oxygen is indicated by shifting of the C=O stretching band to lower frequencies. A comparative study of the spectra of the metal ion exchanged zeolites, zeolite encapsulated and simple complexes of embelin is included with a view to understand the structure of the encapsulated complexes. The magnetic and diffused reflectance data point to an octahedral or nearly octahedral structure for the complexes of Mn(II), Fe(III), Co(II), Ni(II) and a penta coordinated structure for the copper(II) complex. Furthermore, evidence of the ionic environment around the metal ion is obtained from EPR data. The thermogravimetric analysis of the complexes indicates increased thermal stability of the complexes due to encapsulation. The thermal degradation pattern also suggests the possibility of using these systems in high temperature applications. On the basis of the procedural decomposition temperatures, the encapsulated complexes were found to follow the thermal stability sequence, $\text{Co} > \text{Mn} > \text{Fe} > \text{Ni} > \text{Cu}$.

IR spectra of the zeolite encapsulated complexes of 2-aminobenzimidazole reveal that coordination of the ligand is through the ring nitrogen as well as through the nitrogen of the amino group. Octahedral or nearly octahedral structures have been proposed for the Mn(II), Co(II), and Ni(II) complexes on the basis of magnetic moments and diffuse reflectance measurements. These data along with the EPR spectral data suggest a nearly planar structure for the copper(II) complex. The thermal degradation pattern of the complexes (with the exception of the copper(II) complex) does not give a clear idea of the procedural decomposition temperature. It

seems the decomposition of the complex and the removal of water are taking place simultaneously. The copper(II) complex is seen to decompose only after 230°C.

Further evidence for encapsulation of the complexes comes from the surface area analyses. The lowering of the surface area of the zeolite after the ion exchange and encapsulation procedures is an indication of intrazeolite matter. The XRD patterns reveal retention of crystallinity after the ion exchange and encapsulation procedures.

Chapter IV gives an account of the synthesis and characterization of polymer bound complexes of two Schiff bases. The chapter is divided into two sections. The first section deals with the Mn(II), Co(II), Ni(II) and Cu(II) complexes of the Schiff base (PEm) derived from a polymer bound amine and embelin; and the second part deals with the Co(II) and Cu(II) complexes of the polymer bound Schiff base (PAb) derived from a polymer bound aldehyde and 2-aminobenzimidazole. The elemental analyses of the complexes gives the probable composition. Surface area analysis suggests the inclusion of the complexes in the pores of the polymer. FTIR data reveals coordination of the azomethine nitrogen as well as that of the free carbonyl group of the Schiff base, PEm. Based on magnetic moment values and electronic absorption maxima, an octahedral or distorted octahedral structure has been proposed for the Mn(II), Co(II) and Ni(II) complexes of PEm. The Cu(II) complex seems to have a tetragonally distorted planar structure. The EPR data also support the structure. Further, the data indicate strong field nature of the ligand and the covalent nature of the complex. The thermogravimetric data for the complexes suggests the inability to employ the complexes in high temperature applications. All the complexes are found to decompose at lower temperatures.

The FTIR data of the Co(II) and Cu(II) complexes of PAb reveal that the coordination of the ligand to the metal is through the azomethine nitrogen and ring nitrogen. The magnetic and electronic spectral data indicate a tetrahedral structure

for the Co(II) complex and a square planar structure for the Cu(II) complex. However, the EPR data suggests tetragonal distortion of the square planar structure for Cu(II) complex. All these complexes are seen to decompose at lower temperatures.

Chapter V of the thesis presents the details of the activity studies of the complex in the catalysis of the hydrogen-oxygen reaction. A brief introduction of the reaction including review of the literature on this important reaction is given at the beginning. The metal ion exchanged zeolites as well as the complexes were active in catalysing the reaction, whereas the polymer supported complexes were inactive. The encapsulated complexes were more active than their respective metal exchanged ones. This could be only due to the influence of the ligands on the redox potential as well as on the environment about the metal ion. The Cu(II) complexes have come out as the most efficient catalysts for this reaction. However they were active only at a temperature between 230⁰C and 240⁰C. The TG data indicate, this might be due to the removal of coordinated water molecules at ~230⁰C and the consequent creation of vacant sites. The copper embelin complex is more superior catalyst for the deoxo reaction than the copper aminobenzimidazole complex, as the latter gets deactivated after two runs.

Chapter VI of the thesis deals with the catalytic decomposition of hydrogen peroxide using the prepared supported complexes. Screening studies of the complexes were carried out to know their potential as catalysts for this reaction. Zeolite complexes and polymer supported complexes are both active in catalysing the reaction and they follow the same trend for the different metals. The following is the activity pattern. Cu(II) > Co(II) > Mn(II) ~ Fe(III) > Ni(II). The variations in activity were explained on the basis of the structure. The study of the mechanism of the decomposition reaction involving YCuEm as the catalyst indicates a catalase like activity for the complex. Based on the experimental observations a rate equation was formulated for this reaction.



General conclusions drawn from the study:

1. The heterogenization of metal complexes overcomes the practical difficulties associated with their application in catalysis like processing separation from the reactants and products etc.,
2. Heterogenization using an inorganic support like zeolite permits their use at higher temperatures.
3. Zeolite encapsulated complexes are far better when compared to the polymer supported complexes in terms of stability (thermal and mechanical)
4. Embelin acts as an efficient ligand in modifying the properties of transition metal ions. This is evident from the catalytic activity studies.
5. Polymer supported samples can act as catalysts only at low temperatures.